Detection of Optical Brighteners in Morte Femme Peatland

A Major Qualifying Project

Submitted to the Faculty of

WORCESTER POLYTECHNIC INSTITUTE

In partial fulfillment of the requirement for the

Degree of Bachelor of Science in Chemical Engineering

By: Gina Visser

Date: March 29, 2020

Report Submitted to:

Sponsor: Marie-Noëlle Pons (ENSIC)
Advisor: Stephen Kmiotek

Abstract

This report studied the detection of optical brighteners in the Morte Femme peatland located in the Vosges mountains of France. Synchronous fluorescence scans of optical brightener solutions were used to generate fluorescent spectra before and after irradiation with UV light. Tests for pH, conductivity, DOC, ICP, ion chromatography, UV spectroscopy, and synchronous fluorescence spectroscopy were performed on field samples collected at various locations along the Morte Femme and its tributaries. Field samples were also irradiated with UV light, and the effects on their fluorescent intensity observed. A decrease in fluorescence intensity was observed at some sampling locations, and depending on the location this could be due to the presence of dissolved organic matter or optical brighteners.

Acknowledgements

I would like to thank École Nationale Supérieure des Industries Chimiques (ENSIC) for their partnership and for allowing me to conduct this project. Additionally, I would like to thank Dr. Marie Noëlle Pons for allowing me to use her lab facilities, for her help collecting field samples, and for her support and guidance throughout this project. I would also like to thank Professor Stephen Kmiotek at Worcester Polytechnic Institute (WPI) for his support and for giving me the opportunity to complete my Major Qualifying Project in Nancy France

Table of Contents

List of Figures

List of Tables

Executive Summary

Optical brighteners are fluorescent compounds that are commonly used by the textile and detergent industries to make white fibers appear brighter. They do this by emitting blue light between 400 and 440 nm in wavelength after excitation by UV light. The excitation with UV light causes optical brighteners to degrade which corresponds to a decrease in fluorescence. These properties were used to detect the presence of optical brighteners in the Morte Femme peatland.

The Morte Femme peatland is located in the Vosges mountains in the Lorraine region of France. The peatland is located near the source of the Cleurie river, a small mountain river whose pollution levels researchers at the University of Lorraine have been monitoring since 2018. Upstream of the peatland there are several textile plants that each have their own wastewater treatment facilities. People living around the Morte Femme and the Cleurie have noticed strange colors in the water that may be attributed to optical brighteners or dyes used in the textile plants.

Synchronous fluorescent spectroscopy was used to measure the fluorescent intensity of seven optical brightener solutions as well as field samples from the Morte Femme and its tributaries. Following an initial synchronous fluorescence scan, both the optical brighteners and the field samples were irradiated with UV light. If a decrease in fluorescence occurred after irradiation, then it was possible that there was an optical brightener present. However, in the field samples dissolved organic matter could also cause a decrease in fluorescence.

Solutions of the optical brighteners were mixed at concentrations of 0.015 $\frac{g}{L}$, 0.30 $\frac{mg}{L}$, and 0.03 $\frac{mg}{L}$. The optical brighteners studied as part of this report were Tinopal DMA-X, Tinopal CBS-X, Fluorescent Brightener 28, DAS, 4,4’-bis(2-benzoxazolyl) stilbene, 4,4’-diamino-2,2’-stilbenedisulfonic acid, and 2,5-bis(5-tert-butyl-benzoxazol-2-yl) thiophene. Synchronous fluorescent spectra were generated for each of these solutions using a Hitachi F-2500 Fluorescence Spectrophotometer and PMMA cuvettes. These spectra were generated using an excitation wavelength range of 230-600 nm and a difference of 50 nm between excitation and emission wavelengths. After the initial spectra were generated, the cuvettes were placed in a lab made box containing a mirror and a 15-W Vilbert Lourmat 115 L UV lamp where they were irradiated with UV light (365 nm) for 15 minutes. The fluorescent spectra of the irradiated samples were then compared to the initial spectra in order to determine if a decrease in fluorescence had occurred.

The fluorescent spectra of these optical brighteners were compared to those of field samples. Nine series of field samples were collected as part of this project. Eight of these series contained samples of approximately 12 sampling locations in the Morte Femme and its tributaries. The other series was made up of samples collected along the Cleurie river and its tributaries as well as the sites previously discussed. After collection these samples were stored at 4°C until they were able to be analyzed. Tests for pH, conductivity, dissolved organic carbon (DOC), ion chromatography, inductively coupled plasma mass spectroscopy (ICP), UV spectroscopy, and a synchronous fluorescence analysis were performed on each field sample that was collected. The fluorometric analysis performed on the field samples was exactly the same as that previously discussed for the optical brightener solutions. The spectra of the field samples and the optical brighteners were compared in an effort to detect the presence of optical brighteners. Additionally, excitation emission matrices were generated for three field samples as well as three optical brighteners. These provided a more detailed picture of the fluorescent spectra and were used to try and identify a specific optical brightener present in the field samples.

As expected, the optical brightener solutions showed a decrease in fluorescent intensity after irradiation. However, not all the field samples followed this trend. The field samples across all the series were grouped by location for analysis. The Noir Rupt, Corsaire, 2a, 2b and T sampling locations showed a decrease in fluorescent intensity, but this decrease was likely due to dissolved organic matter rather than optical brighteners. Water at the Noir Rupt, Corsaire, 2a, and 2b sampling locations had little contact with humans before arriving at the sampling location thus it was unlikely that optical brighteners were present at these locations. Location T contained excess water from the peatland that percolated through the peat before arriving at the sampling location. Since peat is rich in organic matter, it makes sense that the degradation at this location was from organic matter rather than optical brighteners. Spectra generated from samples taken at locations 6g, 6h, and 6d also showed a decrease in fluorescent intensity. However, as these sample locations had contact with industrial sectors it was possible that this decrease was due to the presence of optical brighteners. Rather than decreasing in fluorescent intensity following irradiation as expected, samples collected at locations 6e, 6f, step 3 aval, and 6 increased in fluorescence. While this was consistent with previous data collected by the University of Lorraine researchers, the reason for this trend is still unknown.

Excitation emission matrices were generated for samples collected at locations 6e, 6h, and T as part of the ninth data series. Matrices were also generated for Tinopal DMA-X, 4,4'-bis(2-benzoxazolyl) stilbene, and 2,5-bis(5-tert-butyl-benzoxazol-2-yl) thiophene. These field samples and optical brighteners were selected as they provided variety in fluorescent intensities and shapes of fluorescent spectra. The matrices of the field samples from locations 6e, and 6h had similar features as that of Tinopal DMA-X. However, the peaks of the field samples spanned a wider range of excitation wavelengths and had maximum intensities much lower than the peaks of Tinopal DMA-X's matrix. This could indicate that there was a mixture of optical brighteners or other fluorescent compounds present in the field samples. Sampling location T's matrix had a peak similar to that of locations 6e, and 6h but had a much higher fluorescent intensity. However, since location T was the old bed of the Cleurie river it was more likely that this peak was due to the presence of dissolved organic matter than optical brighteners.

Introduction

Optical brighteners are a class of chemicals used by the textile and detergent industries to make white fibers appear brighter. Their widespread use combined with their slow biodegradation has resulted in optical brighteners being found in many waterways (Hagedorn et al., 2005). However, optical brighteners do degrade when exposed to UV light. Thus, the presence of optical brighteners can be detected by comparing a fluorescent analysis of water samples before and after UV irradiation.

The goal of this report was to provide evidence of optical brighteners in the Morte Femme peatland located in the Lorraine region of France. This was accomplished through the following objectives: 1) Create synchronous fluorescent spectra of seven commonly used optical brighteners, 2) Collect water samples from various locations in the Morte Femme and its tributaries, 3) Conduct spectrometric characterization of collected water samples, and 4) Compare the fluorescent spectra of optical brighteners and water samples in an effort to determine if optical brighteners were present in the Morte Femme peatland.

Background

Optical Brighteners

Optical brighteners are fluorescent compounds that emit light in the blue range (400-440 nm) after excitation by UV light (360-365 nm) (Assad et al., 2014; Cao et al., 2009). Alternate names for optical brighteners include fluorescent whitening agents, and optical bleaches. The blue light that optical brighteners emit after UV excitation makes them appear whiter to the human eye. This combined with their water solubility and high affinity for binding to cellulose results in their use in the textile industry to mask the yellowing of cotton fabric (AVM Chemical Industries; Kramer et al., 1994).

In addition to their use in the textile industry, optical brighteners are frequently a component of laundry detergent. As a result, large quantities of optical brighteners are present in both domestic and industrial wastewater (Assad et al., 2014). Since optical brighteners are poorly biodegradable, they are often discharged into the wastewater receiving body where they absorb to particulate matter (Hagedorn et al., 2005). Once in surface waters they can be photochemically degraded, but may be hazardous to aquatic life (Gholami et al., 2016). While the main uses of optical brighteners are in textiles and detergents, they are also used in the paper, plastic, medical, chemical and cosmetic industries (Assad et al., 2014).

The structure of each optical brightener molecule determines how well and the pattern in which it will fluoresce. All optical brighteners are composed of highly substituted aromatic structures, and it is the double bonds that are activated by the UV light (Hagedorn et al., 2005; Gholami et al., 2016). This results in a decrease in fluorescent intensity after irradiation with UV light, so by analyzing fluorescence before and after UV exposure optical brighteners can be detected in stream samples (Pitterle and McGinnis-Carter, 2010).

The optical brighteners studied in this report were Tinopal DMA-X, Tinopal CBS-X, Fluorescent Brightener 28, DAS, 4,4’-bis(2-benzoxazolyl) stilbene, 4,4’-diamino-2,2’-stilbenedisulfonic acid, and 2,5-bis(5-tert-butyl-benzoxazol-2-yl) thiophene. Structures of each of these compounds can be found in Figure 1 below.

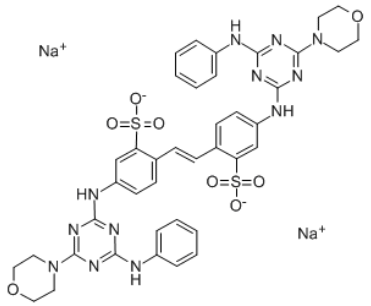

Tinopal DMA-X

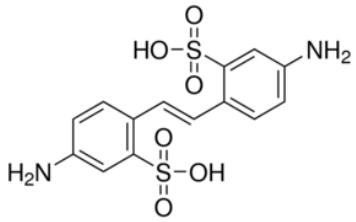

4,4’-diamino-2,2’-stilbenedisulfonic acid

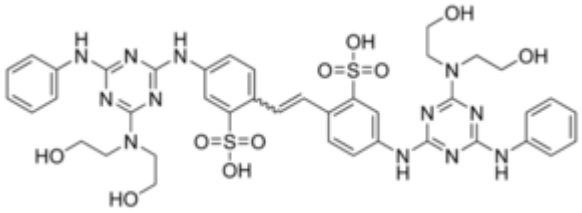

Fluorescent Brightener 28

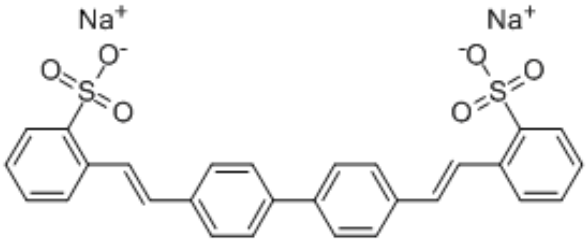

Tinopal CBS-X

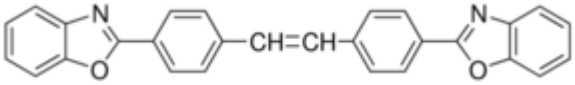

4,4’-bis(2-benzoxazolyl)stilbene

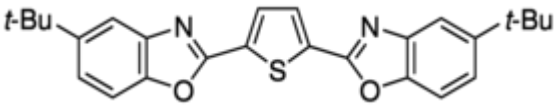

2,5-bis(5-tert-butyl-benzoxazol-2-yl) thiophene

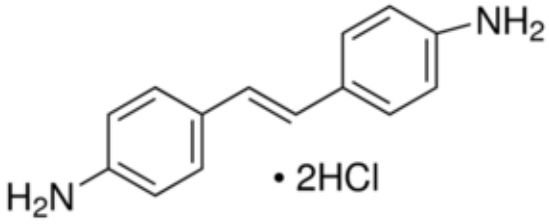

DAS

Figure 1*: Structures of optical brighteners studied in this report*

Geography of the Area

This report focuses on the presence of optical brighteners in Morte Femme peatland. The Morte Femme is located in the Vosges mountains in the Lorraine region of France as seen in Figure 2 below.

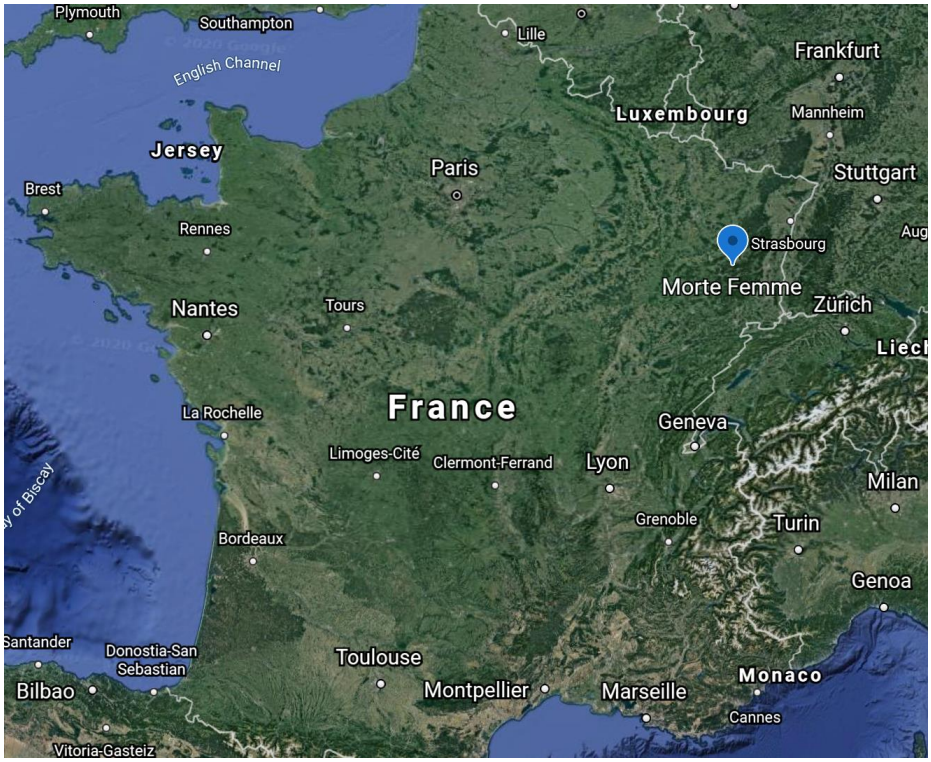

Figure 2: *Location of Morte Femme peatland (Google Earth, n.d.)*

The Morte Femme peatland is located near the source of a small mountain river, the Cleurie. Researchers at the University of Lorraine have been monitoring the pollution in the Cleurie River, its tributaries and the peatland since the summer of 2018 (Pons, 2020). Just upstream from the peatland there are several textile plants as can be seen in Figure 3 where the blue marker represents the Morte Femme, orange line represents the Cleurie River, the purple and red lines represent the Noir Rupt and Corsaire tributaries, and the green markers represent the textile plants.

Figure 3: *Morte Femme peatland and surrounding area (Google Earth, n.d.)*

The textile plants in this area work mainly with cotton yarns, and each have their own water treatment facilities. In past years, people living around or visiting the peatland have noticed strange colors, an example of which is in

Figure **4** below (Pons, 2020). These strange colors may be attributed to optical brighteners and dyes from the textile plants.

Figure 4: *Artificial blue color observed in the peatland during field sampling on January 27*

Fluorescent Spectroscopy

In an effort to detect the presence of optical brighteners in Morte Femme, the field samples collected were analyzed using fluorescent spectroscopy. "Fluorescence is the property of some atoms and molecules to absorb light at a particular wavelength and to subsequently emit light of a longer wavelength after a brief interval… (University of California Irvine)." In the case of optical brighteners, they absorb UV light and emit blue light between 400 and 440 nm (Cao et al., 2009). At a molecular level, this process has three steps. In the first step, the molecule is excited by an incoming photon which results in it transitioning from the ground state to an excited state. Once in the excited state, the second step is the relaxation of the electrons to the lowest energy level. Finally, the electrons return to the ground state by emitting a longer wavelength photon (University of California Irvine). The longer wavelength photon is what is measured by the fluorescent spectrophotometer.

In this study, synchronous fluorescence spectra were generated for each of the field samples. In synchronous fluorescence the excitation and emission monochromators are scanned simultaneously with a fixed wavelength difference between them (Pacheco and Bruzzone, 2013). The methodology section discusses the emission and excitation wavelengths as well as the wavelength difference that were used to generate the spectra in this report. The spectra of the field samples were then compared to solutions of the seven optical brighteners previously mentioned in

order to determine if optical brighteners were present in any of the field samples. However, Cao et al. found that some organic matter and aromatic compounds found in water samples can absorb and emit wavelengths similar to those of optical brighteners (2009). Optical brighteners degrade much faster than dissolved organic matter when exposed to UV light (Cao et al., 2009). In an effort to differentiate between fluorescence as a result of optical brighteners and fluorescence as a result of dissolved organic matter the field samples were irradiated with UV light. If the field samples showed similar degradation as that of the optical brightener solutions, then it was possible that optical brighteners were present in that sample.

Methodology

Optical Brightener Solutions

Solutions of each of the seven optical brighteners were prepared using ultrapure water as the solvent. Ultrapure water was made using an EGLA PURELAB water purification system. For each optical brightener, solutions at concentrations of 0.015 $\frac{g}{L}$, 0.30 $\frac{mg}{L}$, and 0.03 $\frac{mg}{L}$ were prepared. The varying concentrations were used to determine the optimal concentration to be used in further testing. In order to prevent the optical brighteners from photochemically degrading during storage, the volumetric flasks were completely wrapped in aluminum foil and stored at 4 °C.

Once all the solutions of optical brighteners had been created, a fluorometric analysis was performed. A Hitachi F-2500 Fluorescence Spectrophotometer along with 3.5 mL disposable polymethyl methacrylate (PMMA) cuvettes were used to generate fluorescent spectra for each optical brightener solution. A synchronous wavelength scan at the instruments highest sensitivity, 700V, and a scanning speed of 300 nm/min were used to measure the fluorescent spectra. Solutions of Tinopal DMA-X, Tinopal CBS-X, and Fluorescent Brightener 28 at 0.015 $\frac{g}{L}$ were too saturated for the highest sensitivity setting, and thus their spectra were generated using a synchronous wavelength scan at 400V. All scans were conducted at an excitation wavelength ranging from 230-600 nm with a fixed 50 nm difference between emission and excitation wavelengths, and excitation and emission slits of 2.5 nm.

After the initial scan, cuvettes were placed in a laboratory-made closed box fitted with a 15-W Vilbert Lourmat 115 L UV lamp from Fischer Bioblock Scientific and a mirror for reflecting the light. This laboratory setup can be seen in Figure 5. The cuvettes were irradiated with UV light (365 nm) for periods of 15, 30, and 45 minutes with wavelength scans conducted after each period of irradiation. Ultra-pure water was subjected to the same treatment, and its resulting florescent spectrum was used as a baseline.

Figure 5: *Laboratory made closed box shown opened on the left and closed on the right*

The synchronous fluorescence scans previously described were conducted using an excitation wavelength ranging from 230-600 nm and a fixed difference of 50 nm between excitation and emission wavelengths. Additional trials were conducted on a few optical brightener solutions with fixed wavelength differences of 20 nm and 80 nm. These trials were used to confirm that a 50 nm wavelength difference was optimal.

Collecting Field Samples

Several field trips were conducted in order to collect samples of the Cleurie river, its tributaries, and the Morte Femme peatland. Figure 6 below shows the sampling locations along the Cleurie river, and Figure 7 is a close up version showing the sampling locations in Morte Femme. The purple dots represent the sampling locations at Morte Femme peatland, as well as the Corsaire, Noir Rupt, and Costet tributaries which are labeled on Figure 6. The orange dots represent the 11 sampling locations along the Cleurie river, and the pink dots represent sampling locations along the Ruisseau de Voués, Berlingoutte, Pissoire, Cellet, Grand Rupt, Liangoutte, and Meunière tributaries.

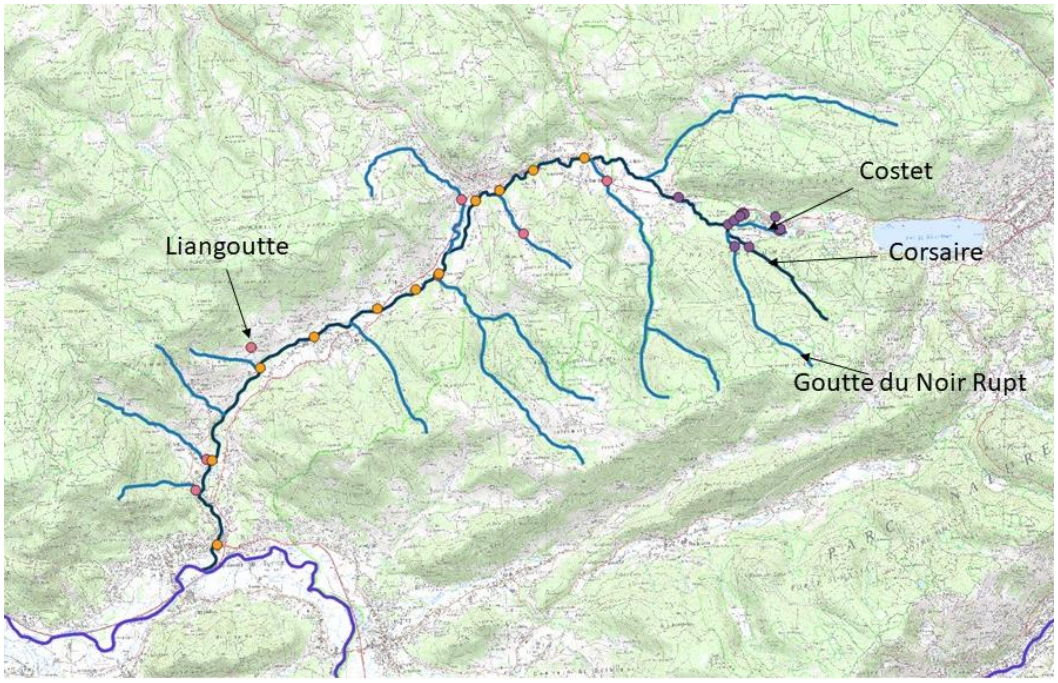

Figure 6: *GIS Map showing sampling locations along Cleurie River, its tributaries, and Morte Femme peatland (Pons, 2020)*

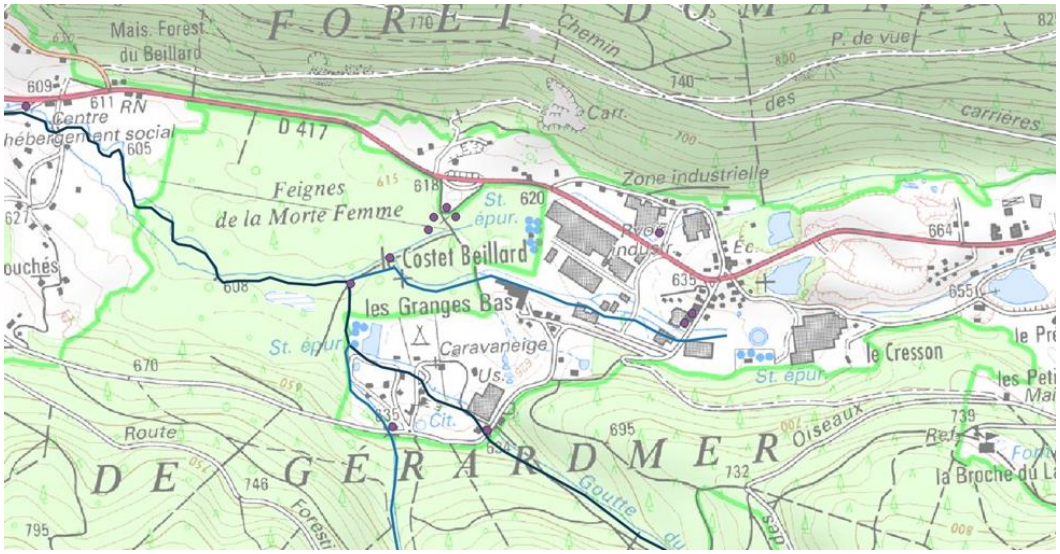

Figure 7*: Close up of sampling locations in Morte Femme peatland (Pons, 2020)*

Field trips on January 23, 29, and 30 as well as February 11 collected samples at each of the purple dot locations. A field trip on January 27 collected samples at all of the locations shown

in Figure 6. On trips when samples of the purple dots were collected, a 5 foot long pole with a cup on the end shown in 

Figure **8** below was used to fill 125 mL bottles with the sample. Both the cup and the sample collection bottle were rinsed with water from the sampling location before the sample was collected.

Figure 8: *Sample collection device*

On the trip when samples were collected at all the locations, multiple collection methods were used. Samples collected from bridges over the waterway used a bailer attached to a length of rope to fill a 125 mL bottle with the sample as shown in the sample.

Figure 9 below. Both the bailer and sample bottle were rinsed with water from the sampling location prior to collection of the sample.

Figure 9: *Bailer used to collect samples from bridges*

Samples collected from the banks of waterways were collected in the same manner previously discussed. Collected samples were stored in a cooler while in the field, and were transferred to a cold room kept at 4°C once back at the lab.

Analyzing Field Samples

Tests for pH, conductivity, dissolved organic carbon (DOC), ion chromatography, inductively coupled plasma mass spectroscopy (ICP), UV-vis spectroscopy, and fluorometric analysis were conducted on each field sample that was collected.

Samples were first removed from the cold room and ordered by sample number as shown in the data tables in Appendix A. A 100 mL plastic bottle, a 50 mL glass vial, a 12 mL disposable test tube, and a 2 mL glass vial for each sample were collected and labeled as can be seen in Figure 10 below.

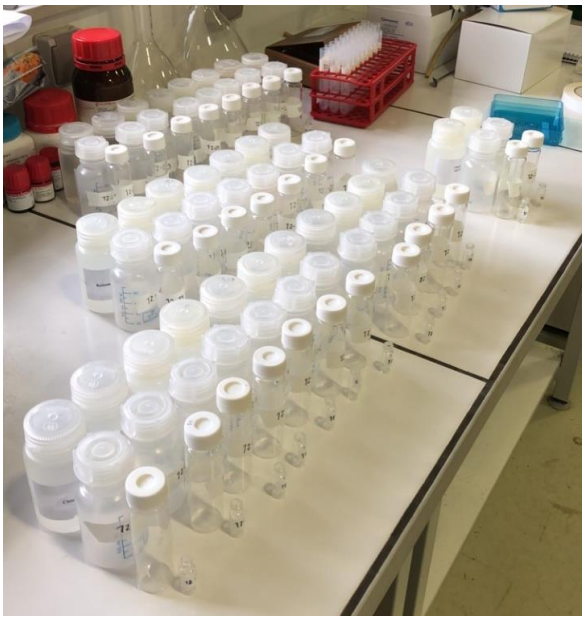

Figure 10: *Samples and necessary containers lined up*

First the samples for ion chromatography were prepared by filtering approximately 2 mL of each sample through a 0.45 µm regenerated cellulose (RC) membrane and into a 2 mL glass vial. Screw tops were used to close all the glass vials. Using the same filter and syringe, the samples for ICP were prepared by filtering 10 mL of the sample into the 12 mL disposable test tube. Parafilm was placed over the top of each test tube. A new filter was used for each sample, and the syringe was rinsed with water from the sample before use. The samples for ion chromatography and ICP were then sent to technicians who would complete the respective analyses.

Next the pH and conductivity of each sample was measured using a Hach HQ40D and its associated pH and conductivity probes which can be seen in Figure 11 below. In between samples, the pH and conductivity probes were dried using a paper towel.

Figure 11: *pH and conductivity meters and probes*

Samples for DOC were then prepared by filtering approximately 30 mL of the sample through a glass microfiber filter using a syringe and into a 50 mL glass vial. The caps were screwed on these vials, and the DOC analysis was performed by Dr. Marie-Noëlle Pons.

The remaining volume of each sample was filtered through the glass microfiber filter using the syringe and into a 100 mL plastic bottle. Caps were screwed onto these bottles and the samples were allowed to come to room temperature. Once at room temperature, samples were poured into a 3.5 mL quartz cuvette and a UV-vis analysis was conducted on them using a Shimadzu UV-2600 UV-Vis Spectrophotometer measuring from 600 to 200 nm. A fluorometric analysis was also conducted on each sample using the same method as was used on the optical brightener solutions discussed previously. However, each sample was only irradiated with UV light for 15 minutes.

Excitation Emission Matrices of Field Samples

Excitation emission matrices are a 3D representation of the sample's fluorescence. The same Hitachi F-2500 Fluorescence Spectrophotometer and PMMA cuvettes were used to create the matrices. Using the FL Solutions 2.0 software, a method was created for a specific excitation wavelength that scanned the emission wavelength starting at 20 nm above the excitation

wavelength and incrementing by one until 600 nm was reached. The excitation wavelengths used incremented by 10 from 250 nm to 600 nm. This data was then compiled using the Scilab software to generate the excitation emission matrices.

Results and Discussion

In an effort to detect the presence of optical brighteners in the Morte Femme peatland, the fluorescent spectra of lab made solutions of seven different optical brighteners were compared to water samples collected at various locations in and around the Morte Femme.

Optical Brighteners- Concentration of Solutions

Solutions of Tinopal DMA-X, Tinopal CBS-X, Fluorescent Brightener 28, DAS, 4,4'-bis(2-benzoxazolyl) stilbene, 4,4'-diamino-2,2'-stilbenedisulfonic acid, and 2,5-bis(5-tert-butyl-benzoxazol-2-yl) thiophene in ultrapure water were created at concentrations of 0.015 $\frac{g}{L}$, 0.30 $\frac{mg}{L}$, and 0.03 $\frac{mg}{L}$. The fluorescent spectra for each of these optical brighteners were compared before and after 15, 30, and 45 minutes of irradiation with UV light. For many of the optical brightener solutions, the spectra generated after 30 and 45 minutes of irradiation showed abnormal trends such as increases in fluorescent intensity or fluorescent intensities below that of the baseline. The increased amount of UV exposure could have caused degradation of the optical brightener molecules which may have been the cause of the abnormal spectra. Thus only the results from the first 15 minutes of irradiation will be discussed. Results from longer irradiation periods can be found in Appendix B. The spectrum of water was included in each figure to serve as a baseline.

The 0.015 $\frac{g}{L}$ solution of Tinopal DMA-X (which will further be referred to as DMA) was too saturated to be read at the fluorimeters highest sensitivity. There is no direct correlation between the highest and lowest sensitivity of the fluorimeter, so the spectrum for this concentration will not be discussed. The 0.30 $\frac{mg}{L}$ solution of DMA was characterized by a single peak spectrum as shown in Figure 12 below.

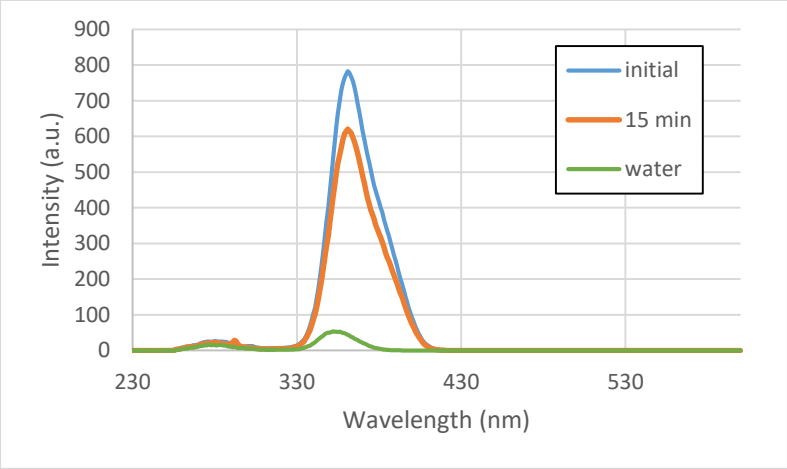

Figure 12: *Fluorescent spectrum for a 0.30 mg/L solution of DMA*

The peak of this spectrum was at 361 nm and had an intensity of 782.7 a.u.. After 15 minutes of irradiation with UV light this peak dropped to an intensity of 620.1 a.u., but remained at 361 nm which was a 20.8% decrease.

By comparison, the peak of the spectrum for a 0.03 $\frac{mg}{L}$ solution of DMA had an intensity of 194.8 a.u. and was located at 355 nm as can be seen in Figure 13 below. This showed that a decrease in concentration of DMA resulted in a decrease in fluorescent intensity which was to be expected as more dilute solutions contain less optical brightener molecules. Note however that the peak intensity was not directly proportional to the concentration; a 90% reduction in concentration resulted in a 76% reduction in intensity.

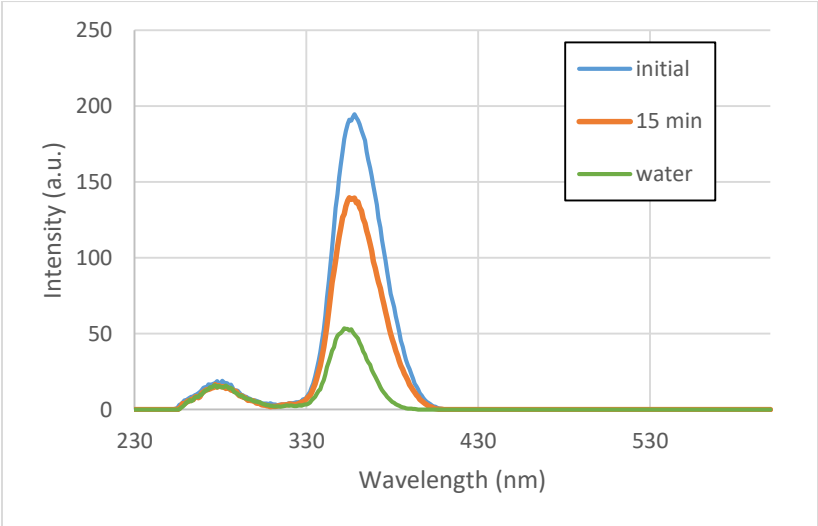

Figure 13: *Fluorescent spectrum for a 0.03 mg/L solution of DMA*

Similar to the higher concentration of DMA, this concentration also had a single peak and experienced a visible decrease in fluorescent intensity after UV irradiation. After 15 minutes of irradiation, the peak's intensity dropped to 139.7 a.u. and was located at 355 nm. This was a 28.3% decrease in intensity.

The 0.015 $\frac{g}{L}$ solution of Tinopal CBS-X (which will further be referred to as CBS) was too saturated to generate a spectrum at the highest sensitivity setting. Since there is no direct correlation between spectra generated using the highest and lowest sensitivity settings, the spectrum for CBS at a concentration of 0.015 $\frac{mg}{L}$ will not be discussed. The spectrum for 0.30 $\frac{mg}{L}$ and 0.03 $\frac{mg}{L}$ solutions of DMA can be seen in Figure 14 below.

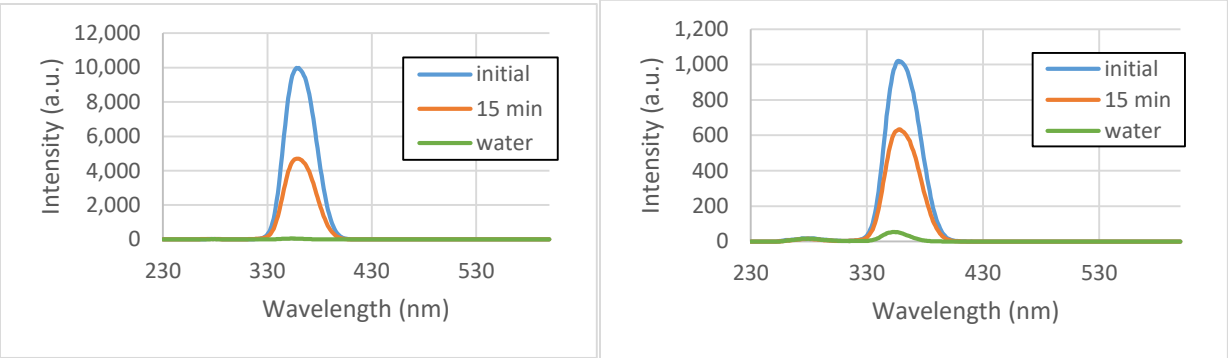

Figure 14: *Fluorescent spectra for a 0.30 mg/L solution of CBS (left) and a 0.03 mg/L solution of CBS (right)*

Both graphs of CBS had a single peak and showed a visible decrease in fluorescent intensity after irradiation with UV light. The maximum intensity on the 0.30 $\frac{mg}{L}$ spectrum was 9,980 a.u. and was located at 358 nm. After irradiation, the peak was located at 360 nm and had an intensity of 4,705 a.u.. The peak of the 0.03 $\frac{mg}{L}$ spectrum was located at 357 nm with an intensity of 1,021 a.u.. After irradiation, the fluorescent intensity dropped to 634.5 a.u. at 358 nm. Similar to DMA, the fluorescence of CBS decreased with decreasing concentration. CBS solutions decreased in fluorescent intensity 52.9% and 37.9% for 0.30 $\frac{mg}{L}$ and 0.03 $\frac{mg}{L}$ respectively. In this case, a 90% reduction in concentration resulted in a 90% reduction in peak intensity and the concentration may have been proportional to intensity. More data would be needed to verify this trend.

For simplicity purposes, 4,4'-diamino-2,2'-stilbenedisulfonic acid was referred to as stilbene acid for the rest of this report. All concentrations of stilbene acid were able to generate spectra at the highest sensitivity setting. The spectra for concentrations of 0.015 $\frac{g}{L}$, 0.30 $\frac{mg}{L}$ and 0.03 $\frac{mg}{L}$ can be found below in Figure 15 parts a, b, and c respectively.

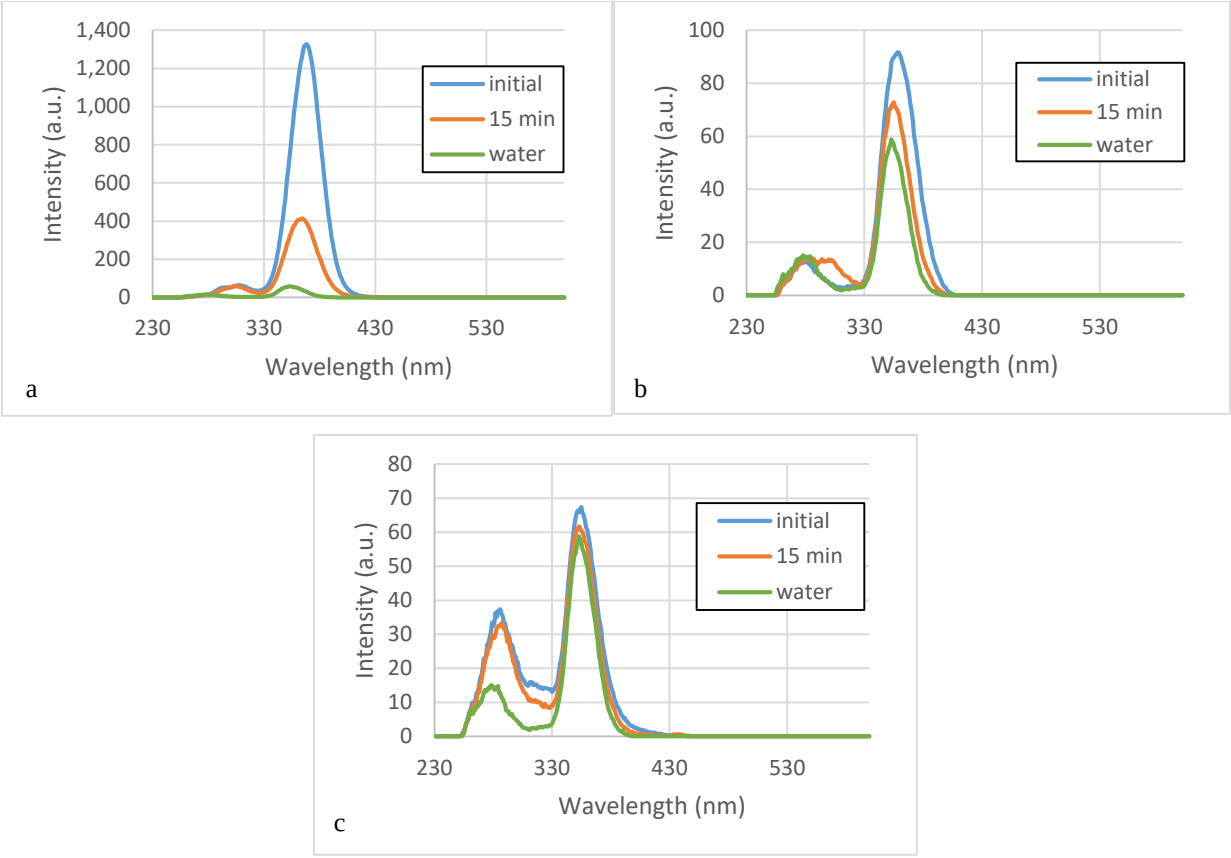

Figure 15: *Fluorescent spectra for 0.015 g/L (a), 0.30 mg/L (b), and 0.03 mg/L (c) solutions of stilbene acid*

The spectra of each concentration had a sharp, tall peak. However, as concentration decreased, a second rounder peak became more apparent. All concentrations showed a visible decrease in intensity after 15 minutes of irradiation with UV light. The most concentrated solution's intensity decreased 68.9% from 1,328 a.u. to 412.9 a.u. peak intensity, and the location of the peak shifted from 368 to 364 nm. The 0.30 $\frac{mg}{L}$ solution decreased from 91.6 a.u. to 72.79 a.u. peak intensity which corresponded to a 20.6% decrease. The peak's location shifted from 359 nm to 355 nm. The peak of the most dilute solution shifted from 355 nm to 353 nm in location and its intensity dropped 8.3% from 67.4 a.u. to 61.6 a.u.. In agreement with the solutions of DMA and CBS, the fluorescent intensity of stilbene acid decreased as the solutions became increasingly

dilute. However, unlike the solutions of DMA and CBS, the relationship between concentration and fluorescent intensity was not linear. It is possible that the presence of additional peaks could be due to a pH dependence of stilbene acid. However, due to time constraints additional trials with solvents of different pHs were not able to be conducted.

The spectra for 4,4'-bis(2-benzoxazolyl) stilbene can be found in Figure 16 below. For the duration of this report, 4,4'-bis(2-benzoxazolyl) stilbene will be referred to as stilbene.

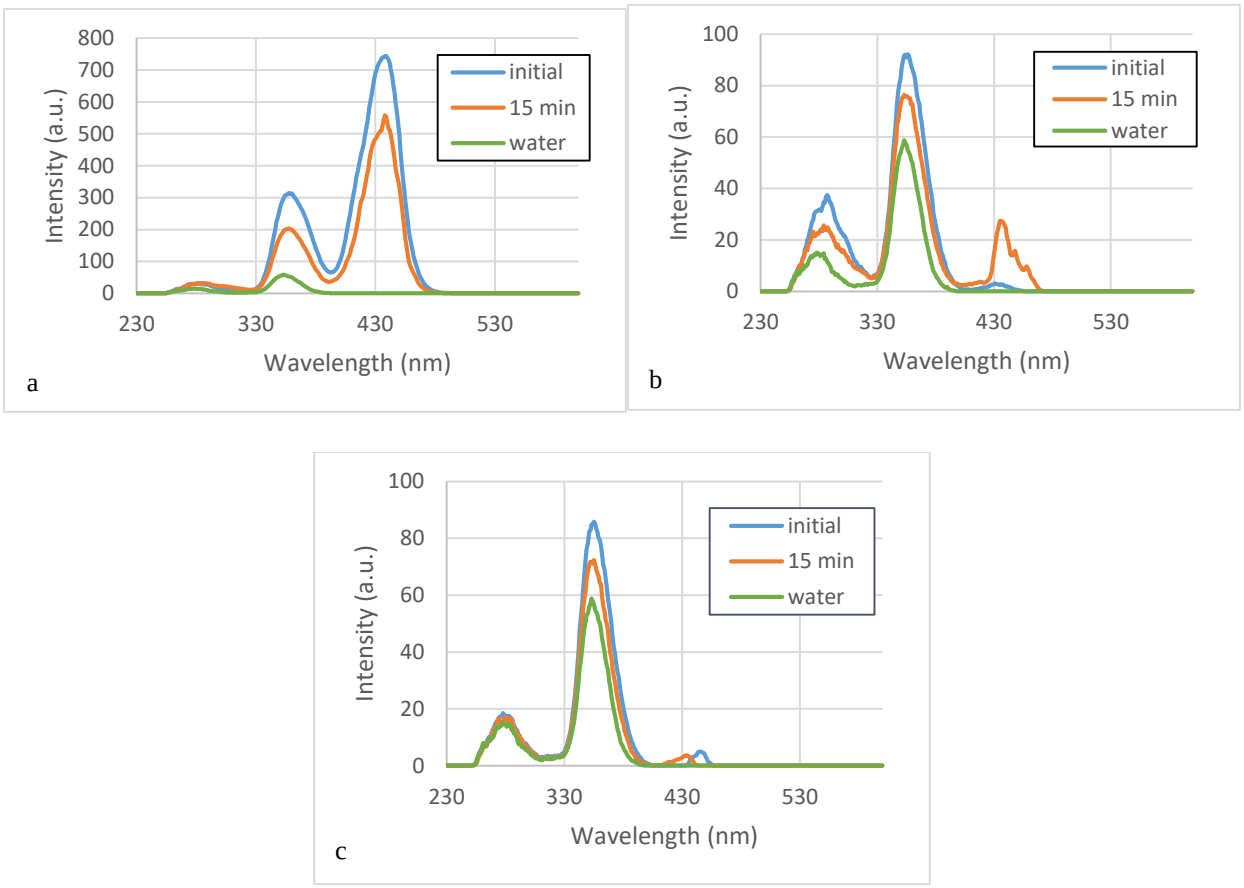

Figure 16: *Fluorescent spectra for 0.015 g/L (a), 0.30 mg/L (b), and 0.03 mg/L (c) solutions of stilbene*

The spectra of stilbene for all concentrations were characterized by a tall sharp peak as well as a secondary small and rounded peak at lower wavelengths. For the 0.30 $\frac{mg}{L}$ and 0.03 $\frac{mg}{L}$ solutions, a very small third peak was present at higher wavelengths. After 15 minutes of UV radiation, all concentrations showed a decrease in fluorescence. For the 0.015 $\frac{g}{L}$ solution, the largest peak occurred at 438 nm, and decreased 25% in intensity from 744.1 a.u. to 577.8 a.u.. The largest peak of the 0.30 $\frac{mg}{L}$ solution shifted from 356 nm to 353 nm and decreased in intensity

17.1% from 92.2 a.u. to 76.4 a.u.. The 0.03 $\frac{mg}{L}$ solution's peak intensity decreased from 85.8 a.u. to 72.3 a.u.. This was a 15.7% decrease. The peak was located at 355 nm both before and after irradiation. As with the optical brighteners previously discussed, the fluorescence intensity decreased with concentration, but similar to stilbene acid the relationship was not linear. Similar to stilbene acid, the presence of additional peaks on the spectra of stilbene may be due to a pH dependence. However, time constraints prohibited additional trials from being conducted with solvents of varying pHs.

The 0.015 $\frac{g}{L}$ solution of Fluorescent Brightener 28 was too saturated to be read at the fluorimeter's highest sensitivity setting and thus will not be discussed in this report. The spectra for 0.30 $\frac{mg}{L}$ and 0.03 $\frac{mg}{L}$ solutions of Fluorescent Brightener 28 were characterized by a single sharp peak as can be seen in Figure 17 below.

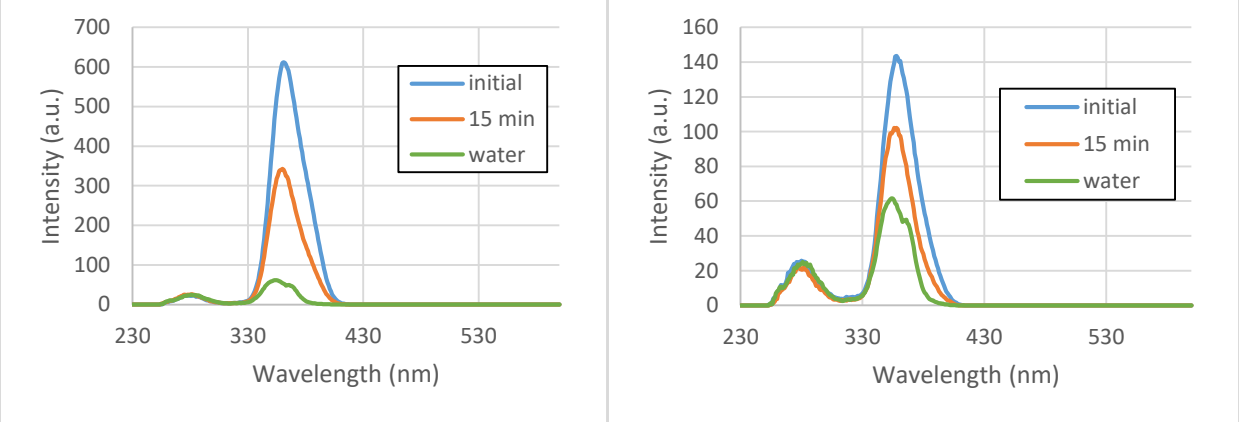

Figure 17: *Fluorescent spectra for 0.30 mg/L (left), and 0.03 mg/L (right) solutions of Fluorescent Brightener 28*

The spectra of both concentrations showed a visible decrease in intensity following irradiation by UV light. The solutions decreased 43.8% and 28.8% for the 0.30 $\frac{mg}{L}$ and 0.03 $\frac{mg}{L}$ solutions respectively. This was due to a drop in maximum intensity from 611.7 a.u. to 342.9 a.u. in the 0.30 $\frac{mg}{L}$ solution and from 143.6 a.u. to 102.2 a.u. in the 0.03 $\frac{mg}{L}$ solution. The peak of the 0.30 $\frac{mg}{L}$ solution shifted from 361 nm to 260 nm while the peak of the 0.03 $\frac{mg}{L}$ shifted from 358 nm to 356 nm. Additionally, it could be seen that as the solution of Fluorescent Brightener 28 became more dilute there was a corresponding drop in fluorescent intensity. However, when the

concentration decreased 90%, the fluorescent intensity only decreased 76.5% meaning that these variables were not directly proportional.

The spectra of DAS contained a tall sharp peak as well as a smaller and broader peak. These features were present regardless of concentration and can be seen in Figure 18 below. Additionally, a decrease in fluorescence after UV irradiation could be seen on all the DAS spectra.

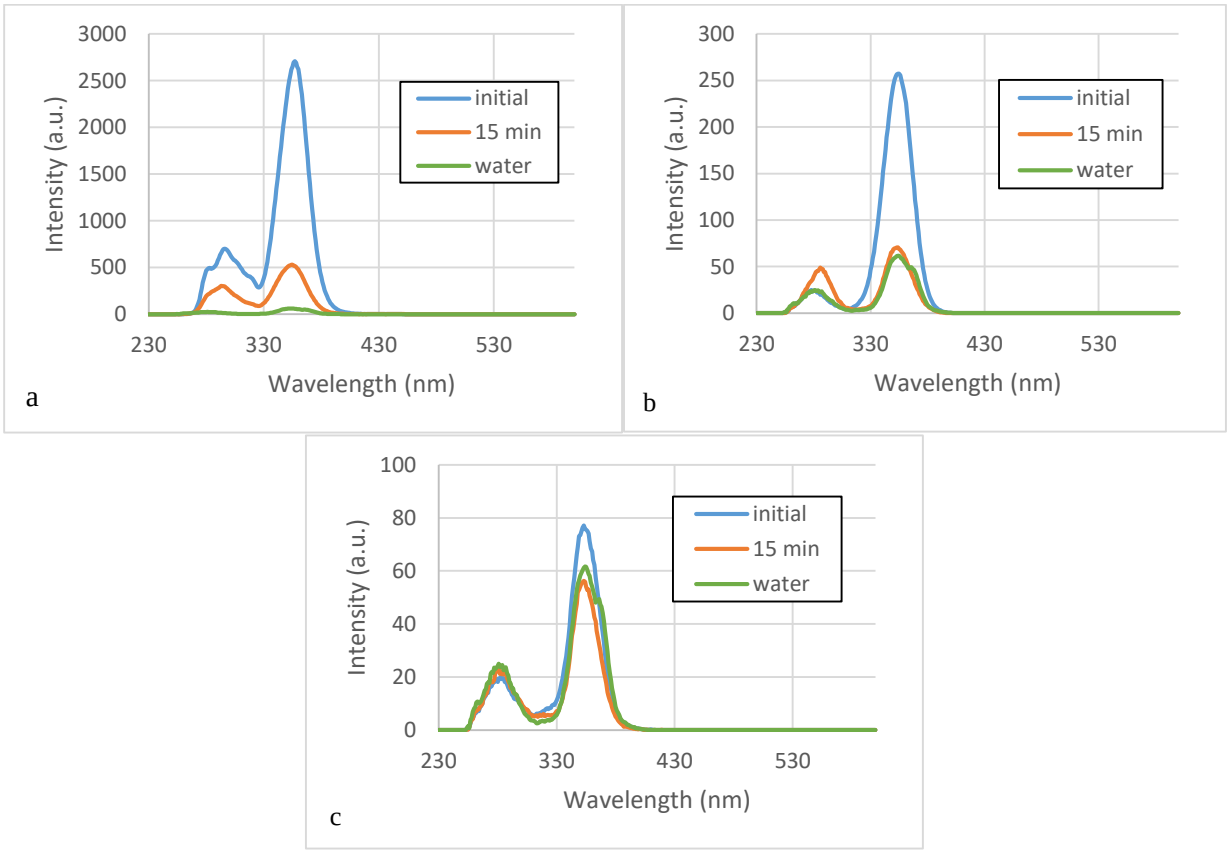

Figure 18: *Fluorescent spectra for 0.015 g/L (a), 0.30 mg/L (b), and 0.03 mg/L (c) solutions of DAS*

The most concentrated solution of DAS had a peak located at 357 nm with an intensity of 2,707 a.u.. After irradiation this peak was located at 354 nm and decreased 80.4% to an intensity of 531.7 a.u.. The 0.30 $\frac{mg}{L}$ solution's peak was located at 534 nm before and after irradiation. Its intensity decreased 72.5% from 257.5 a.u. to 70.79 a.u.. The least concentrated solution decreased 27.1% after irradiation. Its peak remained located at 353 nm after irradiation, but decreased in fluorescent intensity from 77.2 a.u. to 56.2 a.u.. This once again showed that while fluorescent intensity decreases with decreasing concentration, the relationship was not linear.

The final optical brightener studied was 2,5-bis(5-tert-butyl-benzoxazol-2-yl) thiophene which was further referred to as thiophene for simplicity purposes. As can be seen in Figure 19 below, each of the concentrations of thiophene were characterized by spectra of different shapes. The 0.015 $\frac{g}{L}$ solution's spectrum had two tall and sharp peaks that were joined together as well as one short and broad peak located at lower wavelengths. This concentration also increased in fluorescent intensity following irradiation rather than decreasing as was to be expected. By comparison, the 0.30 $\frac{mg}{L}$ solution had only one tall and sharp peak but still had the short and broad peak. This concentration did experience a fluorescent intensity decrease after irradiation, but as can be seen in Figure 19b, its fluorescent intensity was quite similar to that of water. The spectrum of the 0.03 $\frac{mg}{L}$ solution had one very sharp peak located at low wavelengths. Similar to the 0.30 $\frac{mg}{L}$ solution, the 0.03 $\frac{mg}{L}$ solution did experience a decrease in fluorescent intensity after 15 minutes of irradiation with UV light. As it was expected that each concentration of thiophene exhibit similar spectra these results likely indicate an error in preparing the thiophene solutions. It is possible that the thiophene may not have completely dissolved during the preparation of the most concentrated solution and subsequent dilutions. Due to time constraints, additional solutions of thiophene were not able to be prepared and analyzed.

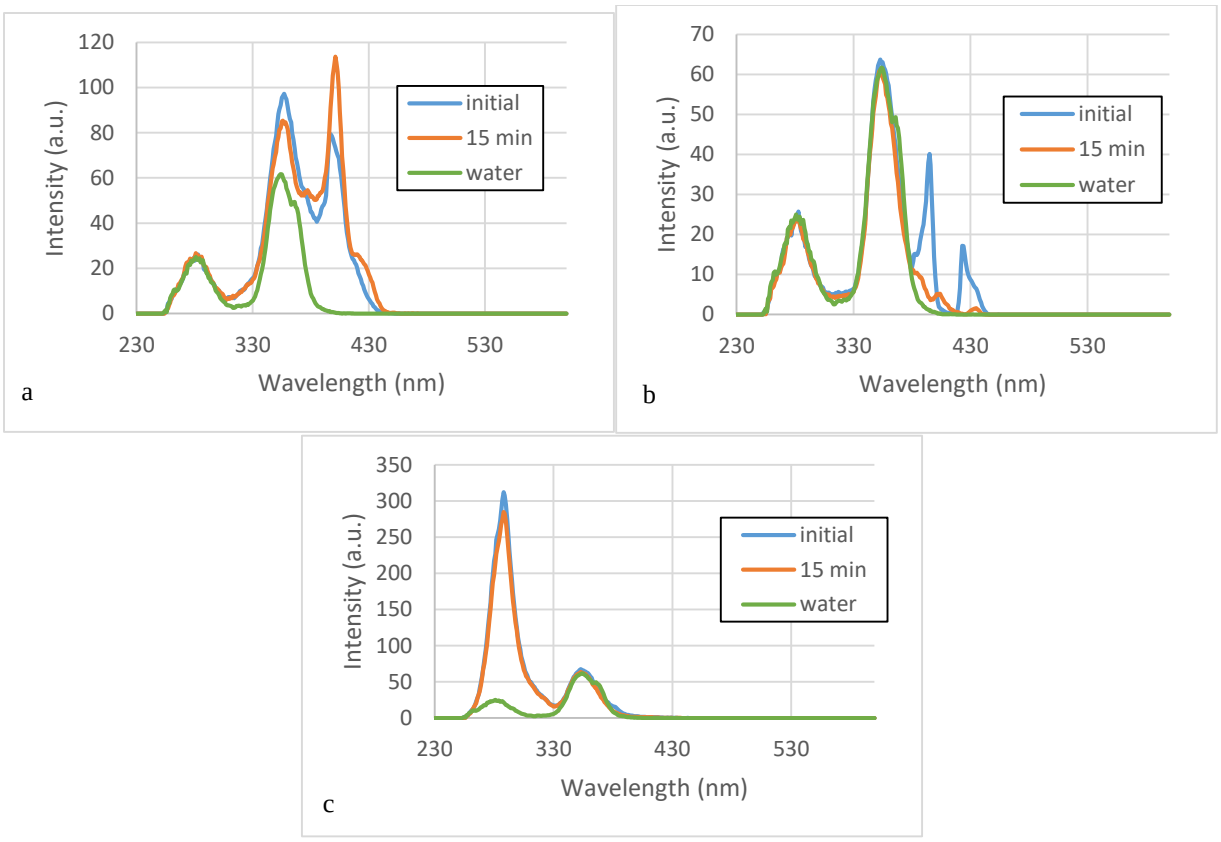

Figure 19: *Fluorescent spectra for 0.015 g/L (a), 0.30 mg/L (b), and 0.03 mg/L (c) solutions of thiophene*

The right most peak of Figure 19a was initially located at 357 nm and had an intensity of 97.25 a.u.. After irradiation this peak was located at 401 nm and had an intensity of 113.7 a.u. which was a 16.9% increase. The reason for this increase is unknown, but will be explained in more detail in the

Field Samples- Fluorescent Trends by **Location** section of this report. The main peak of the 0.30 $\frac{mg}{L}$ solution shifted from 353 nm to 352 nm. It did experience a decrease in fluorescent intensity following irradiation as could be seen from the decrease in intensity from 63.7 a.u. to 60.8 a.u.. This was a 4.6% decrease. The most dilute solution's peak was located at a much lower wavelength of 288 nm. The intensity of this peak decreased 4.6% in intensity after irradiation which corresponded to a decrease in intensity from 312.3 a.u. to 284.9 a.u.. The most dilute solution of thiophene had the strongest fluorescent intensity followed by the most concentrated and then the middle concentration. This trend was not consistent with the trends of the other optical brightener solutions.

Overall, all the optical brighteners except thiophene exhibited a decrease in intensity after irradiation with UV light. This was to be expected as optical brighteners readily photodegrade. Additionally, as the solutions of optical brighteners became more dilute their fluorescent intensity decreased. Some optical brightener solutions showed linear relationships between concentration and fluorescent intensity while others did not, so more data across a wider range of concentrations would be needed to confirm a relationship. For some of the optical brighteners, solutions of higher concentrations were too saturated to be read by the highest sensitivity setting on the fluorimeter. At lower concentrations the fluorescent intensity was quite low and may not have been accurately read by the fluorimeter. Thus it was determined that a middle concentration of 0.30 $\frac{mg}{L}$ was the optimum concentration. This concentration was used for all further testing with optical brighteners.

Optical Brighteners- Synchronous Wavelength Difference

For the optical brightener experiments previously discussed, synchronous fluorescence scans were conducted with excitation wavelengths ranging from 230-600 nm and a fixed difference of 50 nm between emission and excitation wavelengths. In order to ensure that a difference of 50 nm between emission and excitation wavelengths was optimal, tests were also conducted using wavelength differences of 20 nm and 80 nm. Due to time constrains, these tests were only performed on three optical brighteners, DMA, stilbene, and thiophene. These optical brighteners were selected as they range in molecular structure and functional groups.

Figure 20 below shows the spectrum that resulted when DMA was scanned with differences of 20, 50 and 80 nm between excitation and emission wavelengths. For each wavelength difference there was a single broad peak, but as the wavelength difference increased so did the maximum intensity. Additionally, the location of this maximum intensity shifted to greater wavelengths as the wavelength difference increased.

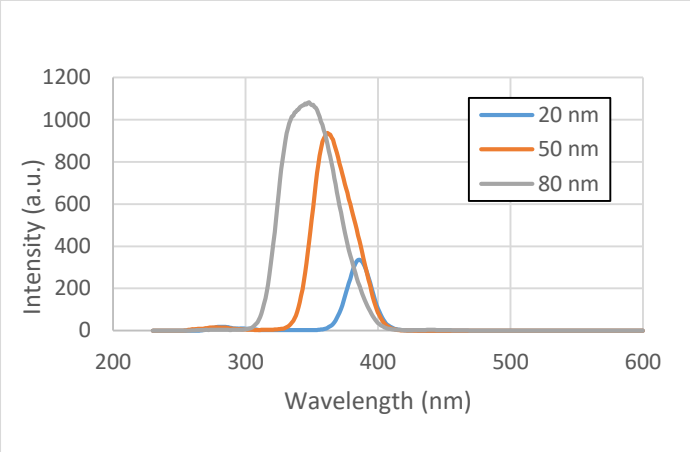

Figure 20: *Fluorescent spectrum of DMA using varying differences between excitation and emission wavelengths*

In contrast, the spectrum for stilbene showed variation in shape with wavelength difference as seen in Figure 21. With a 20 nm wavelength difference, a single short and pointed peak could be seen at low wavelengths. When scanned with a 50 nm wavelength difference this peak was joined by a tall sharp peak located at 353 nm. However, with an 80 nm wavelength difference, the only feature present was a short and broad peak.

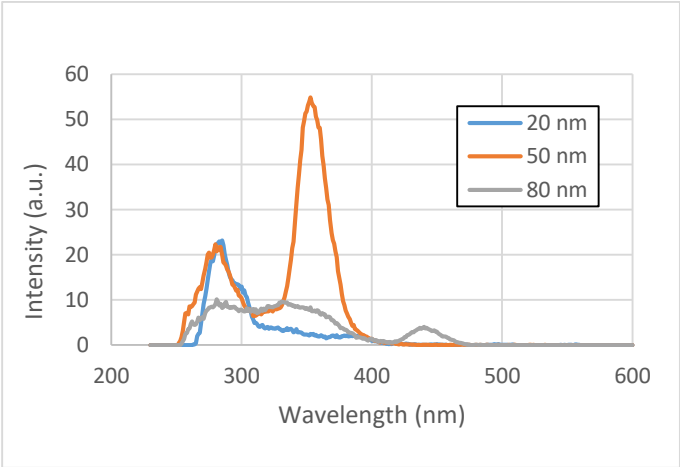

Figure 21: *Fluorescent spectrum of stilbene using varying differences between excitation and emission wavelengths*

The spectrum for thiophene showed similar trends as stilbene in that it exhibited variation in shape with wavelength difference. Figure 22 showed the spectrum for thiophene. At a 20 nm wavelength difference, two short peaks were connected by a small broad peak. When the wavelength difference was 50 nm, a tall and sharp peak as well as a short and broad peak were present. An 80 nm wavelength difference resulted in a single broad peak similar to that of stilbene at the same wavelength difference.

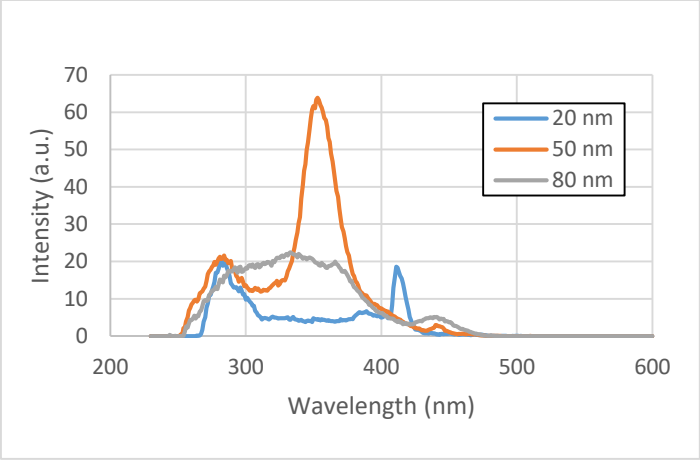

Figure 22: *Fluorescent spectrum of thiophene using varying differences between excitation and emission wavelengths*

These tests confirmed that a 50 nm difference between excitation and emission wavelengths was optimal. The spectrum of DMA showed little difference in definition of features at varying wavelengths. However, on the spectra of stilbene and thiophene, features were most clearly defined when there was a difference of 50 nm between excitation and emission wavelengths. Thus synchronous fluorescent tests were conducted with this wavelength difference for the duration of the report.

Field Samples-Overall Data

Nine series of field samples were collected as previously described in the methodology section. These field samples were a continuation of data that had been collected since 2018 as part of a study by researchers at the University of Lorraine on pollution in the Cleurie River, its tributaries and the Morte Femme peatland. The series collected for this report were labeled 11-19 as they corresponded to the 11^{th}- 19^{th} series' of data collected as part of the University of Lorraine study. Series 11 was collected on January 2, series 12 was collected on January 27, series 13 and 14 were collected on January 29, series 15-18 were collected on January 30, and series 19 was collected on February 11. Series 11, and 13-19 sampled the Morte Femme peatland and its tributaries while series 12 sampled these sites as well as the Cleurie river and its tributaries. Due to weather conditions, some locations were not able to be sampled for all series'. Appendix A shows which locations were sampled as part of each series. Appendix C contains a labeled map of each of the sampling locations along the peatland and its tributaries while Appendix D shows pictures of the locations where samples were collected.

For each sample collected, basic water quality tests such as pH, conductivity, TOC, ion chromatography and ICP were conducted as well as UV and fluorescence spectroscopy. The raw data can be found in Appendix E. Due to similar properties, the University of Lorraine researchers believe locations 2a and 2b to feed location 6h. They also believe the Noir Rupt and Corsaire to feed location step 3 aval. Location 6g feeds 6e which in turn feeds 6f. Locations 6f, 6h, and step 3 aval combine and feed into the peatland. Location 6 is located at the exit of the peatland. Not enough data has been collected to make definite conclusions on how location 6d feeds into the water system, but the University of Lorraine researchers have plans to study this location in more detail in the future.

Field Samples- Fluorescent Trends by Location

In order to determine common trends for each sampling location, the fluorescent spectra of all samples taken at a specific location were compared side by side using a grid setup. The numbers at the bottom left of each spectrum correspond to the series number. Please note that the vertical axis on all the spectra were not the same orders of magnitude as the fluorescent intensity varied greatly between samples.

The spectra generated from samples collected at the Noir Rupt sampling location can be seen in Figure 23 below. Deteriorating road conditions due to snow and hail prohibited samples of the Noir Rupt from being collected as part of series 14 and 19. For this particular site, all the spectra had a similar single broad peak with a smaller bump at low wavelengths. Additionally, the spectra all showed a visible decrease in fluorescent intensity after irradiation with UV light, and had maximum intensities that were of a similar order of magnitude. Following irradiation with UV light, these samples experienced between a 0.54% and 12% decrease. The water at the Noir Rupt sampling location comes directly down the mountain with little human interaction. As a result, it is expected that the broad peak centered around 350 nm corresponded to the presence of dissolved organic matter such as humic acid while the smaller bump around 280 nm corresponded to protein like substances.

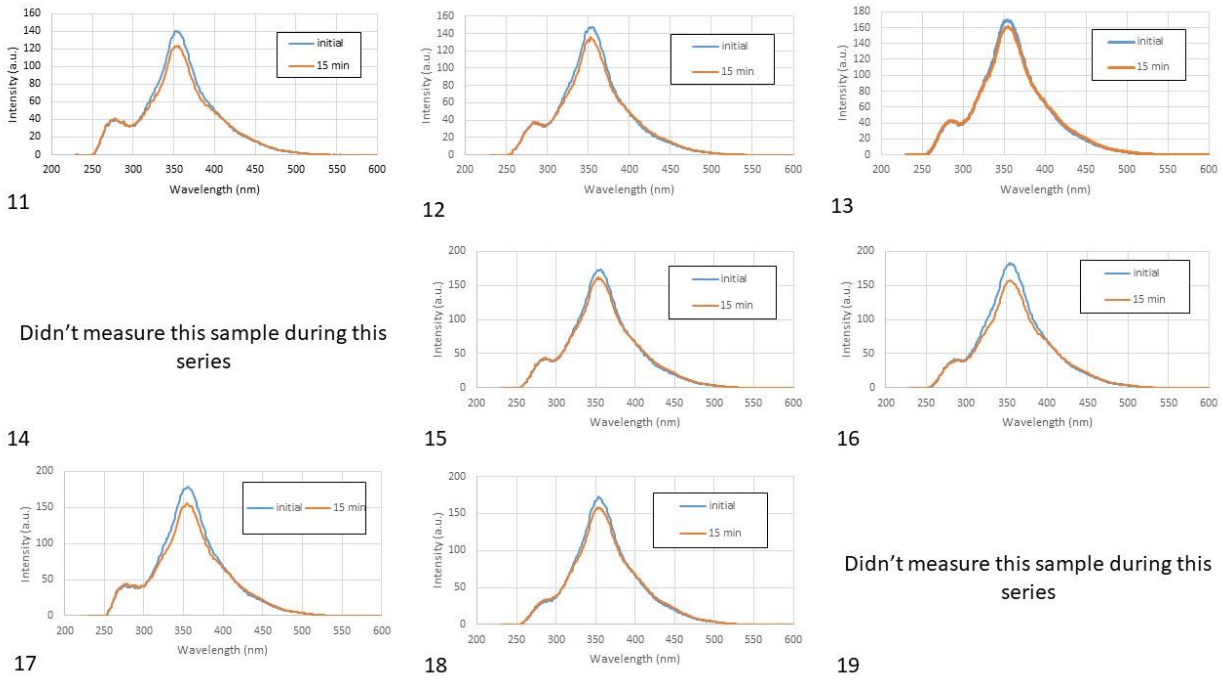

Figure 23: *Fluorescent spectra of the Noir Rupt for all sampling series*

The spectra generated from samples collected at the Corsaire sampling location can be seen in Figure 24 below. Deteriorating road conditions due to snow and hail prohibited samples of Corsaire from being collected as part of series 14 and 19. All of the spectra had a similar shape of two connected peaks with a smaller peak at lower wavelengths and a much taller peak at middle wavelengths. Additionally, the spectra exhibited a visible decrease in intensity and had maximum intensities of similar orders of magnitude. Irradiation caused the samples to experience between a 10% and 14.4% decrease. The broad peak likely indicated the presence of dissolved organic matter in the field samples. However, there are a few houses upstream of the Corsaire sampling location, so the smaller peak on the spectra may be due to protein like substances from untreated domestic wastewater.

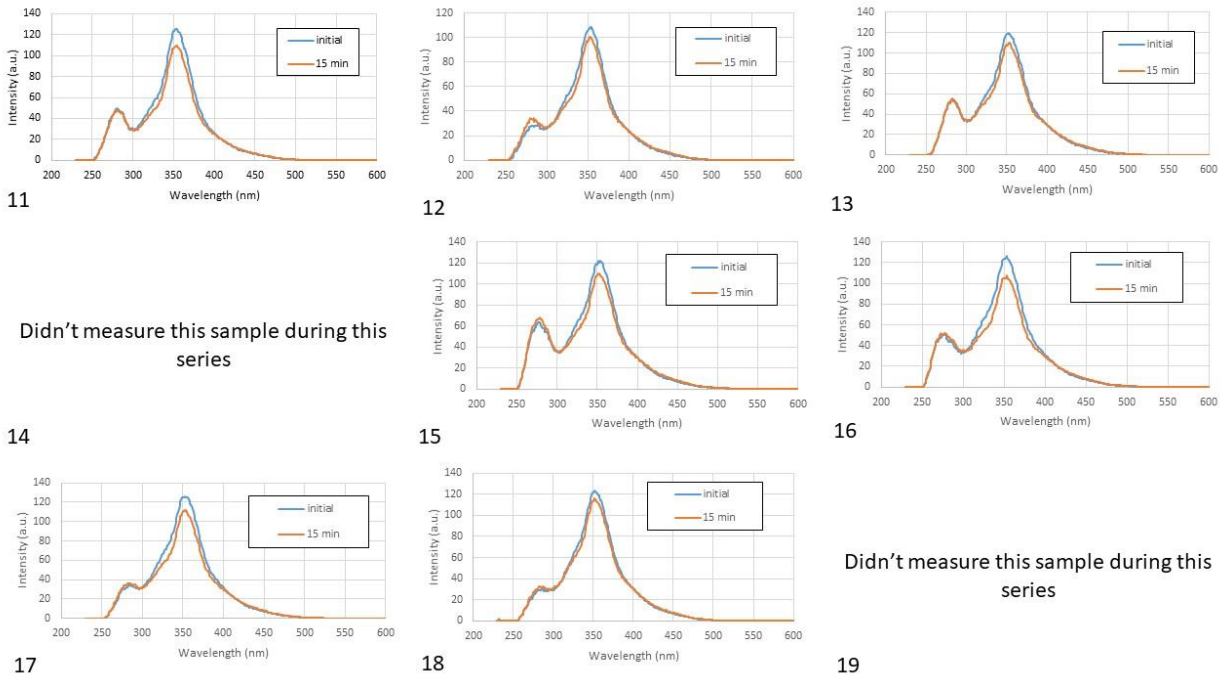

Figure 24: *Fluorescent spectra of the Corsaire for all sampling series*

Due to time constraints, samples of location 2a were unable to be collected as part of series 11 and 12. However, the fluorescent spectra for all other series can be seen in Figure 25 below. All of the spectra were characterized by a smaller peak connected to a taller, sharper peak. Additionally, all the spectra exhibited a decrease in the intensity of the second peak after irradiation with UV light. This decrease ranged from 7% to 19% depending on which series was being considered. Similar to the Noir Rupt and Corsaire, the maximum intensities of all the spectra were of similar orders of magnitude. Location 2a was just downstream from the beginning of the Cleurie, so the fluorescence of the broad peak centered around 350 nm was likely due to dissolved organic matter.

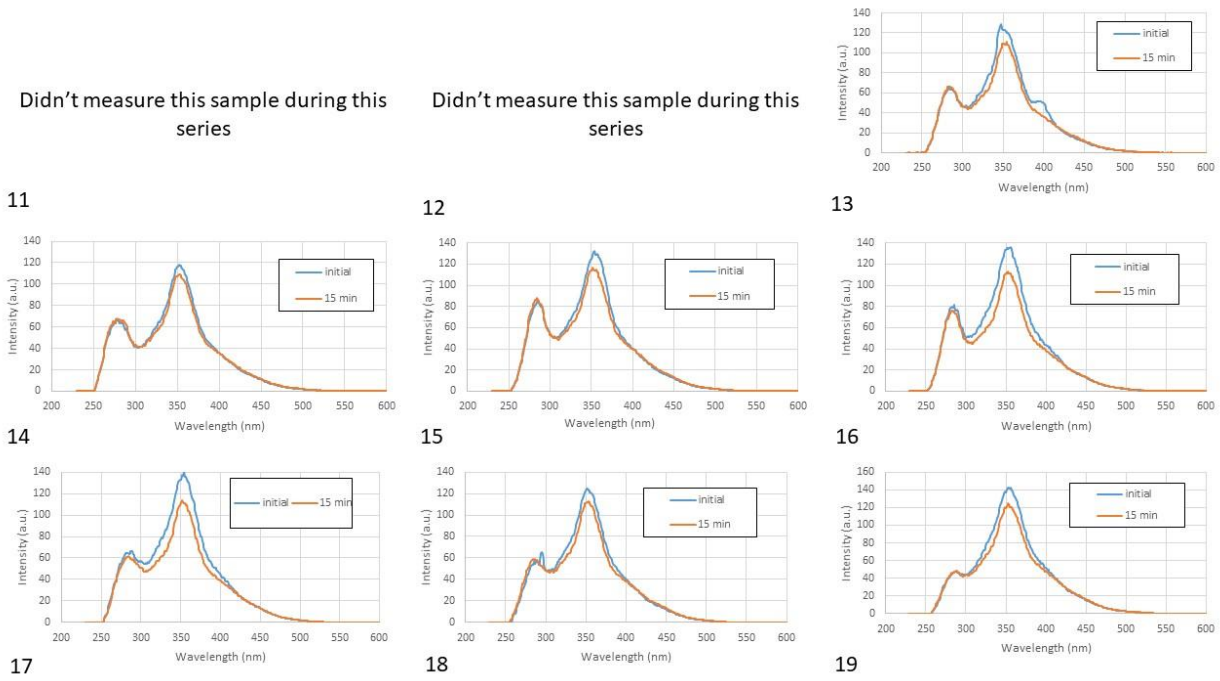

Figure 25: *Fluorescent spectra of sampling location 2a for all sampling series*

Similar to location 2a, time constraints prohibited samples at location 2b from being collected as part of series 11 and 12. The spectra of this location had a similar shape to that of location 2a with a shorter peak connected to a taller, sharper peak. As can be seen in Figure 26 below, the maximum fluorescent intensities of all the spectra were of similar orders of magnitude. With the exception of series 13, all the spectra decreased in fluorescent intensity following irradiation with UV light. The percentage decrease ranged from 0.54% to 12% with series 15 experiencing the least decrease and series 17 experiencing the greatest. Series 13 did not follow these trends, and increased in fluorescent intensity by 6.5% after irradiation. As this series was an outlier the increase in fluorescent intensity was likely due to an error in generation of the spectrum, but due to time constraints additional spectrum of this series were unable to be generated. As with location 2a, location 2b was located just downstream of the start of the Cleurie, so dissolved organic matter was likely the cause of the fluorescence and intensity decrease seen in Figure 26.

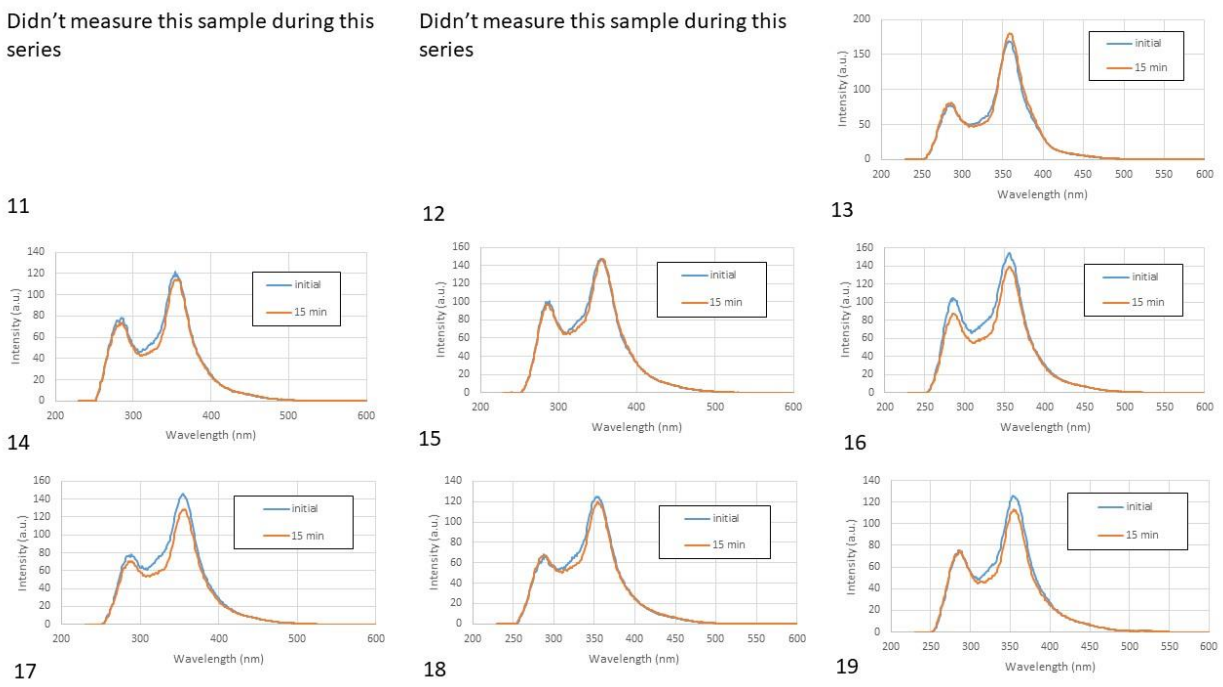

Figure 26: *Fluorescent spectra of location 2b for all sampling series*

The spectra generated from samples collected at sampling location 6g can be seen in Figure 27 below. Regardless of which series they were collected as part of, the spectra all had a smaller, less defined peak connected to a sharper and higher peak. All of the maximum intensities for these spectra were of similar orders of magnitude. The sharper and higher peak exhibited between a 10% and 14.4% decrease after being exposed to UV light for 15 minutes. Location 6g was located near an industrial sector, and there are some houses upstream of this location, so it was possible that the fluorescence and fluorescent intensity decrease seen at this location was due to the presence of optical brighteners or other chemicals used by the various industries.

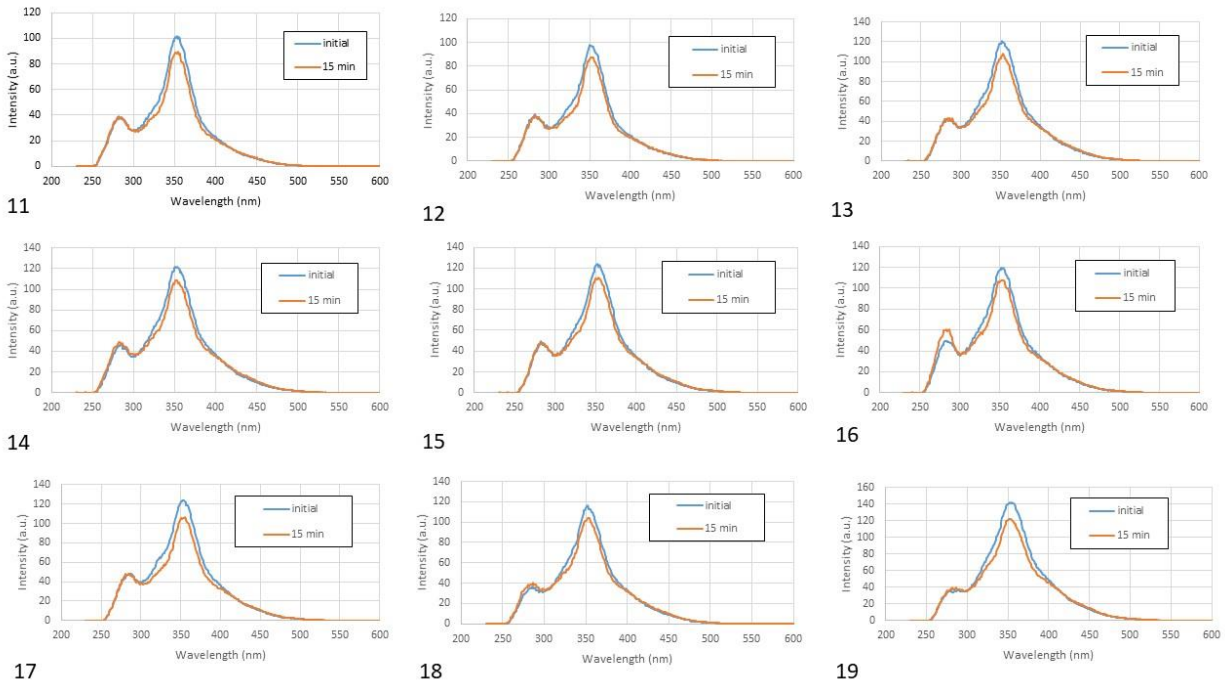

Figure 27: *Fluorescent spectra of location 6g for all sampling series*

The spectra for sampling location 6e can be found in Figure 28 below. With the exception of series 11 and 19, all the spectra were characterized by two tall and sharp peaks. Additionally, series 12-18 increased in fluorescent intensity following irradiation rather than decreasing as expected. This was consistent with previous data collected by the University of Lorraine researchers, and the reason for this trend is still being explored. The maximum fluorescent intensity of each spectrum varied widely among the different series, which was likely due to fluctuating concentrations of the streams. Following periods of rain, the concentration of molecules in the stream would be more dilute and following periods of dry weather these molecules would be present in the stream at higher concentrations. The spectra for series 11 and 19 more closely matched that of the Noir Rupt or Corsaire which likely meant that there was an increased amount of dissolved organic matter present in the samples collected as part of those series'. This makes sense as there was rain in the days before these samples were collected which would have caused runoff of organic matter into the streams.

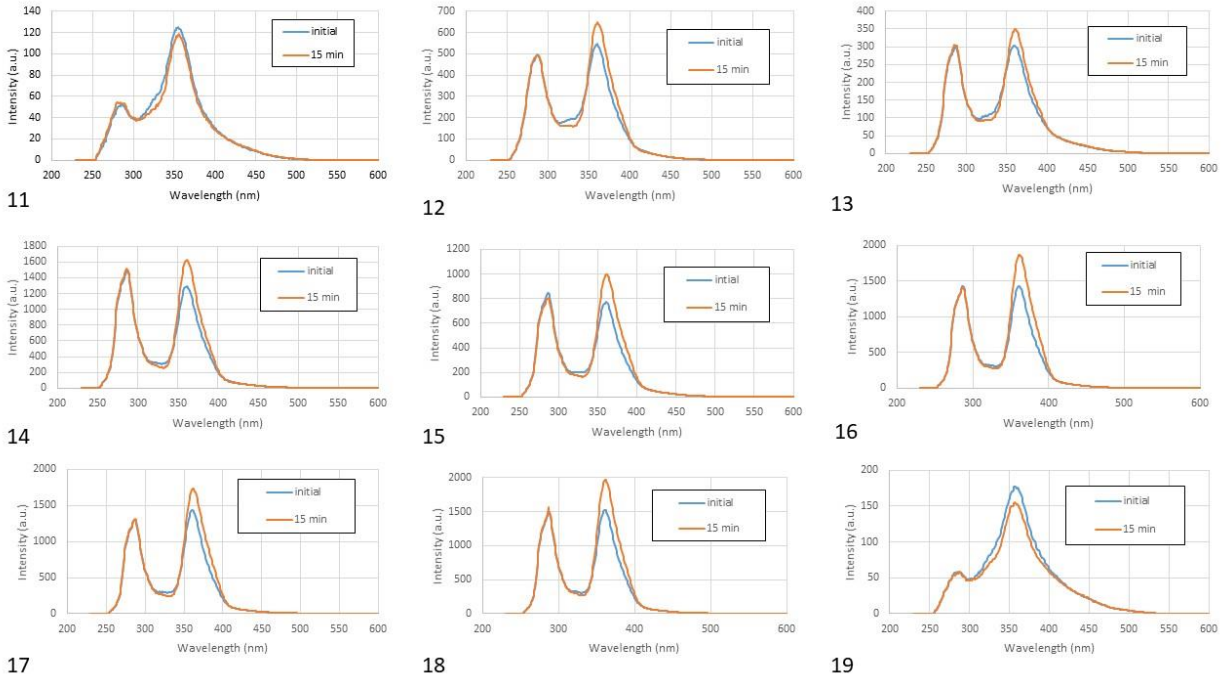

Figure 28: *Fluorescent spectra of location 6e for all sampling series*

Sampling locations 6e and 6d combine and become location 6f, so it makes sense that the spectra of location 6f in Figure 29 below would be similar to that of 6e. Once again series 11 and 19 do not follow the trends exhibited by the other series but more closely matched the spectra of the Noir Rupt and Corsaire. This was likely due to an increased amount of dissolved organic matter in the stream following a period of rain. However, series 12-18 all had similar shaped spectra characterized by two tall and sharp peaks. Similar to location 6e, the fluorescent intensity of series 12-18 increased after irradiation rather than decreased as expected. However, this was consistent with past data collected at this location by the University of Lorraine researchers. The reason for this trend is still being explored. The maximum intensities varied by series which was likely due to varying concentrations of molecules in the stream.

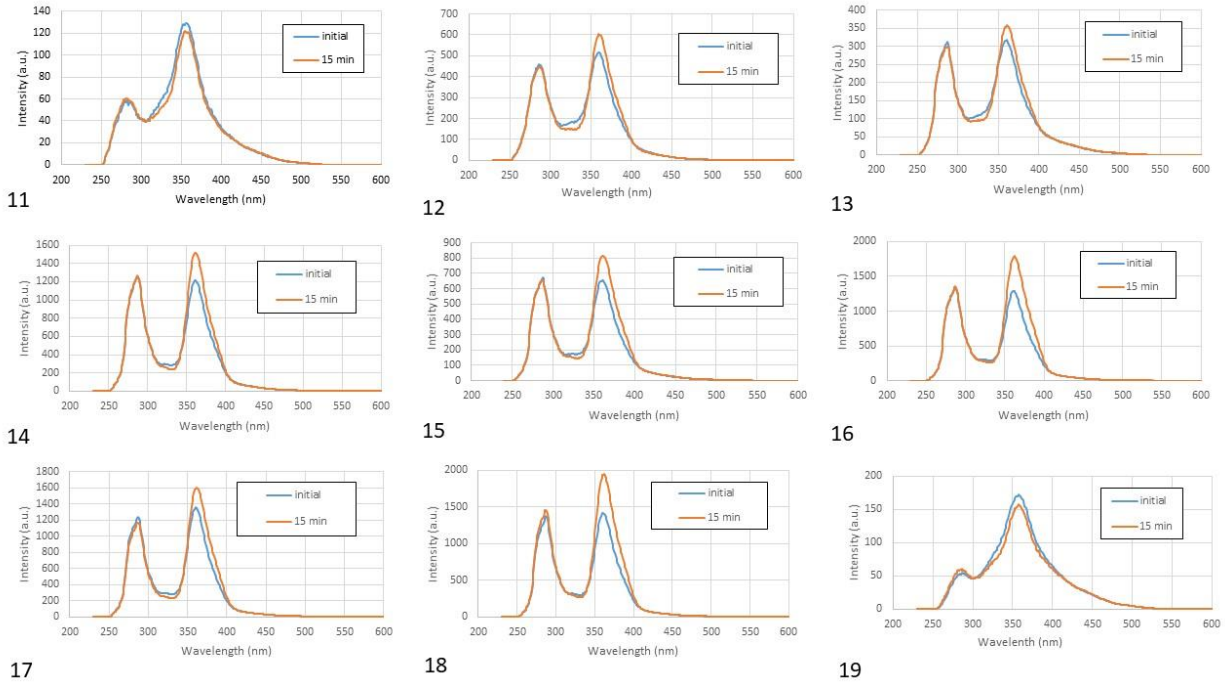

Figure 29: *Fluorescent spectra of location 6f for all sampling series*

The fluorescent spectra generated from samples collected at location 6h can be found in Figure 30 below. All of the spectra except series 19 had a similar shape with a tall, rounded peak at lower wavelengths connected to a second shorter and broader peak at middle wavelengths. Series 19 more closely corresponded to the trends seen at the Noir Rupt and Corsaire sampling locations. Periods of high rain occurred before series 19 was collected, so the trends on this spectrum were likely due to the presence of increased dissolved organic matter. After irradiation with UV light for 15 minutes, all the spectra showed a decrease in fluorescent intensity between 0.36% and 14.1% except series 11 which increased in intensity by 41%. Series 11 not following the trends of the other series was likely due to error in generating the spectrum from this sample. However, due to time constraints additional trials with this sample were unable to be conducted. The variation in fluorescent intensity among different series was likely due to fluctuating concentrations of molecules in the stream. It was believed that locations 2a and 2b fed into location 6h, so it made sense that location 6h showed similar percentages of fluorescent intensity decrease following irradiation as locations 2a and 2b did. However, the fluorescent intensity at location 6h was higher than that at locations 2a and 2b. Between locations 2a, 2b and 6h, the stream flows through an industrial area. It was likely that the larger fluorescence at 6h was due to a chemical

that entered the stream while it was in the industrial area, potentially an optical brightener or a mix of optical brighteners.

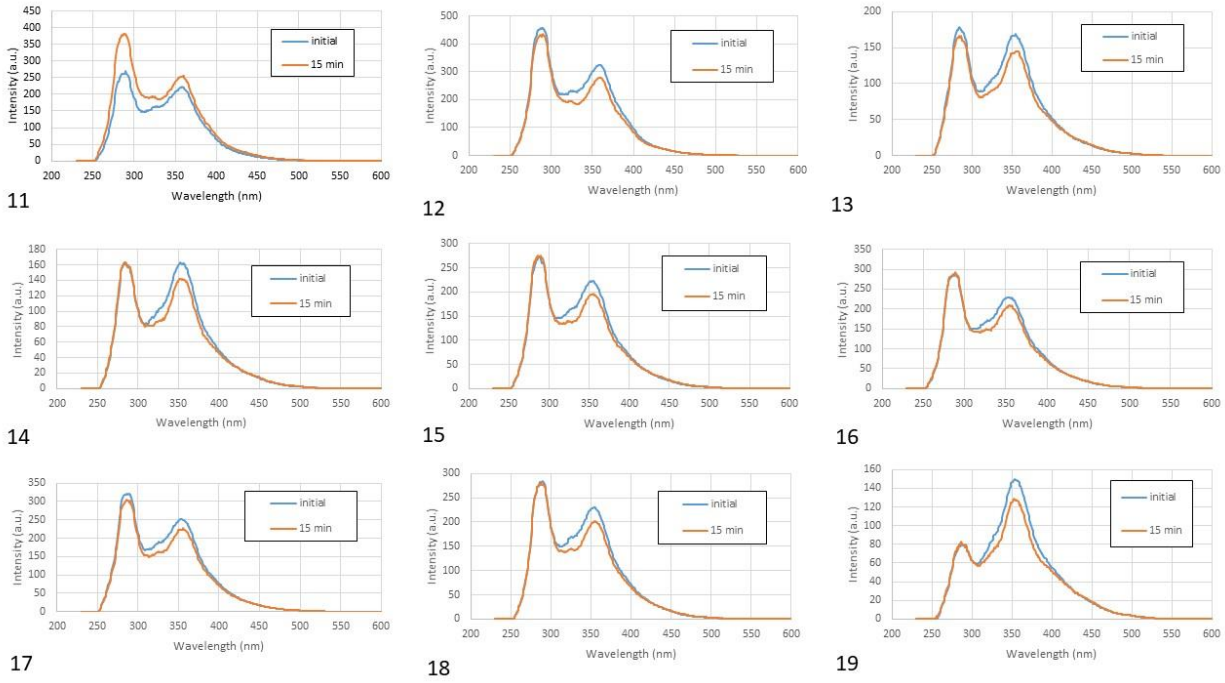

Figure 30: *Fluorescent spectra of location 6h for all sampling series*

The fluorescent spectra at location step 3 aval as seen in Figure 31 were all characterized by a much sharper and narrower peak than those of previous sampling locations. While the maximum fluorescent intensities of the spectra varied in order of magnitude, they all increased in intensity after irradiation with UV light. The variation in order of magnitude was likely due to fluctuations in the concentration of molecules in the stream. However, the reason for the increase in fluorescence following irradiation is still being explored. Step 3 aval was downstream of the Noir Rupt and Corsaire, but also downstream of one of the textile plant's wastewater treatment facilities. It was for this reason that during the collection of series 11 the water at this location was artificially blue as can be seen in Figure 4. The increased fluorescent at step 3 aval when compared to the Noir Rupt and Corsaire could be due to a chemical used in the textile process such as optical brighteners.

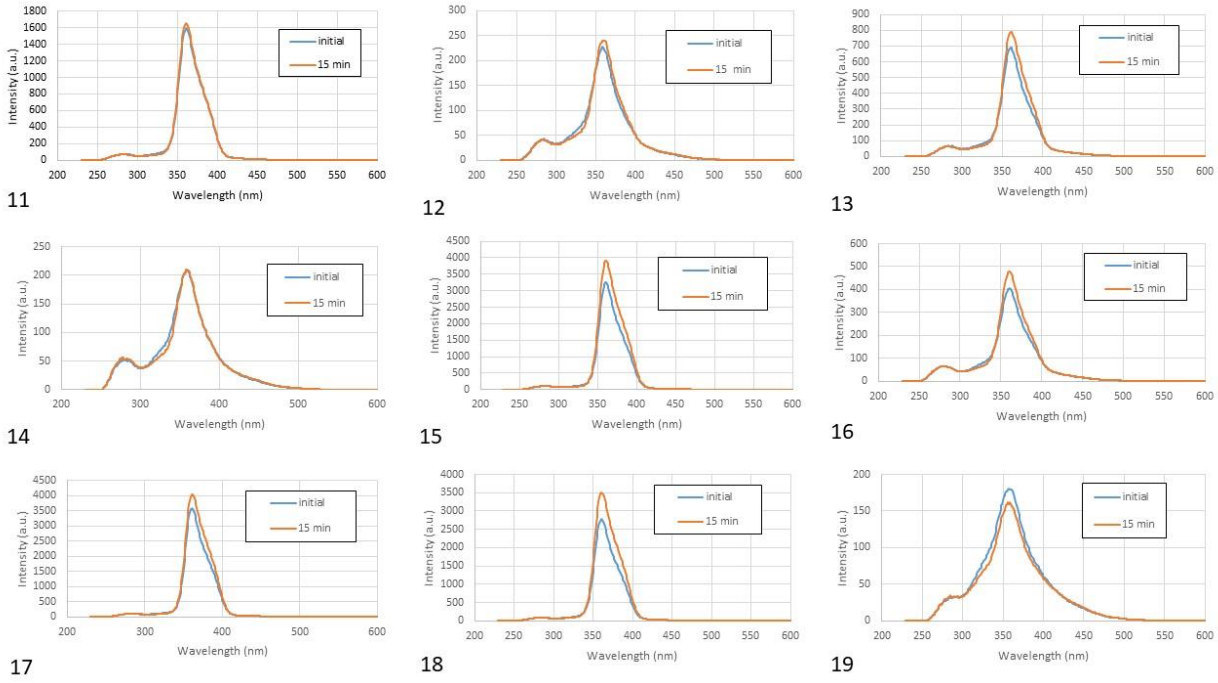

Figure 31: *Fluorescent spectra of step 3 aval location for all sampling series*

Figure 32 shows the spectra generated from samples collected at sampling location 6. Each of these spectra had a short, rounded peak at low wavelengths that was connected to a sharp, and tall peak. There was some variation in the height of the second peak which was due to fluctuating molecular concentrations of the stream water. Following 15 minutes of exposure to UV radiation, all series except series 19 increased in fluorescent intensity. This was consistent with previous data collected by University of Lorraine researchers, but the reason for this trend is still being explored. Locations 6g, 6f, 6h, and step 3 aval feed into location 6 after flowing through the Morte Femme peatland. As locations 6f, and step 3 aval increased in fluorescence following irradiation it could be expected that the unknown molecule causing this phenomenon would also be present downstream at location 6.

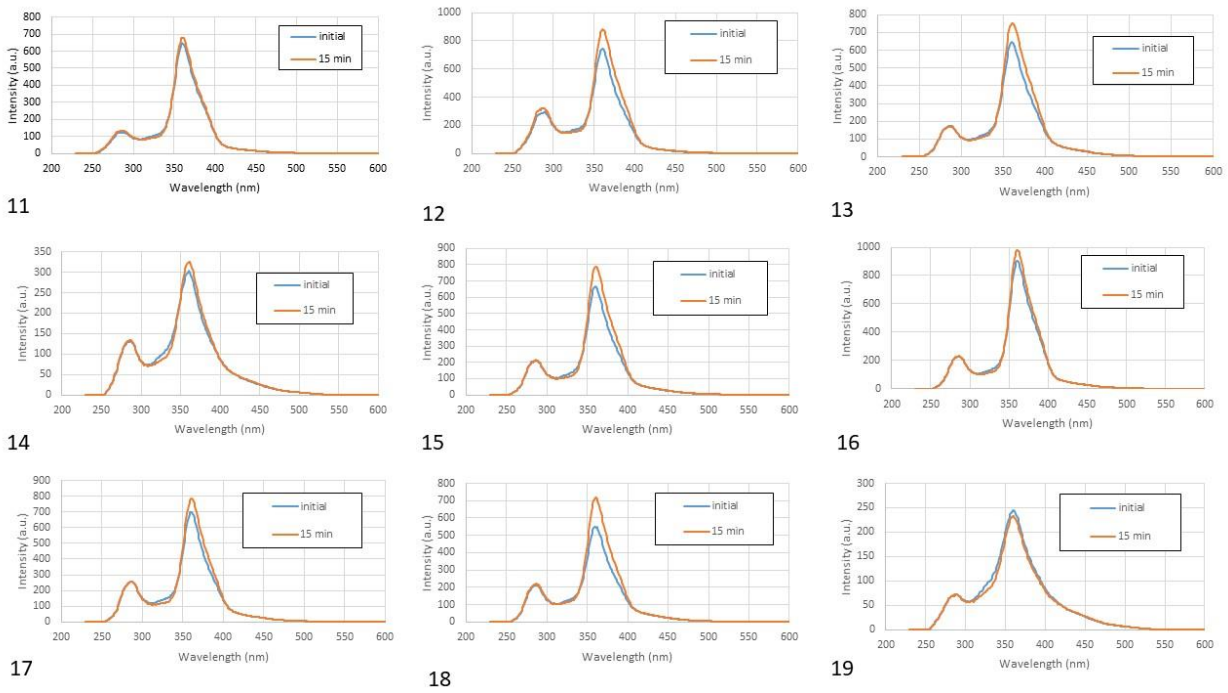

Figure 32: *Fluorescent spectra of location 6 for all sampling series*

Sampling location T was located in the old bed of the Cleurie river. This was where the excess water from the peatland collected after percolating through the peat. If there was enough water, location T flowed into location 6f. The fluorescent spectra for this location all had very similar shapes and fluorescent intensities of similar orders of magnitude as seen in Figure 33 below. The spectra contained a single broad peak that spanned most of the wavelengths measured. Samples collected at location T showed between an 1.5% and 11.8% intensity decrease after irradiation. This decrease was likely due to dissolved organic matter at this location as opposed to human induced chemicals as the water percolates through the peatland, which is rich in organic matter, before arriving at this sampling location.

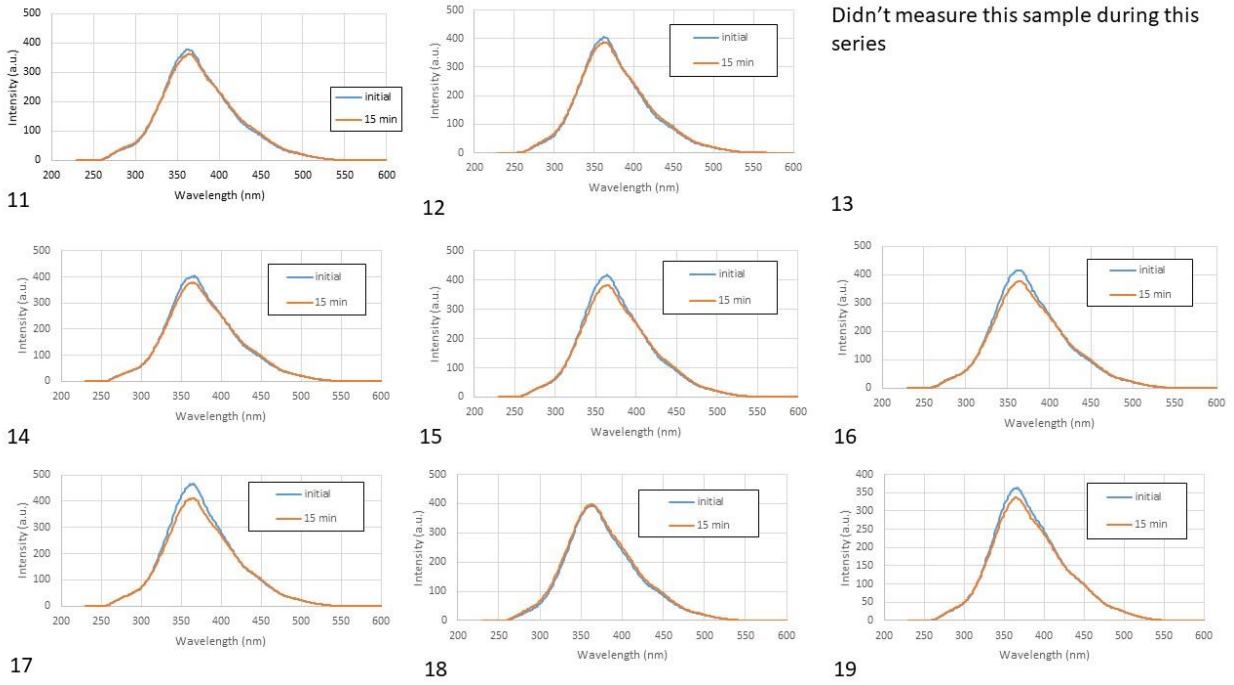

Figure 33: *Fluorescent spectra of location T for all sampling series*

The final sampling location 6d is combined with location 6e to feed into location 6f. The spectra generated at this location can be seen in Figure 34 below. All the spectra were characterized by a broad but tall peak with a much smaller and less defined peak at lower wavelengths. With the exception of series 12, the spectra all showed a decrease in fluorescent intensity after UV irradiation. The maximum intensities of these spectra were at similar orders of magnitude and decreased by between 1.9% and 6.6% after UV exposure. Rather than decreasing in intensity after irradiation, series 12 increased slightly in intensity. Since this was not consistent with the trends of the other series at this location it was likely due to an error in generation of the spectrum. However, due to time constraints additional spectra were not able to be generated for this sample. As seen in Appendix E, location 6d also had unusually high levels of iron and chloride ions. Ferric chloride is commonly used in treatment of textile plant wastewater, so the presence of this chemical suggests that this location was downstream from one of the textile plant's wastewater treatment facilities. Therefore, it was possible that the fluorescent intensity decrease seen at location 6d was due to optical brighteners.

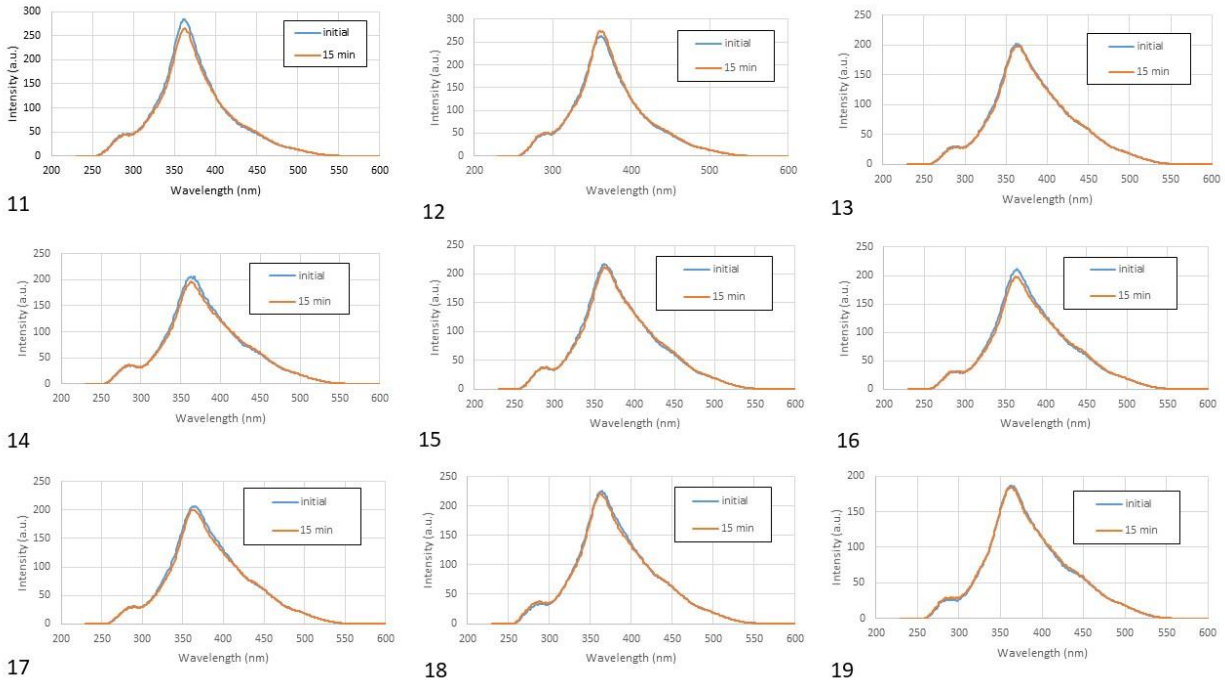

Figure 34: *Fluorescent spectra of location 6d for all sampling series*

Field Samples- Total Fluorescent over Time

In an effort to determine why samples collected at locations 6e, 6f, step 3 aval, and 6 increased in fluorescence after irradiation rather than decreased as was expected, the total fluorescence over time at each location was analyzed. Total fluorescence is a sum of all the fluorescence emitted at each wavelength during the synchronous wavelength scan. Series 15-18 were all collected on January 30 at varying times of day. Series 15 was collected in the late morning while series 16-18 were collected in the afternoon approximately one hour apart from each other. Thus the data for these series could be used to analyze the total fluorescence of locations over the course of a day.

The graph of total fluorescence over time for sampling location 6e can be seen in Figure 35 below. Both the initial fluorescence and fluorescence followed the same trend over time and were approximately equidistance from each other throughout the entire sampling time. However, the total fluorescence after irradiation was always higher than the initial total fluorescence. This was consistent with the previously discussed results from the fluorescent spectra. The total fluorescence was at its lowest at point, greatly increased at series 16, and experienced only small

decreases and increases at series 17 and 18 respectively. This indicated that the molecule in the water that was causing the fluorescence was more concentrated in the afternoon.

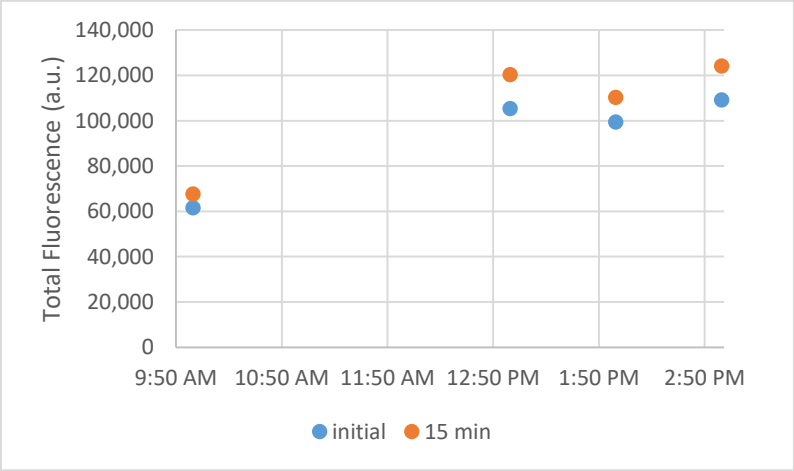

Figure 35: *Total fluorescence over time for sampling location 6e*

The total fluorescence over time for sampling location 6f can be seen in Figure 36 below. Similar to location 6e, the total fluorescence initially and after 15 minutes of UV irradiation followed similar trends. The total fluorescence was at its lowest at series 15, greatly increased to series 16 and then slightly decreased and increased at series 17 and 18 respectively. This once again indicated that the molecule causing the fluorescence was more concentrated in the afternoon. Consistent with the fluorescent spectra previously discussed, the total fluorescence after irradiation was higher than the initial total fluorescence. Since location 6d, and 6e combine to become location 6f it made sense that locations 6e and 6f would have total intensities that were similar orders of magnitude.

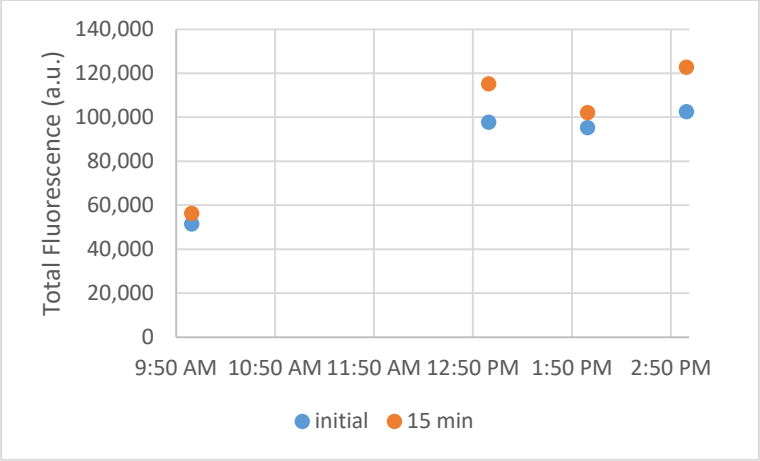

Figure 36: *Total fluorescence over time for sampling location 6f*

The total fluorescence over time for location step 3 aval followed a very different trend from locations 6e and 6f as can be seen in Figure 37 below. At series 15 and 17, the total fluorescence was at its highest. The total fluorescence at series 16 was significantly lower than that of series 15 while series 18 was only slightly lower than series 17. Figure 37 also had the highest range in total fluorescence of any of the locations studied which indicated that the water coming out of the wastewater treatment facility was highly variable in concentration throughout the day. When compared to the initial total fluorescence, the post irradiation total fluorescence was always higher. This was once again consistent with the trends of the fluorescent spectra as previously discussed.

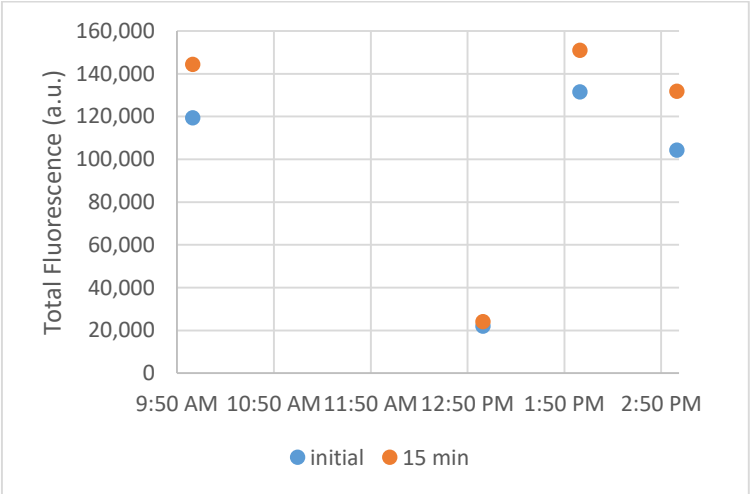

Figure 37: *Total fluorescence over time for sampling location step 3 aval*

Figure 38 shows the total fluorescence over time for sampling location 6. The initial total fluorescence and post irradiation total fluorescence followed similar trends throughout the day. Both increased from series 15 to 16 and decreased after series 16. This showed that the molecule causing fluorescence was at its highest concentration in the early afternoon but became increasingly less concentrated as the afternoon progressed. At all parts of the day, the post irradiation total fluorescence was higher than the initial total fluorescence which was consistent with the results of the fluorescent spectra previously discussed. However, the total fluorescence at this location was significantly lower than that of locations 6e, 6f, and step 3 aval. Location 6 was a mix of locations 6g, 6f, 6h and step 3 aval, but it was also located at the outlet of the Morte Femme peatland, so could have been possible that the peatland absorbed some of the fluorescence.

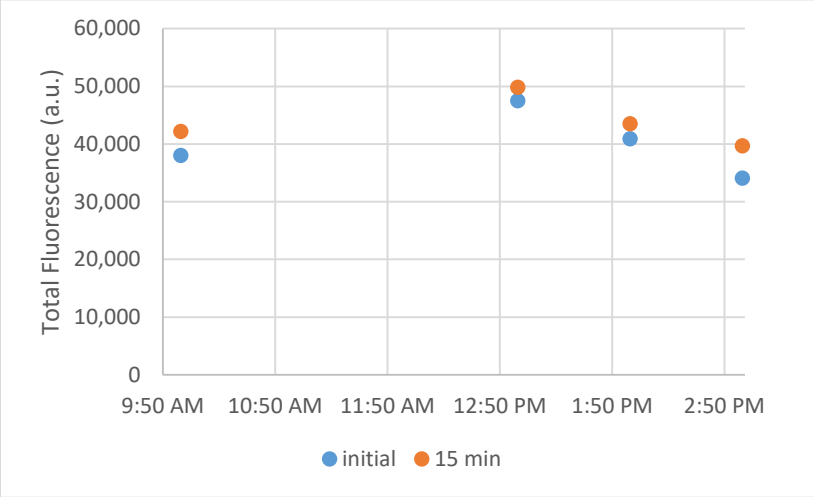

Figure 38: *Total fluorescence over time for sampling location 6*

Field Samples- Excitation Emission Matrices

Excitation emission matrices were created for a few field samples that were part of series 19 as well as a few optical brightener solutions. These matrices provided a 3D picture of the sample's fluorescence and could potentially have been used to identify if a specific optical brightener or a mixture of optical brighteners was present in the field samples. Optical brighteners DMA, stilbene and thiophene were chosen as they provided a range of molecular structures and functional groups. A 0.30 $\frac{mg}{L}$ solution of DMA was used to generate the excitation emission matrix. However, for stilbene and thiophene this concentration was too dilute to yield reasonable results. Thus a 0.015 $\frac{g}{L}$ solution was used to generate the excitation emission spectra for stilbene and

thiophene. For the field samples, locations 6e, 6h, and T were chosen as in previous analyses their spectra contained a variety of shapes and fluorescent intensities.

The excitation emission matrices for the optical brighteners are shown in Figure 39 below. Please note that the y-axis for thiophene had a different scale than those of DMA and stilbene. Additionally, the z-axis represented the brightener's fluorescence and each optical brightener had a different scale on the z-axis. The small sharp peaks on each of the matrices corresponded to the waterline whereas the other features were specific to the optical brightener. The spectrum of DMA contained two large and rounded peaks located at middle emission wavelengths and low excitation wavelengths with maximum intensities around 400 a.u.. Stilbene on the other hand had five sharper peaks located at high emission wavelengths and across the entire range of excitation wavelengths. The two highest peaks on the stilbene matrix had maximum intensities around 500 a.u.. The features on the thiophene matrix are quite different than those of the other optical brightener matrices which is consistent with the results of the synchronous fluorescence spectra. The sharp and wide peak of the thiophene matrix covered the entire emission wavelength range and the majority of the excitation range and had a maximum intensity around 100 a.u.

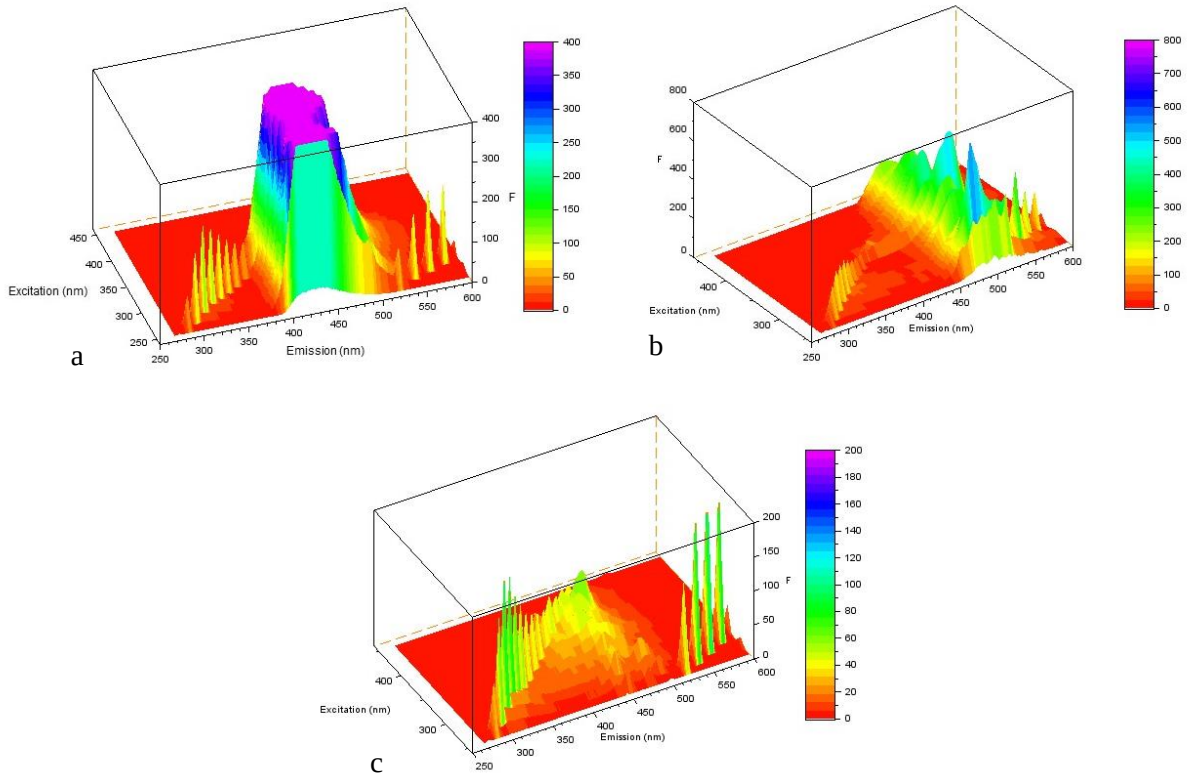

Figure 39: *Excitation emission matrices of DMA (a), stilbene (b) and thiophene (c)*

The excitation emission matrix from the field sample collected as part of series 19 at location 6e can be seen in Figure 40 below. The small, sharp peaks on the matrix corresponded to the waterline. The defining feature of this matrix was the large rounded peak that was located at middle emission wavelengths and ranged across the majority of the excitation wavelengths. This rounded peak had a maximum intensity around 140 a.u. . The presence of rounded peak was similar to that of DMA in Figure 39a. However, the peak for location 6e spanned a wider range of excitation wavelengths and was significantly lower in intensity than that of DMA. It was possible that these differences indicated the presence of a mixture of optical brighteners or an additional fluorescent compound.

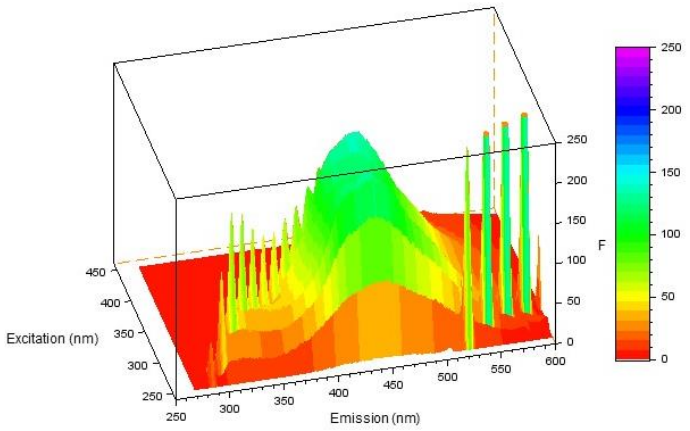

Figure 40: *Excitation emission matrix of location 6e in series 19*

Figure 41 below represents the excitation emission matrix of location 6h that was collected as part of series 19. Once again the sharp peaks were characteristic of the waterline. The defining feature of this spectrum was a broad and rounded peak with a maximum intensity around 100 a.u.. However, this peak was much less defined than that of the matrix for location 6e. Similar to location 6e, this peak was located at middle emission wavelengths and spanned the majority of the excitation wavelengths. This once again spanned a wider excitation wavelength and had a lower intensity than the peak of the DMA matrix. It was possible that DMA was present at this sampling location, but it was also possible that a mixture of optical brighteners or another fluorescent compound was present.

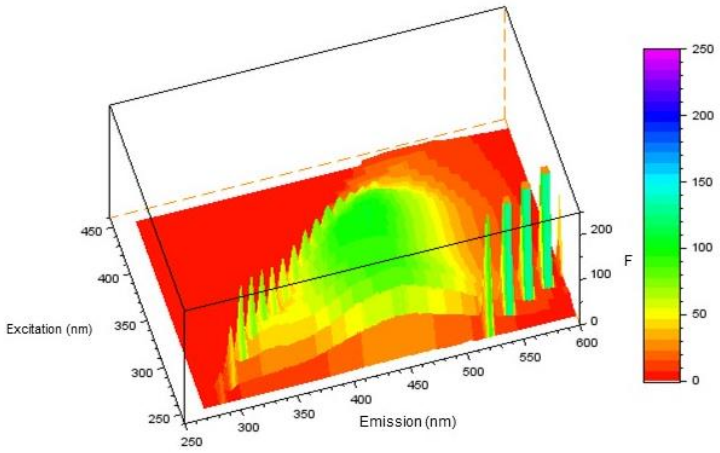

Figure 41: *Excitation emission matrix of location 6h in series 19*

The excitation emission matrix of the sample collected at location T as part of series 19 can be seen in Figure 42 below. The sharp peaks represented the waterline rather than the fluorescence exhibited by the sample. This matrix had a defined rounded peak with a maximum intensity around 400 a.u.. This peak was located at middle emission wavelengths and covered the majority of the excitation wavelength range. However, since sampling location T is in the old bed of the Cleurie river this peak was due to dissolved organic matter rather than optical brighteners.

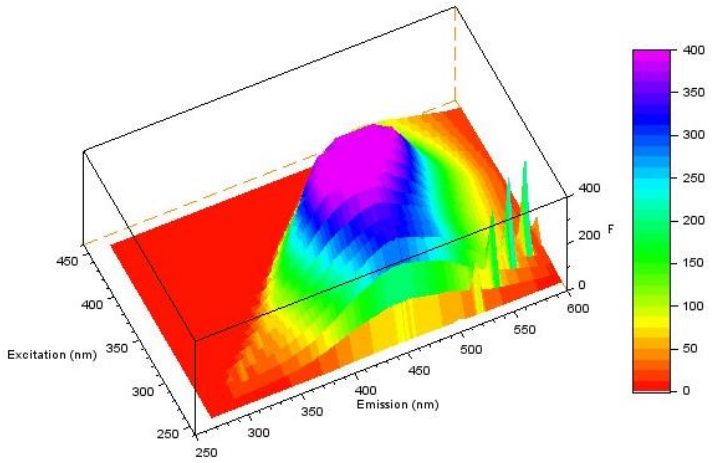

Figure 42: *Excitation emission matrix of location T in series 19*

Error Analysis

As with any process, there was uncertainty associated with the data collected for this report. First the uncertainty associated with the solutions of optical brighteners in water will be discussed. When these solutions were being created some optical brighteners were easier to dissolve in water than others. While all efforts were made to ensure all of the optical brightener had dissolved before further diluting, it was possible that some of the optical brightener did not dissolve entirely. This could have led to a slightly lower than expected concentration, but also undissolved particles could have interfered with the UV light absorption during both the synchronous fluorescence scan and the UV irradiation. Additionally, while mixing the optical brighteners, the dilution flasks were covered in aluminum foil to prevent the optical brighteners from photodegrading. However, while the powdered optical brightener was weighted and while amounts of optical brightener solutions were measured and further diluted they were exposed to light. This could have caused them to degrade and show less fluorescence during the synchronous fluorescent scan than they should have.

Synchronous fluorescent scans appeared to have a measurable baseline of approximately 10 a.u., below which the accuracy of the readings would be uncertain. This level corresponded to a brightener concentration of approximately 0.004 $\frac{mg}{L}$. Based on this, it was assumed that the accuracy of the measurements with concentrations less than this value would be reduced. The synchronous fluorescence scans were conducted in batches as the lab made closed box could only fit 10 cuvettes at a time. Every effort was made to standardize procedures to ensure that all batches experienced exactly 15 minutes of UV irradiation. However, there was some human error in this that was associated with placing the cuvettes in the closed box and setting up the UV irradiation. Additionally, depending on where an individual cuvette fell within a batch it spent varying amounts of time waiting for the UV lamp to be turned on, or to be put in the spectrophotometer after irradiation. During these periods of waiting the cuvettes were exposed to light which could have caused any optical brighteners present to degrade some. This would cause the fluorescence intensity measured to be lower than it should have been.

When collecting field samples, everything was weather dependent. Field samples were collected in all weather conditions including sun, rain, snow, and hail. For a few series, deteriorating road conditions prohibited all the samples in the series from being collected.

Additionally, rain, snow, and hail likely diluted the samples that were collected causing fluorescent intensities to be lower than they would have been in sunny weather. The changing weather conditions also resulted in variable water levels and flow rates in the streams that samples were collected from. This again caused fluctuations in the concentrations of the molecules that were measured which directly impacted the order of magnitudes seen in the fluorescent spectra. It was also possible that when collecting the samples, higher flow rates caused more sediments and organic matter to be present in the samples collected. Sediments were likely filtered out during the initial analysis of the samples when they were brought to the lab. However, organic matter exhibits similar fluorescent characteristics as optical brighteners including degrading following irradiation with UV light. Therefore, it was possible that organic matter could have been mistaken for optical brighteners when the fluorescent spectra were analyzed.

On each day that field samples were collected, the nearby textile plants were running. However, there was no way to know which processes they were running each day. It was possible that they were not using optical brighteners in the processes they were running on the sampling days and thus optical brighteners may not have been discharged into the waterways on days that samples were collected. Series 15-18 were the only series' that were collected at multiple different times of the same day. They were used to analyze trends in total fluorescence throughout the day. However, it was entirely possible that these series and their associated trends were outliers. More data of this nature is needed to confirm the trends discussed in this report.

When analyzing the field samples in the lab, the pH and conductivity meters used had uncertainties of 0.005. For the DOC measurements, C_{inorg} had an uncertainty of 0.05 $\frac{mg\ C}{L}$, C_{org} had an uncertainty of 0.01 $\frac{mg\ C}{L}$, and TN had an uncertainty of 0.20 $\frac{mg\ N}{L}$. The uncertainty of the ion chromatography values varied by species with PO_4 having an uncertainty of 0.50 $\frac{mg}{L}$, and NO_3 , NO_2, SO_4, and Cl having uncertainties of 0.10 $\frac{mg}{L}$. The ICP measurements had an uncertainty of 1.0 $\frac{\mu g}{L}$. Since the fluorescent spectra for field samples were generated using the same method as the optical brighteners, the uncertainty associated with this method also applied to the spectra of the field samples.

Conclusions and Recommendations

Optical Brighteners

Solutions of seven optical brighteners at concentrations of 0.015 $\frac{g}{L}$, 0.30 $\frac{mg}{L}$, and 0.03 $\frac{mg}{L}$ were created and a synchronous fluorescence scan was used to generate fluorescent spectra. With the exception of thiophene, all the optical brighteners decreased in fluorescent intensity after being irradiated with UV light for 15 minutes. An error in preparing the thiophene solutions was likely the reason that thiophene did not follow the trends of the other optical brighteners. However, due to time constraints additional spectra of thiophene were unable to be created. By comparing the spectra of each concentration across all seven optical brighteners it was determined that 0.30 $\frac{mg}{L}$ was the optimal concentration. Higher concentrations were often too saturated to produce accurate results at the fluorimeter's highest sensitivity setting, and lower concentrations were often too dilute and the fluorimeter may not have been able to sense them properly.

The experiments previously described used a synchronous fluorescence scan with a difference of 50 nm between excitation and emission wavelengths. To ensure that this was the optimal wavelength difference, scans also using 20 nm and 80 nm wavelength differences were conducted on DMA, stilbene, and thiophene. Due to time constraints it was not feasible to run these test on all optical brighteners. DMA, stilbene and thiophene were chosen due to their wide range of molecular structures and functional groups. The spectra generated from these scans showed the most clearly defined features when a 50 nm wavelength difference was used, so this wavelength difference was used for all future synchronous wavelength scans.

Field Samples

As part of this project, nine series of field samples were collected. Eight of these series included approximately 12 sampling locations at the Morte Femme peatland and its tributaries. Series 12 included 28 sampling locations at the Cleurie river, the Morte Femme, and their respective tributaries. The fluorescent spectra for each of the samples collected were analyzed by location in order to find trends in the fluorescence at each location. Many of these locations showed large fluctuations in fluorescent intensity between series' which were due to variable concentrations of the molecules causing the fluorescence. This variable concentration was likely due to changing weather conditions such as rain and snow that affected the flow and water level at the sampling locations.

After being irradiated with UV light for 15 minutes, samples collected at the Noir Rupt, Corsaire, 2a, 2b, and T sampling locations all showed a decrease in fluorescent intensity. This decrease was linked to the degradation of the fluorescent molecule. The degradation experienced at the Noir Rupt, Corsaire, 2a, 2b, and T sampling locations was likely due to the presence of dissolved organic matter rather than optical brighteners as the water at the Noir Rupt, and Corsaire sampling locations came down from the mountains and had little human contact before reaching the sampling location. Similarly, water at locations 2a and 2b came from the start of the Cleurie river and thus had limited human interactions. Sampling location T was made up of excess water from the Morte Femme peatland that percolates through the peat which was rich in organic matter before reaching the sampling location. Thus it made sense that the degradation at all these locations was due to dissolved organic matter rather than optical brighteners.

Samples collected at locations 6g, 6h, and 6d also showed degradation after UV irradiation. However, at these locations this degradation could be due to the presence of optical brighteners. The streams on which locations 6g and 6h were located flow through an industrial zone. High amounts of iron and chloride ions found in samples collected at location 6d show that there was likely a textile wastewater treatment plant upstream. For these reasons it was possible that the decrease in fluorescent intensity seen after UV irradiation was due to optical brighteners or a similar fluorescent chemical.

It was expected that after 15 minutes of UV irradiation the fluorescent intensity of the samples should have decreased. However, the samples collected at locations 6e, 6f, step 3 aval, and 6 increased in fluorescent intensity. This was consistent with the data previously collected at these locations by University of Lorraine researchers, but the reason for this trend is still unknown. In an effort to see the bigger picture of what was happening at these locations the total fluorescence at each location was analyzed over a period of one day. Since series 15-18 were collected in the same day, the total fluorescence of these series before and after irradiation at locations 6e, 6f, step 3 aval and 6 were analyzed. For all of these locations, and over the entire day studied, the total fluorescence after 15 minutes of irradiation was higher than the initial total fluorescence which was consistent with the trends seen on the fluorescent spectra at this location.

Excitation Emission Matrices

Excitation emission matrices show the 3D fluorescent spectrum of a particular solution and could be used to identify if a specific optical brightener was present in the sample. Due to time constraints, excitation emission matrices for only three field samples and three optical brighteners were generated. Locations 6e, 6h, and T were chosen for field samples and DMA, stilbene, and thiophene were chosen for optical brighteners. The broad and rounded peak that was present on the matrices at locations 6e, and 6h was similar to that on the matrix of DMA. However, the peak on the field samples covered a larger range of excitation wavelengths, and was generally lower in fluorescent intensity than that of DMA. This meant that there may have been additional optical brighteners or fluorescent compounds in addition to DMA present in the field samples. The matrix of location T had a similar peak to that of locations 6e and 6h, but since location T was the old bed of the Cleurie river this peak was likely due to dissolved organic matter.

References

Assad, A.; Pontvianne, S.; Pons, M. Photodegredation-based detection of fluorescent whitening agents in a mountain river. *Chemosphere* 2014, *100*, 27-33.

AVM Chemical Industries Chemistry of Optical Brightener and uses in Textile Industries and its Mechanism. *AVM Chemical Industries*.

Cao, Y.; Griffith, J. F.; Weisberg, S. B. Evaluation of optical brightener photodecay characteristics for detection of human fecal contamination. *Water Research* 2009, *34*, 2273-2279.

Gholami, A.; Masoum, S.; Mohsenikia, A.; Abbasi, S. Chemometrics-assisted excitation-emission fluorescence analytical data for rapid and selective determination of optical brighteners in the presence of uncalibrated interferences. *Spectrochimica Acta Part A: Molecular and Biomolecular Spectroscopy* 2016, *153*, 108-117.

Google Earth Morte Femme peatland and surrounding area. n.d. a.

Google Earth Location of Morte Femme peatland in France. n.d. b.

Hagedorn, C.; Saluta, M.; Hassall, A.; Dickerson, J. Fluorometric Detection of Optical Brighteners as an Indicator of Human Sources of Water Pollution. Part 1. Description and Detection of Optical Brighteners.

Kramer, J. B.; Canonica, S.; Hoigneé, J.; Kaschig, J. Degradation of Fluorescent Whitening Agents in Sunlit Natural Waters. *Environmental Science and Technology* 1994, *30*, 2227-2234.

Pacheco, M. E.; Bruzzone, L. Synchronous fluorescence spectrometry: Conformational investigation or inner filter effect? *Journal of Luminescence* 2013, *137*, 138-142.

Pitterle, B.; McGinnis-Carter, F. Optical Brightener Monitoring in Goleta Streams. *Santa Barbara Channelkeeper* 2010.

Pons, M.N. GIS Map of the Cleurie. 2020.

Pons, M. N. Morte Femme peatland. 2020.

Povrozin, Y.; Barbieri, B. Fluorescence Spectroscopy. *Handbook of Measurement in Science and Engineering* 2016, *3*, 2475-2499.

University of California Irvine Fluorescence Excitation and Emission Fundamentals. *n.d.*

Appendices

Appendix A- List of Samples Collected as Part of Each Series

Table 1: *List of sampling locations included in series 11*

Number	Location Name
11-1	Corsaire
11-2	Noir Rupt
11-3	Cleurie 6g
11-4	Cleurie 6e
11-5	Cleurie 6f
11-6	Cleurie 6h
11-7	Step 3 aval
11-8	Cleurie 6
11-9	T
11-10	Cleurie 6d

Table 2: *List of sampling locations included in series 12*

Number	Location Name
12-1	Cleurie 1
12-2	Cleurie 2
12-3	Cleurie 3
12-4	Cleurie 4
12-5	Cleurie 5
12-6	Cleurie 6
12-7	Cleurie 7
12-8	Cleurie 8
12-9	Cleurie 9
12-10	Cleurie 10
12-11	Cleurie 11
12-12	Noir Rupt
12-13	Corsaire
12-14	Ruisseau des Voués
12-15	Berlingoutte
12-16	Pissoire
12-17	Cellet
12-18	Grand Rupt
12-19	Liangoutte
12-20	Meunière
12-21	Cleurie 6g
12-22	Cleurie 6e
12-23	Cleurie 6f
12-24	Cleurie 6h
12-25	Step 3 aval
12-26	Cleurie 6
12-27	T
12-28	Cleurie 6d

Table 3: *List of sampling locations included in series 13*

Number	Location Name
13-1	Corsaire
13-2	Noir Rupt
13-3	Cleurie 2a
13-4	Cleurie 2b
13-5	Cleurie 6g
13-6	Cleurie 6e
13-7	Cleurie 6f
13-8	Cleurie 6h
13-9	Step 3 aval
13-10	Cleurie 6
13-11	Cleurie 6d

Table 4: *List of sampling locations included in series 14*

Number	Location Name
14-1	T
14-2	Cleurie 2a
14-3	Cleurie 2b
14-4	Cleurie 6g
14-5	Cleurie 6e
14-6	Cleurie 6f
14-7	Cleurie 6h
14-8	Step 3 aval
14-9	Cleurie 6
14-10	Cleurie 6d

Table 5: *List of sampling locations included in series 15*

Number	Location Name
15-1	Corsaire
15-2	Noir Rupt
15-3	Cleurie 2a
15-4	Cleurie 2b
15-5	Cleurie 6g
15-6	Cleurie 6e
15-7	Cleurie 6f
15-8	Cleurie 6h
15-9	Step 3 aval
15-10	Cleurie 6
15-11	T
15-12	Cleurie 6d

Table 6: *List of sampling locations included in series 16*

Number	Location Name
16-1	Corsaire
16-2	Noir Rupt
16-3	Cleurie 2a
16-4	Cleurie 2b
16-5	Cleurie 6g
16-6	Cleurie 6e
16-7	Cleurie 6f
16-8	Cleurie 6h
16-9	Step 3 aval
16-10	Cleurie 6
16-11	T
16-12	Cleurie 6d

Table 7: *List of sampling locations included in series 17*

Number	Location Name
17-1	Corsaire
17-2	Noir Rupt
17-3	Cleurie 2a
17-4	Cleurie 2b
17-5	Cleurie 6g
17-6	Cleurie 6e
17-7	Cleurie 6f
17-8	Cleurie 6h
17-9	Step 3 aval
17-10	Cleurie 6
17-11	T
17-12	Cleurie 6d

Table 8: *List of sampling locations included in series 18*

Number	Location Name
18-1	Corsaire
18-2	Noir Rupt
18-3	Cleurie 2a
18-4	Cleurie 2b
18-5	Cleurie 6g
18-6	Cleurie 6e
18-7	Cleurie 6f
18-8	Cleurie 6h
18-9	Step 3 aval
18-10	Cleurie 6
18-11	T
18-12	Cleurie 6d

Table 9: *List of sampling locations included in series 19*

Number	Location Name
19-1	Cleurie 2a
19-2	Cleurie 2b
19-3	Cleurie 2c
19-4	Cleurie 6g
19-5	Cleurie 6e
19-6	Cleurie 6f
19-7	Cleurie 6h
19-8	Step 3 aval
19-9	Cleurie 6
19-10	T
19-11	Cleurie 6d

Appendix B- Fluorescent Spectra of Optical Brighteners for all Irradiation Periods

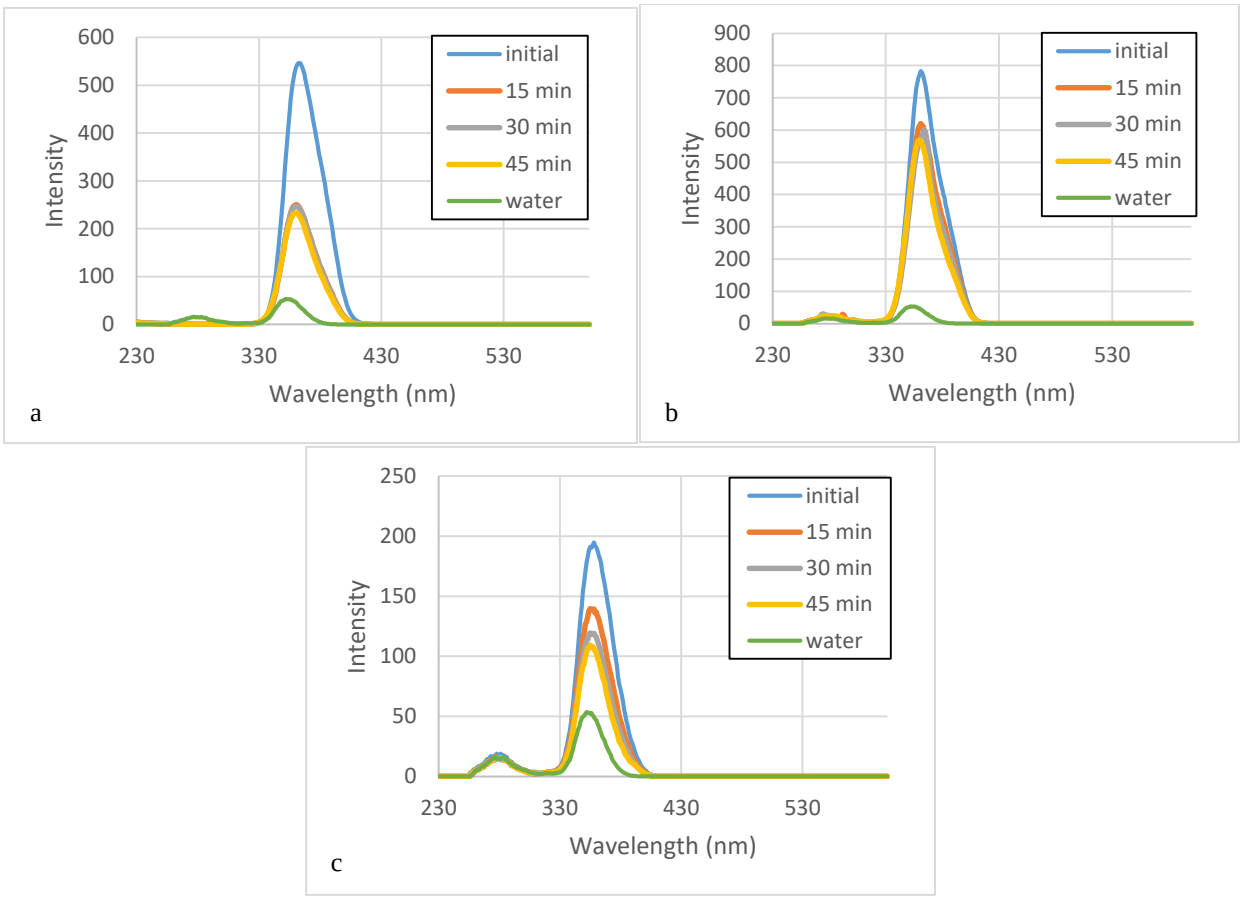

Figure 43: *Fluorescent spectra for 0.015 g/L (a), 0.30 mg/L (b), and 0.03 mg/L (c) solutions of DMA*

<u>Note:</u> Figure 43a was generated using a 400V sensitivity rather than a 700V sensitivity like the other figures were.

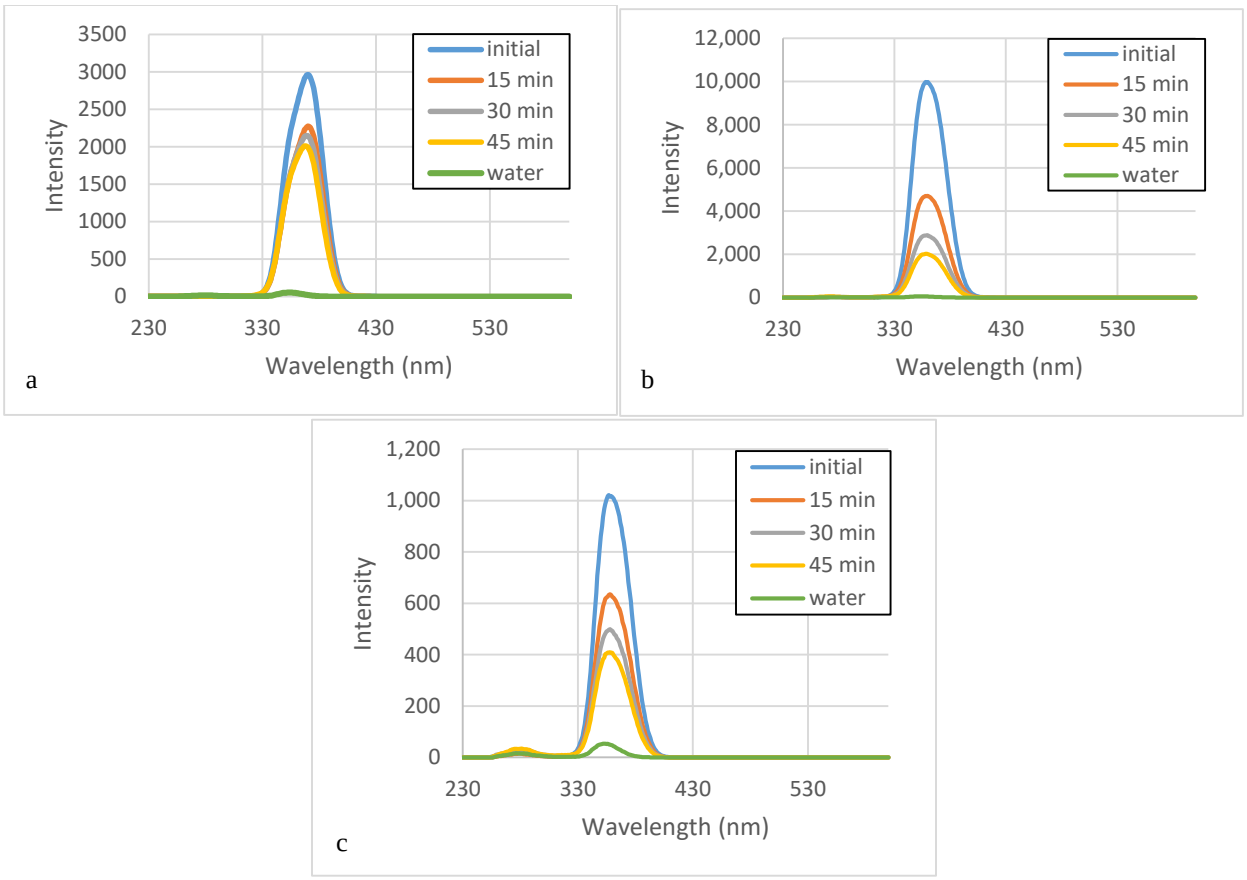

Figure 44: *Fluorescent spectra for 0.015 g/L (a), 0.30 mg/L (b), and 0.03 mg/L (c) solutions of CBS*

Note: **Figure 44***a was generated using a 400V sensitivity rather than a 700V sensitivity like the other figures were.*

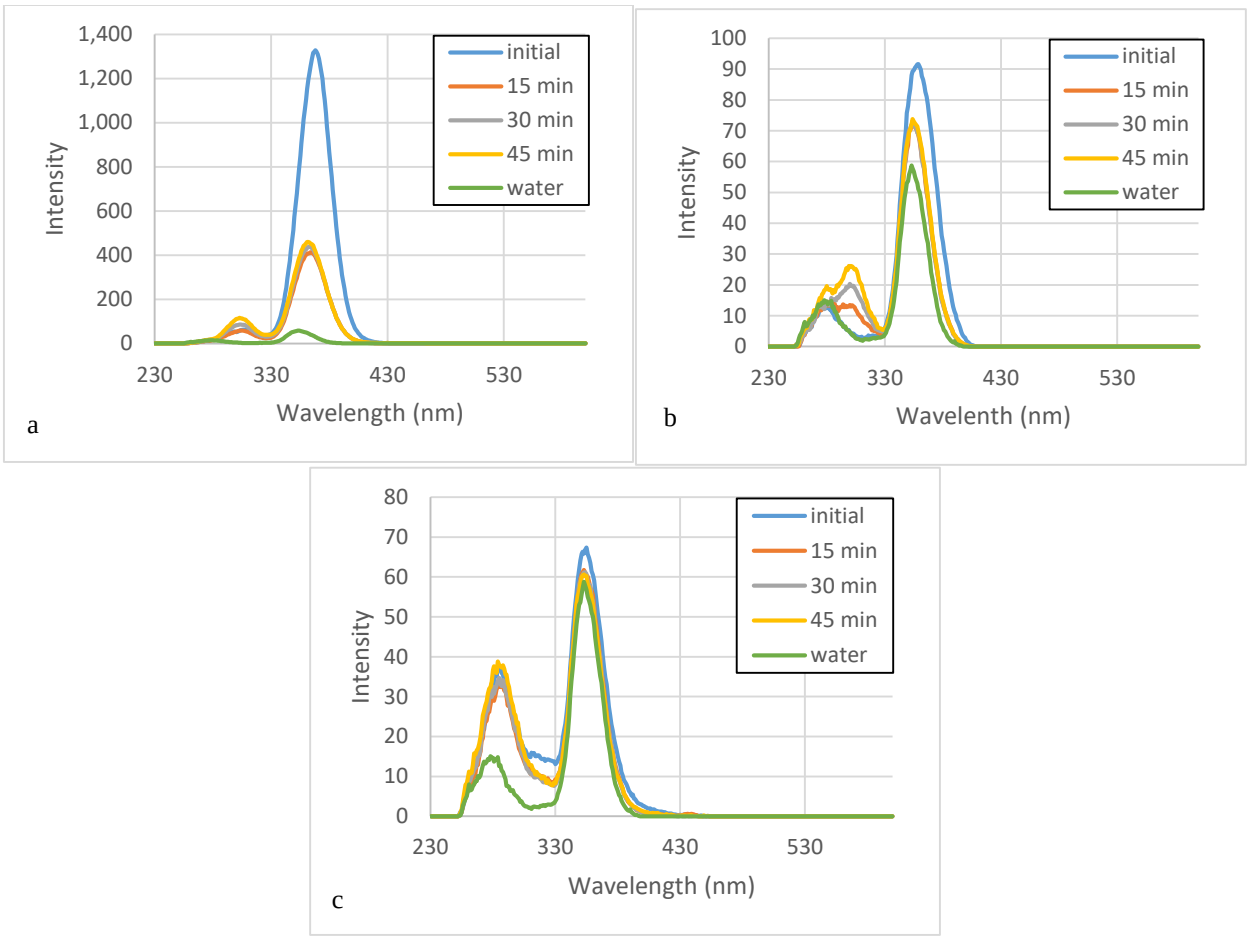

Figure 45: *Fluorescent spectra for 0.015 g/L (a), 0.30 mg/L (b), and 0.03 mg/L (c) solutions of stilbene acid*

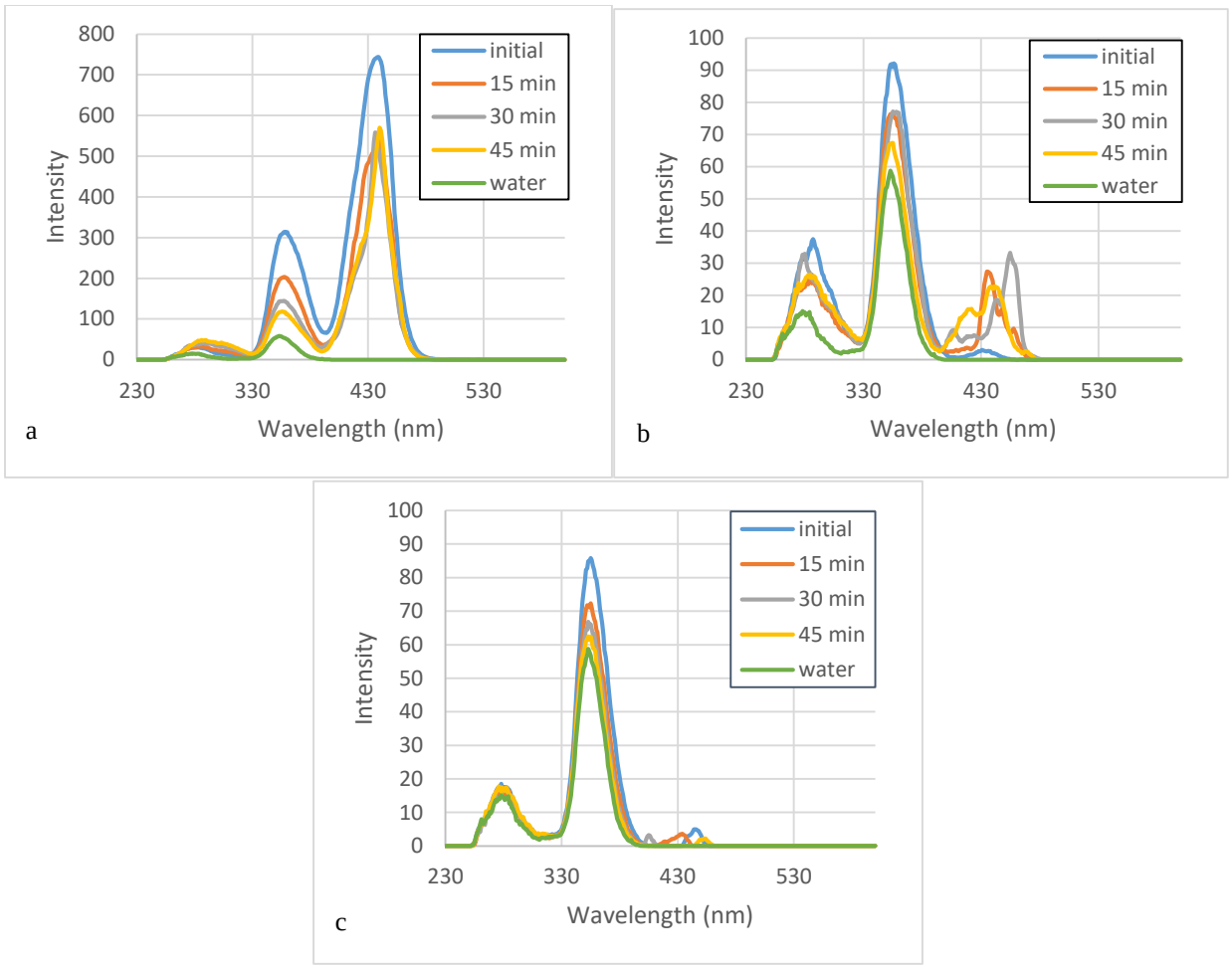

Figure 46: *Fluorescent spectra for 0.015 g/L (a), 0.30 mg/L (b), and 0.03 mg/L (c) solutions of stilbene*

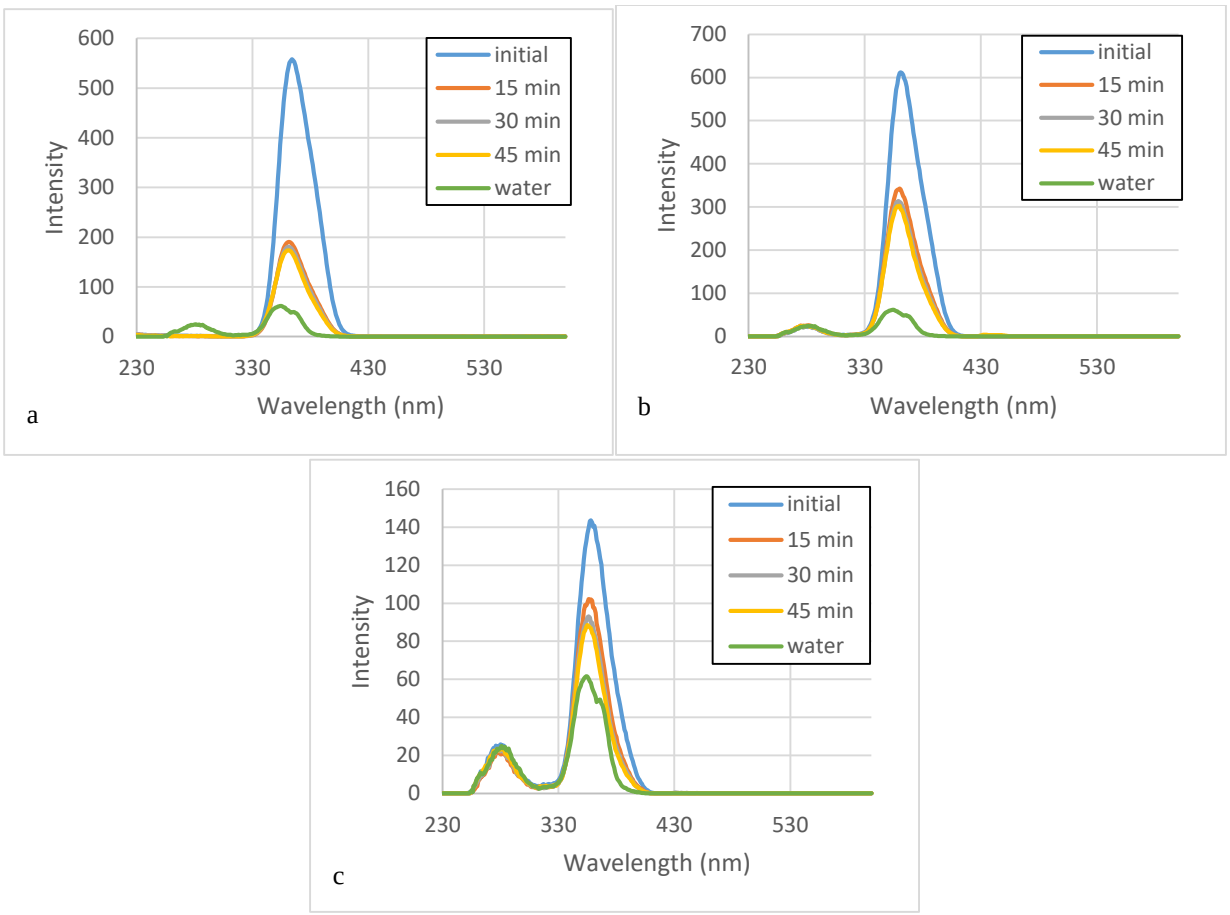

Figure 47: *Fluorescent spectra for 0.015 g/L (a), 0.30 mg/L (b), and 0.03 mg/L (c) solutions of Fluorescent Brightener 28*

Note: **Figure 47***a was generated using a 400V sensitivity rather than a 700V sensitivity like the other figures were.*

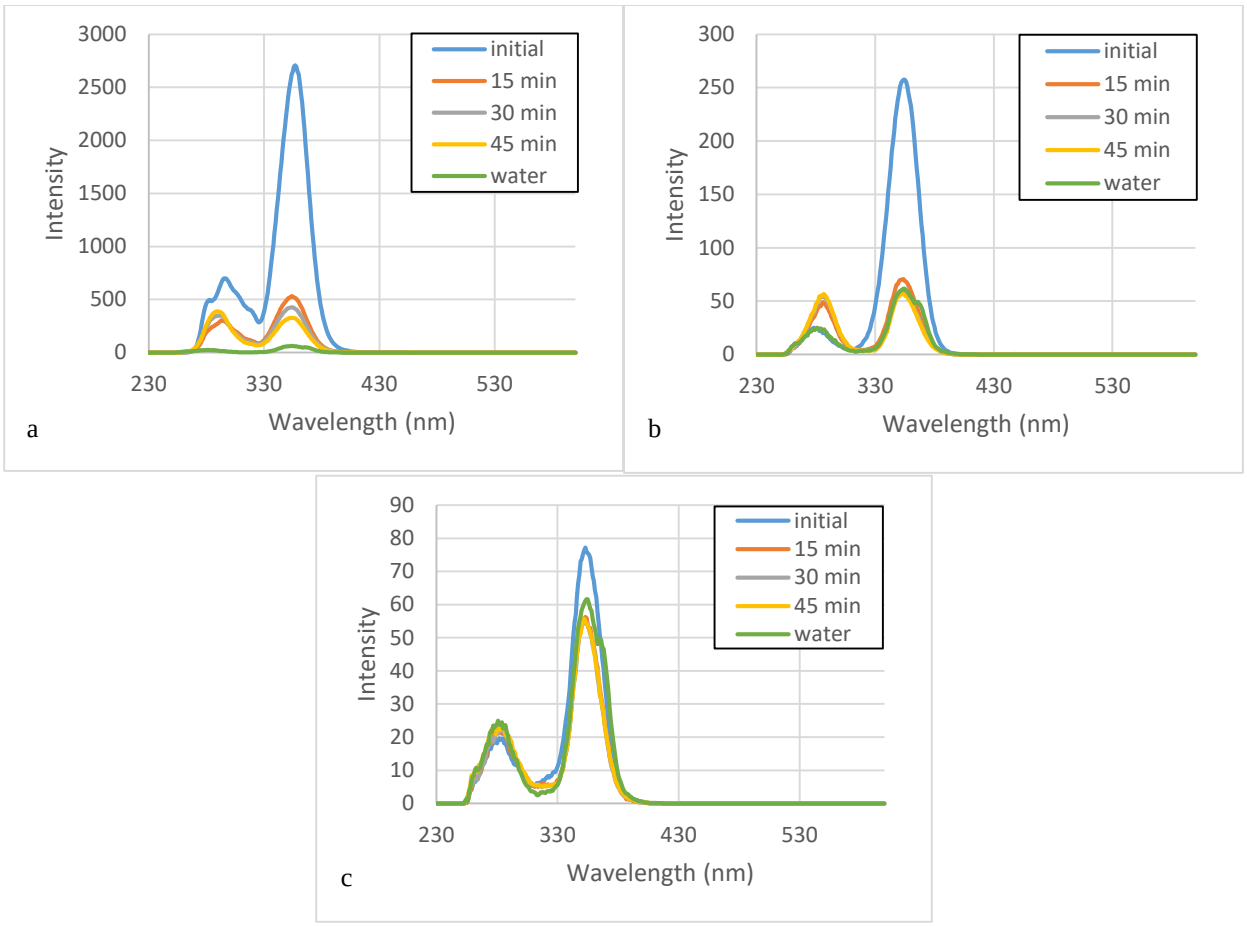

Figure 48: *Fluorescent spectra for 0.015 g/L (a), 0.30 mg/L (b), and 0.03 mg/L (c) solutions of DAS*

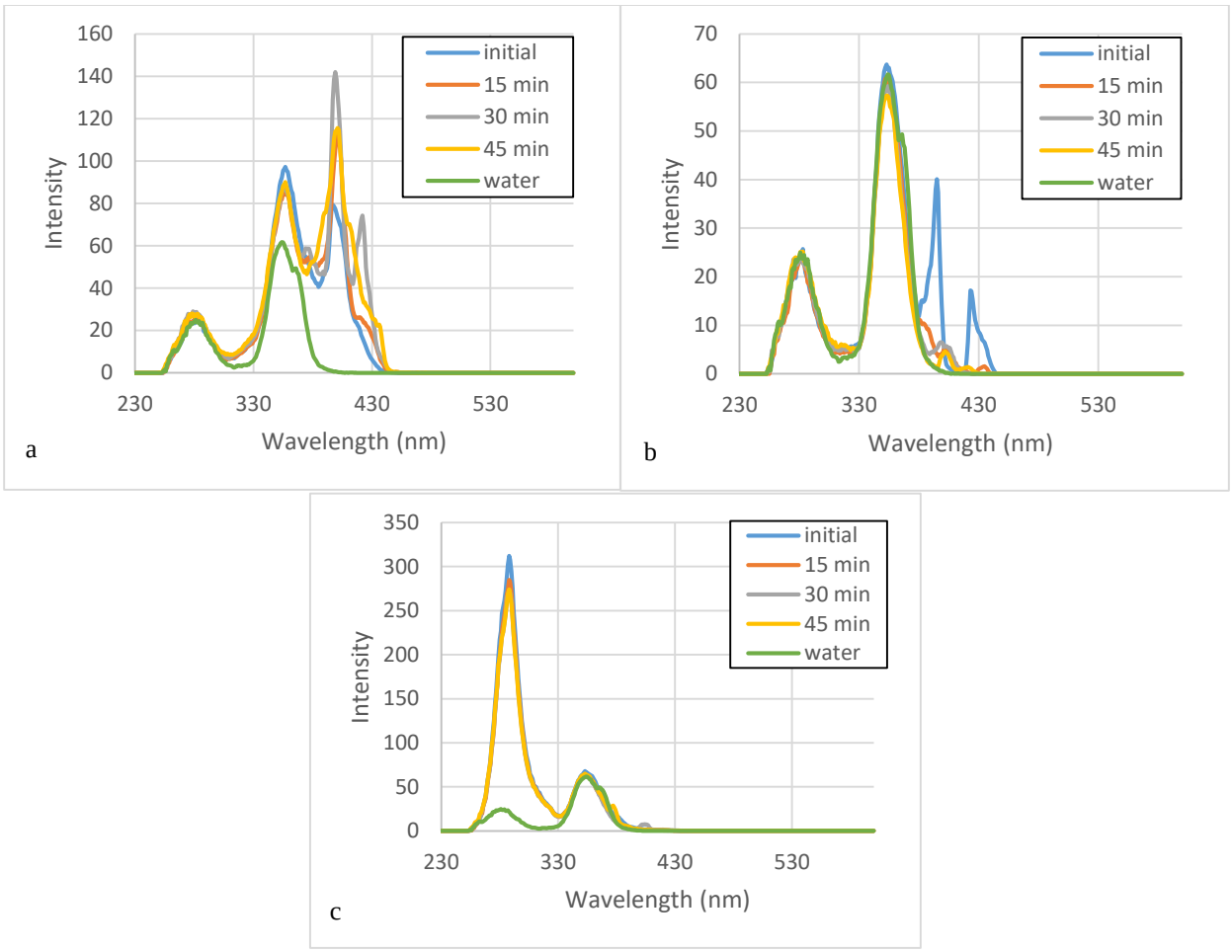

Figure 49: *Fluorescent spectra for 0.015 g/L (a), 0.30 mg/L (b), and 0.03 mg/L (c) solutions of thiophene*

Appendix C-Map of Sampling Locations

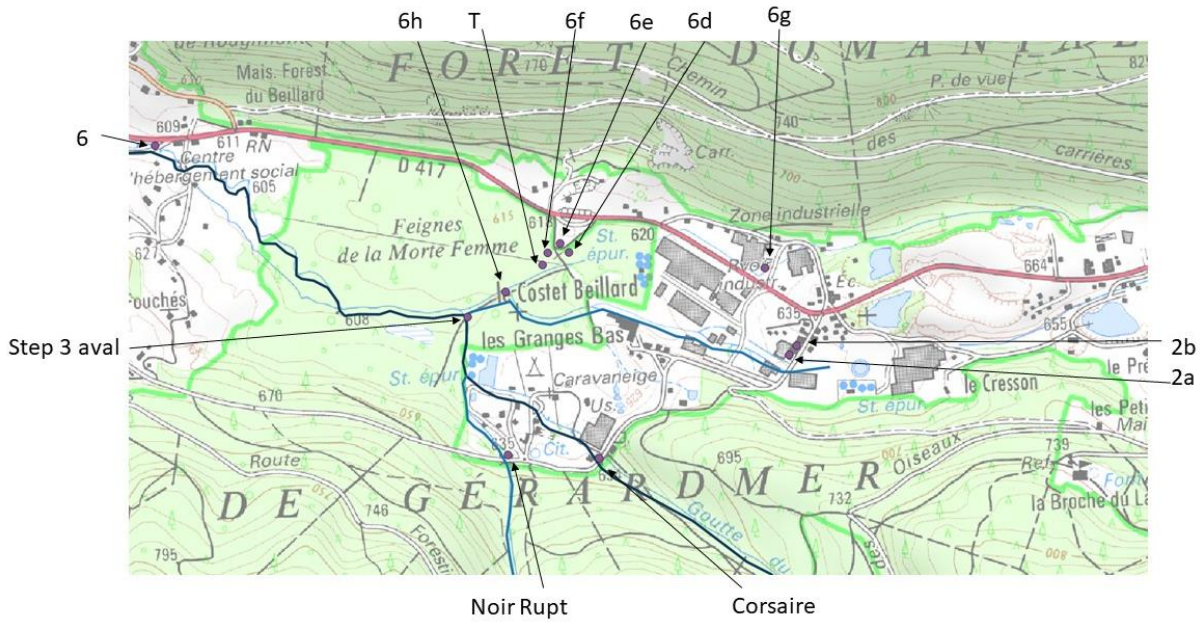

Figure 50: *Labeled map showing sampling locations*

Appendix D- Photos of Sampling Locations

Figure 51: *Noir Rupt sampling location*

Figure 52: *Corsaire sampling location*

Figure 53: *Sampling location 2a*

Figure 54: *Sampling location 2b*

Figure 55: *Sampling location 6g*

Figure 56: *Sampling location 6e*

Figure 57: *Sampling location 6f*

Figure 58: *Sampling location 6h*

Figure 59: *Step 3 aval sampling location*

Figure 60: *Sampling location 6*

Figure 61: *Sampling location T*

Figure 62: *Sampling location 6d*

Appendix E- Raw Data

Table 10: *pH, conductivity, and DOC results for series 11*

Number	X (µS/cm)	pH	C_{inorg} (mgC/L)	C_{org} (mgC/L)	TN (mg/L)
11-1	12.48	7.93	0.76	3.70	0.61
11-2	7.16	7.78	0.53	5.53	0.72
11-3	45.70	6.95	5.02	2.83	0.62
11-4	61.20	6.55	7.10	3.73	0.80
11-5	63.90	6.51	7.11	4.11	0.71
11-6	214.60	6.68	33.50	7.32	1.47
11-7	71.70	6.99	15.23	9.68	0.73
11-8	121.40	6.82	16.81	8.47	1.00
11-9	16.20	6.07	4.65	30.94	0.68
11-10	124.80	6.18	7.29	22.80	0.83

Table 11: *ICP results for series 11*

Number	Ca (µg/L)	K (µg/L)	Na (µg/L)	Mg (µg/L)	Si (µg/L)	Mn (µg/L)	Fe (µg/L)	Cu (µg/L)	Zn (µg/L)	Al (µg/L)
11-1	428	127	1,721	133	3,041	59	48	17	28	1,606
11-2	247	182	917	84	2,868	134	541	27	22	2,812
11-3	3,358	906	7,448	1,059	4,506	959	347	n.a	3	580
11-4	4,124	1,671	11,814	1,082	4,372	433	432	n.a	17	557
11-5	4,093	1,794	12,513	1,065	4,339	422	708	n.a	16	646
11-6	4,970	16,069	60,624	1,789	4,721	177	738	n.a	173	558
11-7	753	4,432	23,082	335	2,712	108	458	n.a	60	2,264
11-8	3,204	6,545	33,486	990	3,710	242	1,112	n.a	53	1,257
11-9	280	316	1,813	88	4,559	123	3,838	n.a	53	15,177
11-10	1,440	5,159	36,527	394	4,023	777	12,117	n.a	4	3,402

Table 12: *Ion chromatography results for series 11*

Number	NO_3 (mg/L)	PO_4 (mg/L)	NO_2 (mg/L)	SO_4 (mg/L)	Cl (mg/L)
11-1	0.32	<LOQ	<LOQ	2.42	2.54
11-2	0.32	<LOQ	<LOQ	1.59	0.89
11-3	0.89	<LOQ	<LOQ	6.08	11.38
11-4	1.44	0.61	0.12	7.60	14.60
11-5	1.36	0.61	0.13	7.54	15.43
11-6	2.27	1.04	<LOQ	18.92	41.81
11-7	0.50	0.79	<LOQ	9.09	4.11
11-8	1.48	0.68	<LOQ	11.57	27.95
11-9	<LOQ	0.66	<LOQ	0.89	1.94
11-10	0.44	<LOQ	<LOQ	5.64	49.82

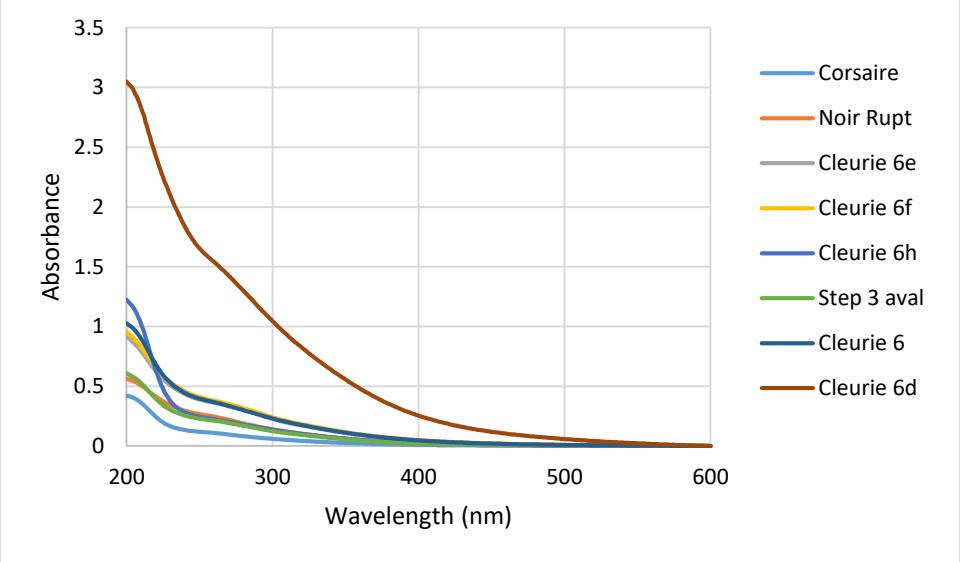

Figure 63: *UV spectroscopy results for series 11*

Table 13: *pH, conductivity, and DOC results for series 12*

Number	X (µS/cm)	pH	C_{inorg} (mgC/L)	C_{org} (mgC/L)	TN (mgN/L)
12-1	56.40	7.26	5.11	4.64	1.16
12-2	58.60	7.19	5.60	4.25	1.11
12-3	62.50	7.16	5.83	3.94	1.08
12-4	58.40	7.09	5.65	4.13	1.03
12-5	69.70	7.05	6.72	3.78	1.11
12-6	64.20	7.03	6.51	3.80	1.09
12-7	72.60	7.01	7.52	3.86	0.99
12-8	54.70	7.03	6.64	4.20	1.09
12-9	61.00	7.07	7.72	4.29	1.09
12-10	71.20	7.04	10.45	5.07	0.99
12-11	75.70	7.13	11.37	5.84	0.90
12-12	6.46	7.31	0.55	4.90	0.44
12-13	9.54	6.73	0.57	2.47	0.53
12-14	12.13	6.61	1.00	2.09	0.55
12-15	18.42	6.57	1.12	1.52	1.01
12-16	13.16	6.53	0.74	3.09	0.71
12-17	10.59	6.51	0.91	2.25	0.65
12-18	19.14	6.37	1.94	5.55	1.06
12-19	13.19	6.33	0.70	4.02	0.86
12-20	36.50	6.12	2.85	4.67	1.49
12-21	49.70	6.49	5.13	2.59	0.77
12-22	195.60	7.06	35.53	8.94	1.22
12-23	189.60	7.24	34.59	9.29	1.21
12-24	226.00	7.43	34.20	9.57	1.36
12-25	23.90	7.60	3.92	5.00	0.60
12-26	184.20	7.23	30.69	10.83	1.12
12-27	14.96	5.66	3.11	30.95	0.65
12-28	124.20	6.16	7.77	21.36	0.83

***Table 14**: ICP results for series 12*

Number	Ca (µg/L)	K (µg/L)	Na (µg/L)	Mg (µg/L)	Si (µg/L)	Mn (µg/L)	Fe (µg/L)	Cu (µg/L)	Zn (µg/L)	Al (µg/L)
12-1	2,008	4,321	19,961	654	4,007	135	927	0	22	1,261
12-2	265	148	882	85	2,830	142	563	n.a	14	2,772
12-3	385	104	1,675	127	3,019	52	32	n.a	3	1,552
12-4	960	307	1,356	332	3,448	12	83	n.a	4	564
12-5	1,299	567	2,699	316	3,116	9	61	n.a	7	344
12-6	562	483	2,229	143	3,006	44	216	8	7	1,164
12-7	775	309	1,335	169	3,366	172	189	n.a	2	1,039
12-8	1,315	447	1,920	911	4,039	44	638	n.a	13	1,531
12-9	949	236	1,423	277	3,491	83	348	n.a		1,933
12-10	2,802	981	5,368	625	3,663	72	591	n.a	10	750
12-11	3,416	935	7,588	1,093	4,480	860	329	n.a	2	484
12-12	4,137	15,763	69,646	1,659	6,690	238	582	n.a	114	618
12-13	3,898	15,064	67,018	1,598	6,575	239	791	n.a	97	626
12-14	4,882	15,945	75,561	1,835	4,906	145	633	n.a	172	387
12-15	683	1,011	6,092	174	2,926	148	432	n.a	37	2,295
12-16	3,163	12,857	52,531	1,299	4,559	207	1,386	n.a	107	1,263
12-17	270	272	2,005	85	4,440	117	3,627	n.a	53	15,027
12-18	1,391	5,194	2,015	364	4,170	731	11,454	n.a	10	3,314
12-19	2,008	4,321	19,961	654	4,007	135	927	0	22	1,261
12-20	265	148	882	85	2,830	142	563	n.a	14	2,772
12-21	385	104	1,675	127	3,019	52	32	n.a	3	1,552
12-22	960	307	1,356	332	3,448	12	83	n.a	4	564
12-23	1,299	567	2,699	316	3,116	9	61	n.a	7	344
12-24	562	483	2,229	143	3,006	44	216	8	7	1,164
12-25	775	309	1,335	169	3,366	172	189	n.a	2	1,039
12-26	1,315	447	1,920	911	4,039	44	638	n.a	13	1,531
12-27	949	236	1,423	277	3,491	83	348	n.a	8	1,933
12-28	2,802	981	5,368	625	3,663	72	591	n.a	10	750

Table 15: *Ion chromatography results for series 12*

Number	NO_3 (mg/L)	PO_4 (mg/L)	NO_2 (mg/L)	SO_4 (mg/L)	Cl (mg/L)
12-1	2.34	0.44	n.a.	5.61	11.59
12-2	2.37	0.42	n.a.	5.84	14.22
12-3	2.19	0.47	n.a.	6.09	15.50
12-4	2.15	0.45	n.a.	5.92	14.51
12-5	2.24	0.46	n.a.	6.65	17.43
12-6	2.22	n.a.	n.a.	6.34	15.52
12-7	2.47	0.49	n.a.	7.05	17.89
12-8	0.17	n.a.	n.a.	0.58	1.00
12-9	2.50	0.90	0.16	7.01	11.66
12-10	1.80	0.53	n.a.	7.72	11.95
12-11	1.60	0.54	n.a.	8.33	11.60
12-12	0.31	n.a.	n.a.	2.16	1.08
12-13	0.28	n.a.	n.a.	2.60	2.56
12-14	1.40	n.a.	n.a.	3.95	1.68
12-15	2.46	n.a.	n.a.	2.86	3.93
12-16	1.66	n.a.	n.a.	4.00	3.19
12-17	1.30	n.a.	n.a.	3.48	1.89
12-18	1.63	n.a.	n.a.	3.53	2.09
12-19	1.41	n.a.	n.a.	3.49	1.65
12-20	3.16	n.a.	0.15	4.47	8.66
12-21	0.94	0.55	n.a.	6.23	11.77
12-22	1.23	0.58	0.06	11.94	27.45
12-23	1.22	0.59	0.05	11.75	27.89
12-24	2.40	1.29	n.a.	20.17	43.99
12-25	0.46	0.44	n.a.	4.05	2.10
12-26	1.54	0.98	n.a.	17.98	26.94
12-27	0.12	0.48	n.a.	1.02	1.96
12-28	0.48	n.a.	n.a.	6.13	47.48

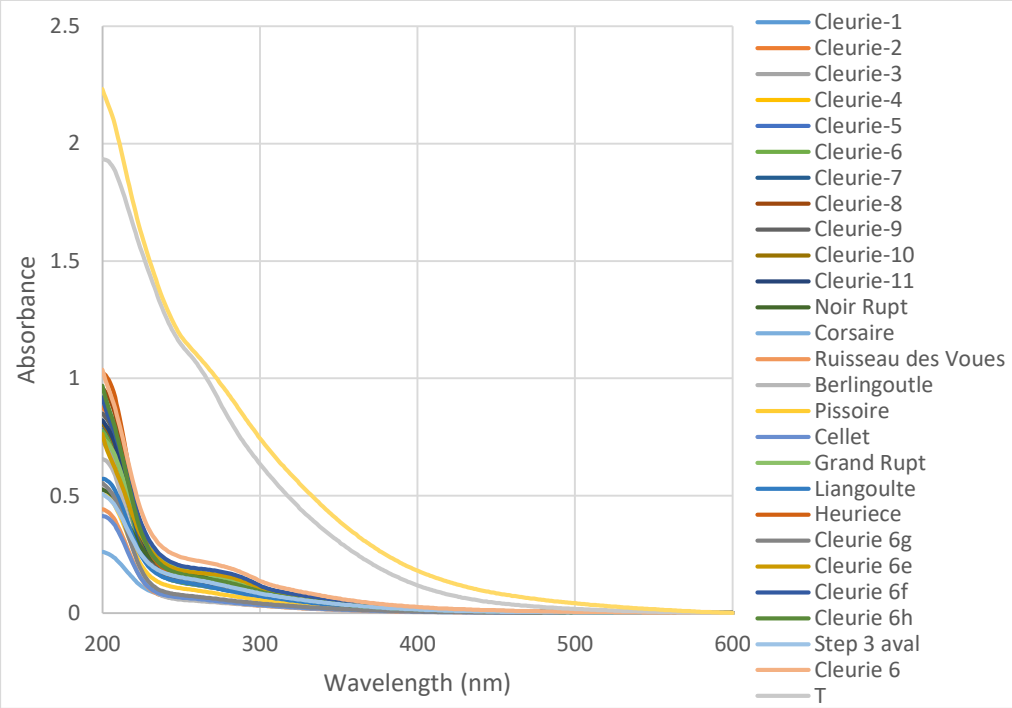

Figure 64: *UV spectroscopy results for series 12*

Table 16: *pH, conductivity, and DOC results for series 13*

Number	X (µS/cm)	pH	C_{inorg} (mgC/L)	C_{org} (mgC/L)	TN (mgN/L)
13-1	12.01	7.92	0.63	4.15	0.72
13-2	6.81	7.95	0.41	7.11	0.52
13-3	72.50	7.11	4.46	4.81	1.01
13-4	64.90	6.75	8.28	2.65	1.02
13-5	38.20	6.78	3.78	4.04	0.67
13-6	133.30	6.41	12.82	8.49	0.80
13-7	135.80	6.54	12.98	8.25	0.92
13-8	120.40	6.71	11.25	6.19	1.11
13-9	59.00	6.81	11.12	8.23	0.64
13-10	124.20	6.73	18.98	13.60	1.12
13-11	71.20	6.87	5.08	29.67	0.76

Table 17: *ICP results for series 13*

Number	Ca (µg/L)	K (µg/L)	Na (µg/L)	Mg (µg/L)	Si (µg/L)	Mn (µg/L)	Fe (µg/L)	Cu (µg/L)	Zn (µg/L)	Al (µg/L)
13-1										
13-2										
13-3										
13-4										
13-5										
13-6										
13-7										
13-8										
13-9										
13-10										
13-11										

Note: ICP results for this series have not yet been received from the technician. This appendix will be updated once they are received.

Table 18: *Ion chromatography results for series 13*

Number	NO_3 (mg/L)	PO_4 (mg/L)	NO_2 (mg/L)	SO_4 (mg/L)	Cl (mg/L)
13-1	0.47	n.a.	2.30	2.57	n.a.
13-2	0.56	n.a.	1.02	1.47	n.a.
13-3	2.26	n.a.	26.22	6.78	n.a.
13-4	2.70	n.a.	16.12	6.68	n.a.
13-5	0.93	n.a.	10.77	5.28	n.a.
13-6	0.79	n.a.	44.02	7.15	n.a.
13-7	0.75	n.a.	44.02	7.08	n.a.
13-8	2.00	n.a.	37.59	9.95	0.56
13-9	0.66	n.a.	3.31	11.93	0.82
13-10	1.30	n.a.	21.09	15.89	0.71
13-11	0.50	n.a.	25.33	3.94	n.a.

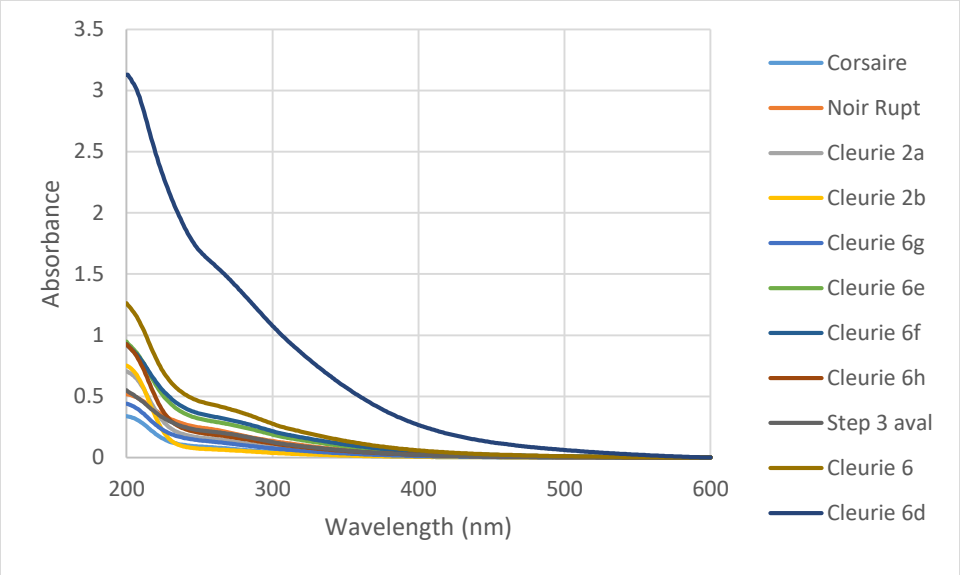

Figure 65: *UV spectroscopy results for series 13*

Table 19: *pH, conductivity, and DOC results for series 14*

Number	X (µS/cm)	pH	C_{inorg} (mgC/L)	C_{org} (mgC/L)	TN (mgN/L)
14-1	16.47	5.85	3.16	32.03	0.73
14-2	82.80	5.84	4.07	4.52	0.78
14-3	57.20	6.03	7.55	2.97	0.98
14-4	36.00	6.04	3.51	4.29	0.54
14-5	279.00	6.82	56.08	16.94	1.49
14-6	279.00	6.93	55.88	18.77	1.36
14-7	109.30	7.37	11.63	5.75	1.28
14-8	22.70	7.51	2.90	5.96	0.52
14-9	89.40	6.86	9.97	10.92	0.99
14-10	69.60	6.94	4.75	27.83	0.74

Table 20: *ICP results for series 14*

Number	Ca (µg/L)	K (µg/L)	Na (µg/L)	Mg (µg/L)	Si (µg/L)	Mn (µg/L)	Fe (µg/L)	Cu (µg/L)	Zn (µg/L)	Al (µg/L)
14-1										
14-2										
14-3										
14-4										
14-5										
14-6										
14-7										
14-8										
14-9										
14-10										

Note: ICP results for this series have not yet been received from the technician. This appendix will be updated once they are received.

Table 21: *Ion chromatography results for series 14*

Number	NO_3 (mg/L)	PO_4 (mg/L)	NO_2 (mg/L)	SO_4 (mg/L)	Cl (mg/L)
14-1	0.56	n.a.	1.75	1.67	n.a.
14-2	1.82	n.a.	32.57	6.06	n.a.
14-3	2.28	n.a.	13.51	5.83	n.a.
14-4	0.82	n.a.	10.01	5.00	n.a.
14-5	0.73	n.a.	39.73	15.90	0.57
14-6	0.73	n.a.	39.28	15.74	0.60
14-7	1.74	n.a.	32.95	9.27	0.54
14-8	0.58	n.a.	3.69	4.61	0.67
14-9	1.10	n.a.	23.17	8.60	0.53
14-10	0.49	n.a.	24.92	3.93	n.a.

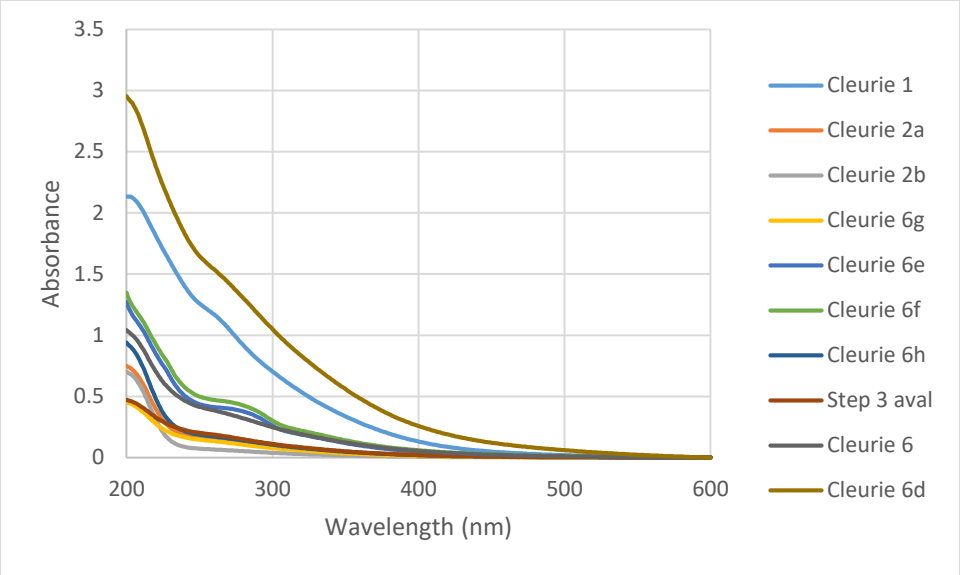

Figure 66: *UV spectroscopy results for series 14*

Table 22: *pH, conductivity, and DOC results for series 15*

Number	X (µS/cm)	pH	C_{inorg} (mgC/L)	C_{org} (mgC/L)	TN (mgN/L)
15-1	12.83	7.88	0.58	2.95	0.61
15-2	7.04	7.82	0.49	6.46	0.47
15-3	55.70	7.00	4.34	5.41	0.95
15-4	71.60	6.56	10.19	2.99	1.12
15-5	32.90	6.52	4.09	3.97	0.65
15-6	258.00	6.64	31.13	11.74	1.10
15-7	236.00	6.76	25.84	11.30	1.29
15-8	149.90	6.88	20.56	7.27	1.23
15-9	169.30	7.16	33.57	15.15	0.75
15-10	118.90	7.46	19.72	12.38	1.10
15-11	15.34	5.60	3.49	32.05	0.61
15-12	75.70	5.89	5.42	29.14	0.81

Table 23: *ICP results for series 15*

Number	Ca (µg/L)	K (µg/L)	Na (µg/L)	Mg (µg/L)	Si (µg/L)	Mn (µg/L)	Fe (µg/L)	Cu (µg/L)	Zn (µg/L)	Al (µg/L)
15-1										
15-2										
15-3										
15-4										
15-5										
15-6										
15-7										
15-8										
15-9										
15-10										
15-11										
15-12										

Note: ICP results for this series have not yet been received from the technician. This appendix will be updated once they are received.

Table 24: *Ion chromatography results for series 15*

Number	NO_3 (mg/L)	PO_4 (mg/L)	NO_2 (mg/L)	SO_4 (mg/L)	Cl (mg/L)
15-1	0.61	n.a.	2.27	2.61	n.a.
15-2	0.39	n.a.	1.02	1.34	0.44
15-3	2.69	0.19	17.19	6.41	0.57
15-4	3.24	0.11	13.64	8.65	n.a.
15-5	1.16	n.a.	9.97	5.99	n.a.
15-6	0.89	n.a.	75.42	10.60	0.52
15-7	0.87	n.a.	72.41	9.64	0.50
15-8	2.03	0.08	32.76	14.24	0.76
15-9	0.51	n.a.	5.83	32.57	1.21
15-10	1.10	n.a.	16.47	15.04	0.72
15-11	0.22	n.a.	1.58	1.44	n.a.
15-12	0.51	n.a.	27.11	4.23	n.a.

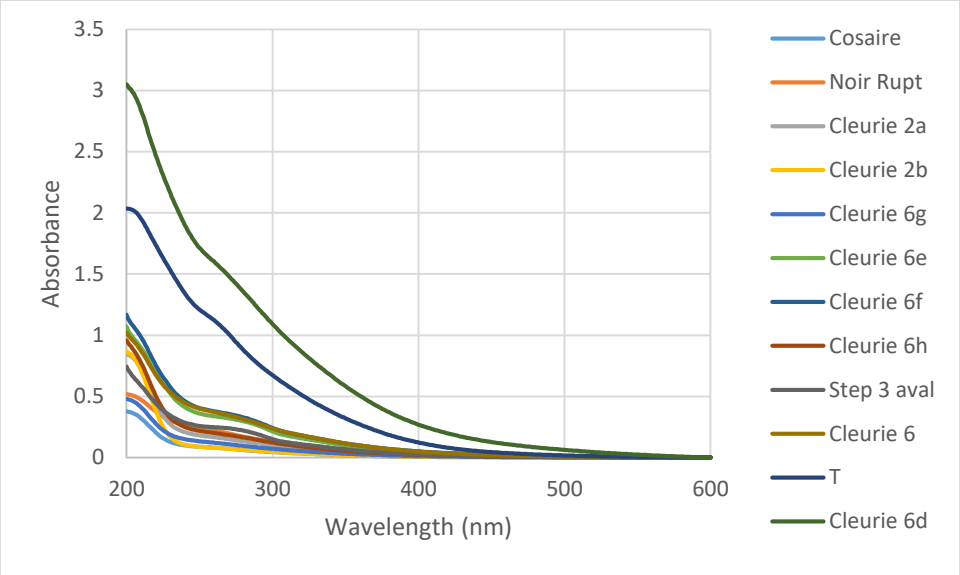

Figure 67: *UV spectroscopy results for series 15*

Table 25: *pH, conductivity, and DOC results for series 16*

Number	X (µS/cm)	pH	C_{inorg} (mgC/L)	C_{org} (mgC/L)	TN (mgN/L)
16-1	9.77	6.43	0.72	2.96	0.37
16-2	7.02	6.08	0.52	6.88	0.48
16-3	55.60	5.81	4.65	5.18	0.96
16-4	75.30	6.03	10.14	2.62	1.03
16-5	40.50	6.30	5.36	4.12	0.58
16-6	293.00	6.97	53.31	16.92	1.48
16-7	290.00	7.16	51.75	17.85	1.50
16-8	153.30	7.41	20.78	7.37	1.17
16-9	37.50	7.49	6.63	7.71	0.51
16-10	125.60	7.11	20.31	12.81	0.96
16-11	15.46	5.72	1.23	33.42	0.84
16-12	77.20	6.05	4.40	29.72	0.72

Table 26: *ICP results for series 16*

Number	Ca (µg/L)	K (µg/L)	Na (µg/L)	Mg (µg/L)	Si (µg/L)	Mn (µg/L)	Fe (µg/L)	Cu (µg/L)	Zn (µg/L)	Al (µg/L)
16-1										
16-2										
16-3										
16-4										
16-5										
16-6										
16-7										
16-8										
16-9										
16-10										
16-11										
16-12										

Note: ICP results for this series have not yet been received from the technician. This appendix will be updated once they are received.

Table 27: *Ion chromatography results for series 16*

Number	NO_3 (mg/L)	PO_4 (mg/L)	NO_2 (mg/L)	SO_4 (mg/L)	Cl (mg/L)
16-1	0.63	n.a.	2.24	2.84	n.a.
16-2	0.31	n.a.	1.00	1.37	n.a.
16-3	2.11	0.17	16.75	6.04	n.a.
16-4	2.93	n.a.	15.22	7.92	n.a.
16-5	0.87	n.a.	7.70	5.48	n.a.
16-6	1.11	n.a.	50.36	15.68	0.57
16-7	1.22	n.a.	52.00	15.35	0.58
16-8	2.01	0.09	32.32	14.31	0.81
16-9	0.43	n.a.	2.51	7.09	0.55
16-10	1.06	n.a.	16.37	16.10	0.74
16-11	0.25	n.a.	2.00	1.42	0.45
16-12	0.27	n.a.	27.11	3.68	n.a.

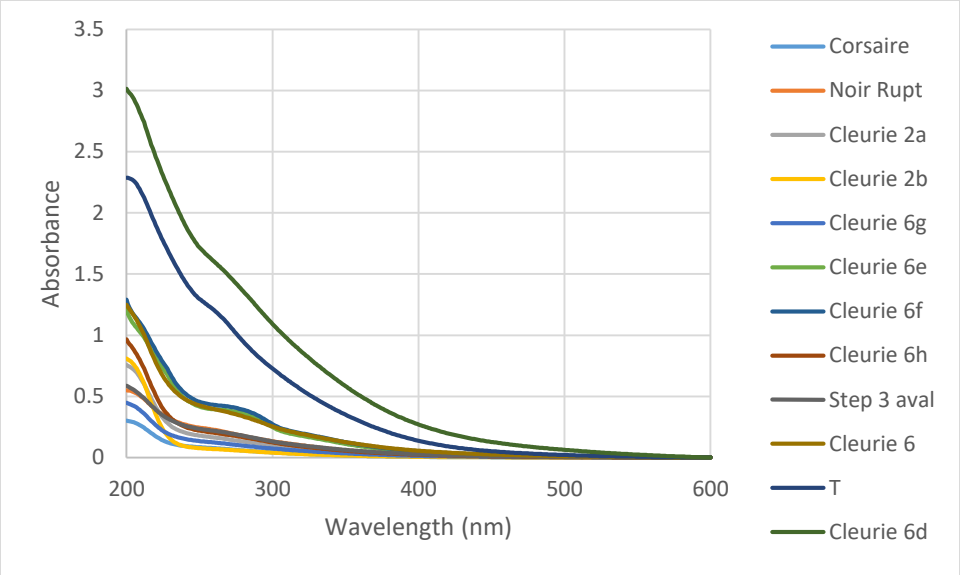

Figure 68: *UV spectroscopy results for series 16*

Table 28: *pH, conductivity, and DOC results for series 17*

Number	X (µS/cm)	pH	C_{inorg} (mgC/L)	C_{org} (mgC/L)	TN (mgN/L)
17-1	10.88	7.76	0.53	2.86	0.56
17-2	6.88	7.77	0.45	7.22	0.38
17-3	59.70	7.01	4.95	5.81	0.87
17-4	80.20	6.46	9.75	2.62	1.06
17-5	34.80	6.49	3.49	4.18	0.58
17-6	219.30	6.65	43.54	15.94	1.38
17-7	213.90	7.26	40.95	15.86	1.29
17-8	164.90	7.20	21.66	7.36	1.28
17-9	165.20	7.38	32.47	15.42	0.73
17-10	127.40	7.52	20.23	12.20	0.87
17-11	15.11	5.83	3.44	33.61	0.72
17-12	77.20	6.02	5.88	29.57	0.97

Table 29: *ICP results for series 17*

Number	Ca (µg/L)	K (µg/L)	Na (µg/L)	Mg (µg/L)	Si (µg/L)	Mn (µg/L)	Fe (µg/L)	Cu (µg/L)	Zn (µg/L)	Al (µg/L)
17-1										
17-2										
17-3										
17-4										
17-5										
17-6										
17-7										
17-8										
17-9										
17-10										
17-11										
17-12										

Note: ICP results for this series have not yet been received from the technician. This appendix will be updated once they are received.

Table 30: *Ion chromatography results for series 17*

Number	NO_3 (mg/L)	PO_4 (mg/L)	NO_2 (mg/L)	SO_4 (mg/L)	Cl (mg/L)
17-1	0.36	n.a.	2.38	2.31	n.a.
17-2	0.33	n.a.	0.96	1.40	n.a.
17-3	1.81	0.04	16.93	5.10	0.46
17-4	3.02	n.a.	20.10	7.88	n.a.
17-5	0.93	n.a.	7.82	5.61	n.a.
17-6	1.28	n.a.	26.35	14.42	0.95
17-7	1.09	n.a.	25.67	13.96	0.91
17-8	2.00	0.11	37.64	14.87	0.81
17-9	0.77	n.a.	5.52	32.27	1.22
17-10	1.26	n.a.	21.12	15.31	0.93
17-11	0.24	n.a.	1.86	1.76	0.46
17-12	0.28	n.a.	27.88	3.71	n.a.

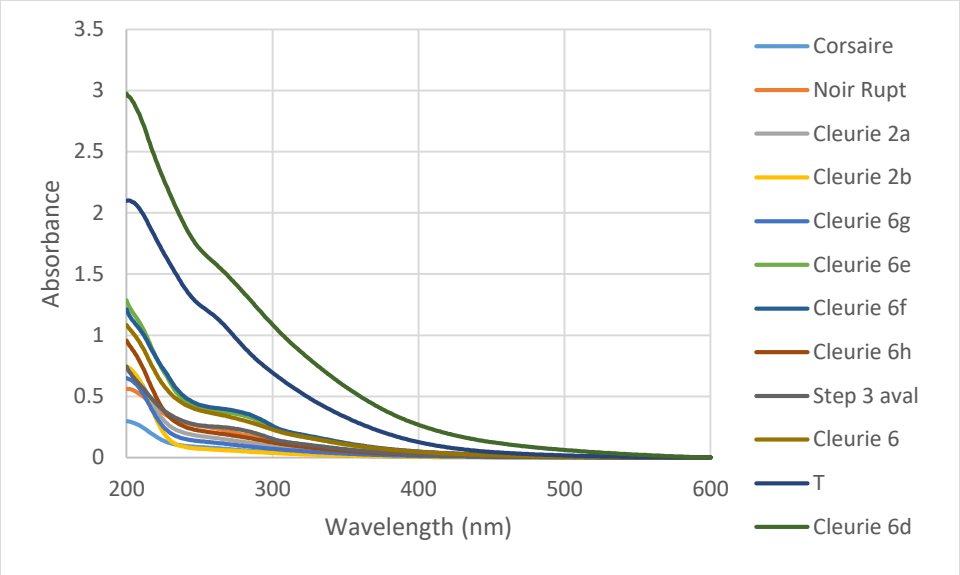

Figure 69: *UV spectroscopy results for series 17*

Table 31: *pH, conductivity, and DOC results for series 18*

Number	X (µS/cm)	pH	C_{inorg} (mgC/L)	C_{org} (mgC/L)	TN (mgN/L)
18-1	9.91	6.13	0.54	2.88	0.50
18-2	6.81	5.94	0.48	7.00	0.47
18-3	58.00	5.84	4.89	5.54	0.97
18-4	76.00	6.03	9.68	2.48	1.07
18-5	35.10	6.16	3.87	4.00	0.67
18-6	264.00	6.89	56.51	17.80	1.67
18-7	268.00	6.99	57.51	19.02	1.54
18-8	161.10	7.40	22.24	7.48	1.21
18-9	162.00	7.47	31.98	14.89	0.71
18-10	124.00	7.60	19.10	11.87	0.96
18-11	15.72	5.80	3.32	31.86	0.64
18-12	78.60	5.99	5.76	30.05	0.83

Table 32: *ICP results for series 18*

Number	Ca (µg/L)	K (µg/L)	Na (µg/L)	Mg (µg/L)	Si (µg/L)	Mn (µg/L)	Fe (µg/L)	Cu (µg/L)	Zn (µg/L)	Al (µg/L)
18-1										
18-2										
18-3										
18-4										
18-5										
18-6										
18-7										
18-8										
18-9										
18-10										
18-11										
18-12										

Note: ICP results for this series have not yet been received from the technician. This appendix will be updated once they are received.

Table 33: *Ion chromatography results for series 18*

Number	NO_3 (mg/L)	PO_4 (mg/L)	NO_2 (mg/L)	SO_4 (mg/L)	Cl (mg/L)
18-1	0.34	n.a.	2.11	1.94	n.a.
18-2	0.31	n.a.	1.19	1.42	n.a.
18-3	1.90	0.04	16.96	5.17	n.a.
18-4	3.18	n.a.	17.09	8.60	n.a.
18-5	0.70	n.a.	7.65	4.57	n.a.
18-6	0.93	n.a.	29.17	15.77	0.61
18-7	0.87	n.a.	29.60	15.73	0.59
18-8	2.08	0.07	34.37	15.00	0.83
18-9	0.74	n.a.	5.37	31.18	1.20
18-10	1.24	n.a.	21.30	14.43	0.85
18-11	0.18	n.a.	1.67	1.68	0.44
18-12	0.32	n.a.	28.06	3.86	n.a.

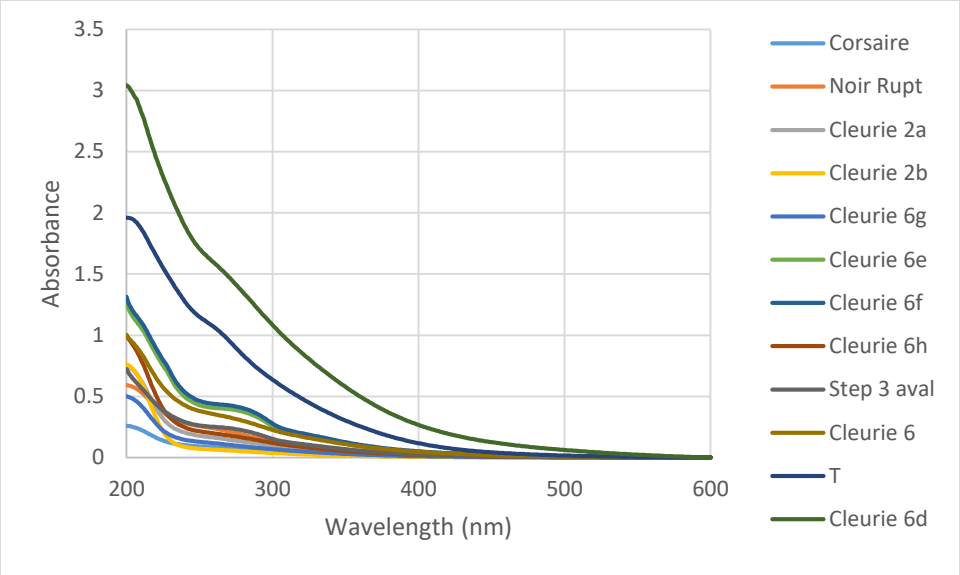

Figure 70: *UV spectroscopy results for series 18*

Table 34: *pH, conductivity, and DOC results for series 19*

Number	X (µS/cm)	pH	C_{inorg} (mgC/L)	C_{org} (mgC/L)	TN (mgN/L)
19-1	56.20	7.36	2.72	6.10	0.84
19-2	50.40	7.16	6.64	2.98	1.01
19-3	20.45	7.20	1.26	4.66	0.48
19-4	18.65	6.93	2.20	5.29	0.42
19-5	38.60	6.77	3.13	6.93	0.56
19-6	37.60	6.62	3.30	7.59	0.53
19-7	61.60	6.61	4.54	6.18	0.96
19-8	12.20	6.89	1.68	6.02	0.52
19-9	47.70	6.55	5.32	8.60	0.72
19-10	18.54	5.76	2.98	35.35	0.67
19-11	49.00	5.98	4.09	25.74	0.73

Table 35: *ICP results for series 19*

Number	Ca (µg/L)	K (µg/L)	Na (µg/L)	Mg (µg/L)	Si (µg/L)	Mn (µg/L)	Fe (µg/L)	Cu (µg/L)	Zn (µg/L)	Al (µg/L)
19-1										
19-2										
19-3										
19-4										
19-5										
19-6										
19-7										
19-8										
19-9										
19-10										
19-11										

Note: ICP results for this series have not yet been received from the technician. This appendix will be updated once they are received.

Table 36: *Ion chromatography results for series 19*

Number	NO_3 (mg/L)	PO_4 (mg/L)	NO_2 (mg/L)	SO_4 (mg/L)	Cl (mg/L)
19-1	1.00	n.a.	19.53	3.55	n.a.
19-2	2.36	0.24	12.04	5.15	n.a.
19-3	0.25	n.a.	7.44	2.02	n.a.
19-4	0.31	n.a.	4.47	2.96	n.a.
19-5	0.66	n.a.	12.06	3.91	n.a.
19-6	0.35	n.a.	12.09	3.53	n.a.
19-7	2.07	n.a.	20.56	5.05	0.49
19-8	0.61	n.a.	2.19	2.64	n.a.
19-9	1.22	n.a.	11.70	5.09	0.48
19-10	0.37	n.a.	2.46	0.89	0.64
19-11	0.21	n.a.	16.02	2.10	n.a.

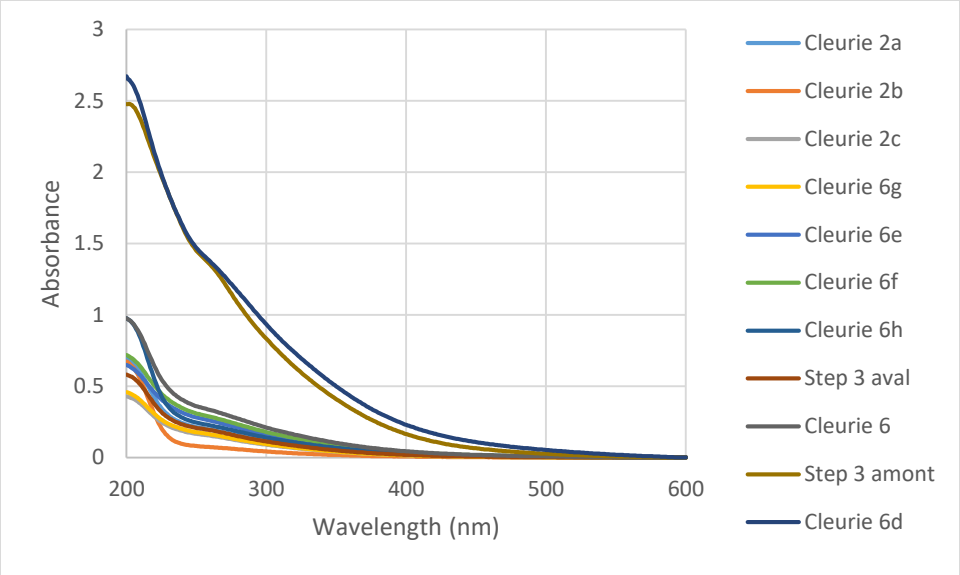

Figure 71: *UV spectroscopy results for series 19*